Probing cardiac repolarization reserve in drug safety assessment

Bepaling van de cardiale repolarisatiereserve in de beoordeling van geneesmiddelenveiligheid
(met een samenvatting in het Nederlands)

Proefschrift

ter verkrijging van de graad van doctor aan de Universiteit Utrecht op gezag van de rector magnicus prof.dr. G.J. van der Zwaan, ingevolge het besluit van het college voor promoties in het openbaar te verdedigen op vrijdag 16 september 2011 des ochtends te 10.30 uur

door

Lukáš Nalos

geboren 5 maart 1976 te Ústí nad Labem, Tsjechië

Promotor:	prof. dr. M.A. Vos
Co-promotoren:	dr. M.A.G. van der Heyden
	dr. M.B. Rook

Financial support by the Heart & Lung Foundation Utrecht for the publication of this thesis is gratefully Acknowledged.
The study described in this thesis was supported by a grant of the Top Institute Pharma, (D2-101), Leiden, The Netherlands.

Probing cardiac repolarization reserve in drug safety assessment

Bepaling van de cardiale repolarisatiereserve in de beoordeling van geneesmiddelenveiligheid
(met een samenvatting in het Nederlands)

Proefschrift

Lukáš Nalos

Cover design: Tomáš Barčík
ISBN: 978-80-260-0355-7

For all that constitutes my cardiac reserve

Chapter 1

Introduction

1

Electrical activity of the heart

The normal electrical activity of the heart is crucial for synchronous and effective cardiac contraction and thus for the normal heart function. The ventricular action potential (AP) is the result of the fine balance between inward and outward currents operating with different time and voltage dependencies, in perfect harmony. The AP can be subdivided into five phases (Fig 1.): phase 0 is known as initial depolarization and rapidly brings the membrane potential from negative to positive values due to fast activation of sodium channels (I_{Na}). Phase 1 is early repolarization and returns the membrane potential close to 0 mV. Most prominent currents in this phase are the transient outward current (I_{to}) and ultrarapid potassium current (I_{Kur}). Phase 1 proceeds more or less smoothly into phase 2 – the "plateau phase" which is characterized by a gradual increase and decrease of L-type calcium current (I_{CaL}) combined with a slow increase in

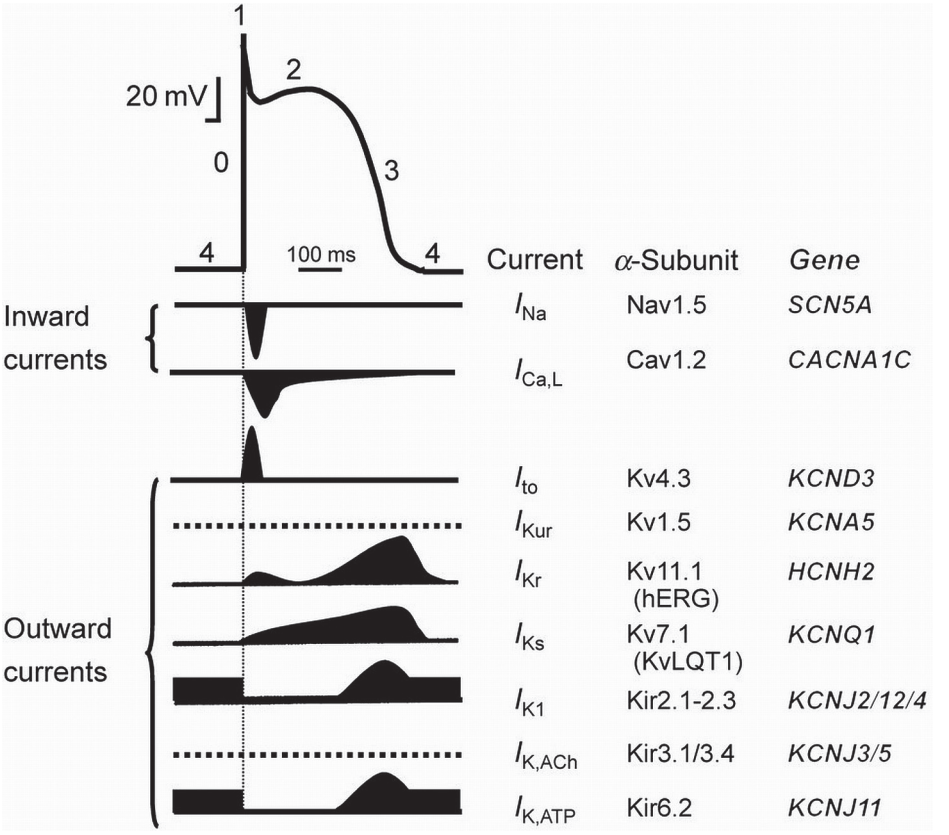

Figure 1. Action potential and main currents responsible for the AP shape (Ravens and Cerbai, 2008).

rapid (I_{Kr}) and slow (I_{Ks}) delayed rectifying currents. As the repolarizing currents become more prominent in time, the plateau phase proceeds into phase 3 – the final repolarization. In this phase, largely carried by I_{Kr} and I_{Ks}, also the inward rectifying potassium current (I_{K1}) is contributing to the return of the membrane potential to the resting membrane potential (phase 4). I_{K1} is then maintaining the stable resting membrane potential during the whole diastole.

When focusing on repolarization, during the plateau phase, inward currents are almost balanced by outward K^+ currents. I_{CaL} together with late sodium current (I_{NaL}) keep the membrane potential at positive voltages. In physiological conditions, I_{CaL} is primarily inhibited by binding of calcium to the channel - Ca^{2+}-dependent inactivation (CDI; Cens *et al.*, 2006). That is accompanied by a slow shift of membrane potential to negative values which is leading to an increase in voltage sensitive repolarizing current I_{Kr} and in I_{K1}, resulting in the final repolarization (Sanguinetti and Jurkiewicz, 1990; Ibarra *et al.*, 1991). I_{Ks} is activated by prolonged depolarization and the importance of this current is increasing with adrenergic stimulation of the heart (Volders *et al.*, 2003). Although I_{Kr} is considered to be the main repolarizing current, also I_{Ks} and I_{K1} are contributing to the repolarization capacity. This is called repolarization reserve - disruption of one repolarizing current is partially compensated by other currents (Roden, 1998a).

Repolarization disturbances caused by a decrease in repolarization reserve are projecting in the ECG as prolongation of the QT interval: the long QT syndrome (LQT). LQT can precipitate in Torsade de Pointes arrhythmia (TdP) which is a polymorphic ventricular tachycardia with a characteristic twist of the QRS complex around the isoelectric baseline on ECG. This arrhythmia can be self terminating or can degenerate into life threatening ventricular fibrillation. There are several LQT syndromes, which are associated with genetic disease (OMIM®; in overview Table 1.). Nevertheless, LQT can be also induced by drugs affecting currents involved in repolarization – acquired LQT (Roden *et al.*, 1996). Although most often the target of these drugs is I_{Kr}, it is believed that block of a single current is not enough for TdP arrhythmia, because of the repolarization reserve. For example the incidence of TdP after clinical treatment with dofetilide (selective I_{Kr} blocker) is only 2.1% (Pedersen *et al.*, 2007). In most cases repolarization reserve is capable to control the normal heart rhythm. Also experiments in animals or isolated right papillary muscles show that blocking of a single repolarizing current is not enough to reach the arrhythmogenic outcome (Lengyel *et al.*, 2007; Biliczki *et al.*, 2002). Thus a decrease of more than one repolarization current or a combination of decrease in an outward current and increase in an inward current (multiple hit) is necessary for TdP occurrence.

Type	Mutation	Description	
LQT1	KCNQ1	alpha subunit of the slow delayed rectifier potassium channel	I_{Ks}
LQT2	KCNH2	alpha subunit of the rapid delayed rectifier potassium channel	I_{Kr}
LQT3	SCN5A	alpha subunit of the sodium channel	I_{Na}
LQT4	ANK1	anchor protein Ankyrin B	
LQT5	KCNE1	beta subunit (MinK) which coassembles with KCNQ1	I_{Ks}
LQT6	KCNE2	beta subunit (MiRP1) which coassembles with KCNH2	I_{Kr}
LQT7	KCNJ2	inward rectifier potassium channel	I_{K1}
LQT8	CACNA1c	alpha subunit of the calcium channel Cav1.2	I_{CaL}
LQT9	CAV3	Caveolin 3	I_{Na}
LQT10	SCN4B	beta subunit type IV which coassembles with SCN5A	I_{Na}
LQT11	AKAP9	A-kinase anchor protein 9	
LQT12	SNTA1	Alpha-1-syntrophin	
LQT13	KCNJ5	G protein-activated inward rectifier potassium channel 4	I_{KATP}

Table 1. Overview of genetic LQT syndromes

Repolarizing currents

This thesis is focused on two currents involved in cardiac repolarization. The first is I_{Kr}, the main repolarizing current. The second one is I_{K1}, the current that is maintaining the stable resting membrane potential and contributing to final part of repolarization. I_{Kr} is extensively studied and its role in cardiac arrhythmias is well accepted (Sanguinetti and Tristani-Firouzi, 2006). On the other hand, there is not much known about the contribution of I_{K1} to LQT related arrhythmias, although the connection in genetically determined LQT7 is clear.

I_{Kr}

The KCNH2 gene, also known as human Ether-a-go-go-related gene (hERG) codes for $K_v11.1$ protein. The gene was first described by Warmke and Ganetzky in 1994. $K_v11.1$ is the alpha subunit of the I_{Kr}. The structure of $K_v11.1$ is similar to other voltage-gated ion channels. It consists of six transmembrane helices, numbered S1-S6, a pore helix situated between S5 and S6 and cytoplasmatically located N- and C- termini. Four $K_v11.1$ proteins

form a functional channel. After translation the protein is transported to the Golgi apparatus where it is glycosylated. N-linked glycosylation is required for surface membrane expression (Petrecca *et al.*, 1999). Several beta subunits were described to associate with K_v11.1. MinK, MiRP1 and MiRP2 modulate the kinetic behavior of the I_{Kr} (Yang *et al.*, 1995a; Abbott *et al.*, 1999; Schroeder *et al.*, 2000). Not much is known about degradation or backward trafficking of the I_{Kr} channel. Ubiquitine was identified as crucial player in degradation of the protein in the lysosomal as well as the proteosomal pathway (Gong *et al.*, 2005; Chapman *et al.*, 2005).

The electrophysiological properties of I_{Kr} are unique compared to other voltage sensitive potassium channels. The main difference is the speed of gating of I_{Kr}. I_{Kr} has two gates, activation and inactivation. In general potassium channel activation gates operate faster than inactivation gates. This means that upon activation the channel is conducting the current until the inactivation gates closed. However, inactivation gates in I_{Kr} operate faster than activation gates (Spector *et al.*, 1996). After voltage dependent activation of I_{Kr} the inactivation gates are closing before the activation gates can fully open. Therefore at the beginning of the plateau phase I_{Kr} is quite small. As the membrane potential shifts during plateau phase to more negative voltages, the inactivation gates are again opening faster than activation gates are closing and the current is flowing through the channel. Thus, although I_{Kr} is activated by depolarization, in fact it is opened by repolarization.

There are a variety of drugs that can block I_{Kr} channel. Their structural and therapeutic heterogeneity is striking. Part of the explanation could be found in the structure of the channel. The cytoplasmic mouth of the channel is wide and access to the channel pore is relatively easy for larger molecules. Molecular determinants of the binding sites were identified using Alanine-scanning mutagenesis studies. Mutation of four residues located in the S6 domain (G648, Y652, F656, and V659; Mitcheson *et al.*, 2000) and three of the "K^+ channel signature sequence" (Heginbotham *et al.*, 1994) residues (TSVGFG) located near the base of the pore helix (T623, S624, and V625) reduced block of hERG channels by the methanesulfonanilide class III drugs (MK-499, dofetilide, and E-4031; Fig 2B). Inactivation of the channel is also important for drug binding as many drugs bind to open or inactivated state of the channel (Yang *et al.*, 2004).

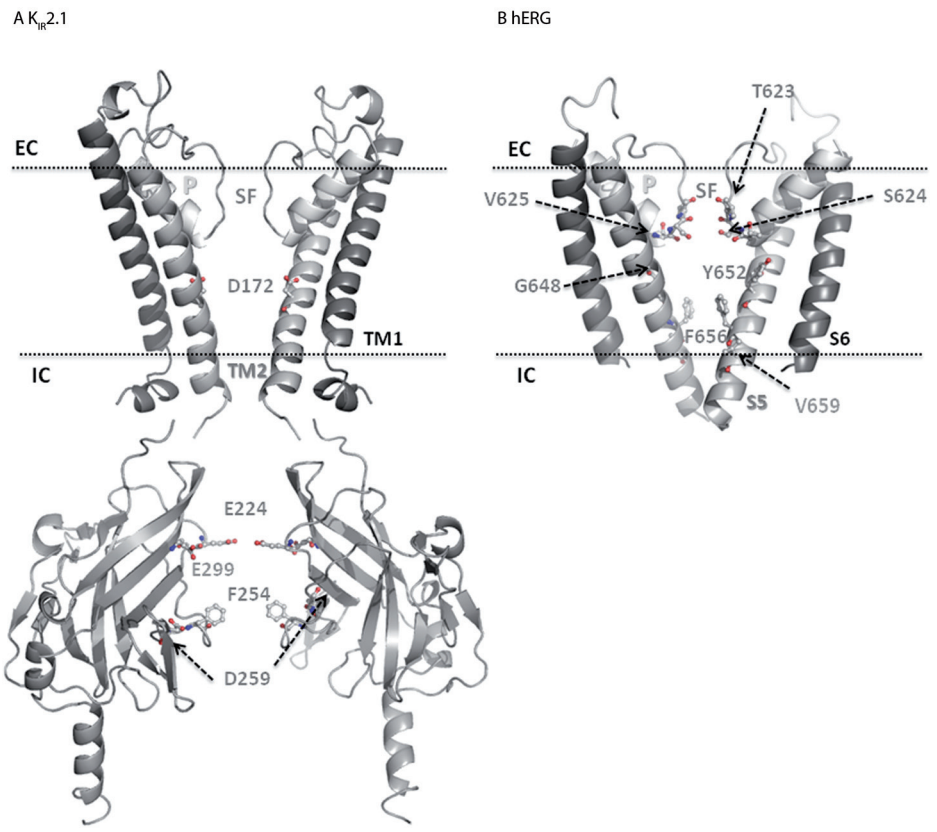

Figure 2. K_{IR}2.1 and hERG structure with depicted aminoacids residues important in drug binding. EC = Extracellular, IC = Intracellular, SF = Selectivity filter, TM = Transmembrane domain, P = P-loop, SX = Segment X.

I_{K1}

The inward rectifier potassium channel of the heart is formed by protein subunits K_{IR}2.1, K_{IR}2.2 and K_{IR}2.3 encoded by KCNJ2, KCNJ12 and KCNJ4 gene respectively (Redell *et al.*, 1998; Hugnot *et al.*, 1997; Makhina *et al.*, 1994). Although the crystal structure of the K_{IR}2.x channels is not available, it is known that K_{IR}2.x proteins have two transmembrane domains with the P-loop in between and C- and N-termini facing the cytoplasma. Four K_{IR}2.x proteins tetramerize to form an I_{K1} ion channel. The P-loop frames the selectivity filter. The protein is not known to undergo posttranscriptional modifications in sarcoplasmic reticulum or Golgi. K_{IR}2.x channel activity is dependent on the interaction of the channel with phosphatidylinositol-4,5-bisphosphate (PIP2;

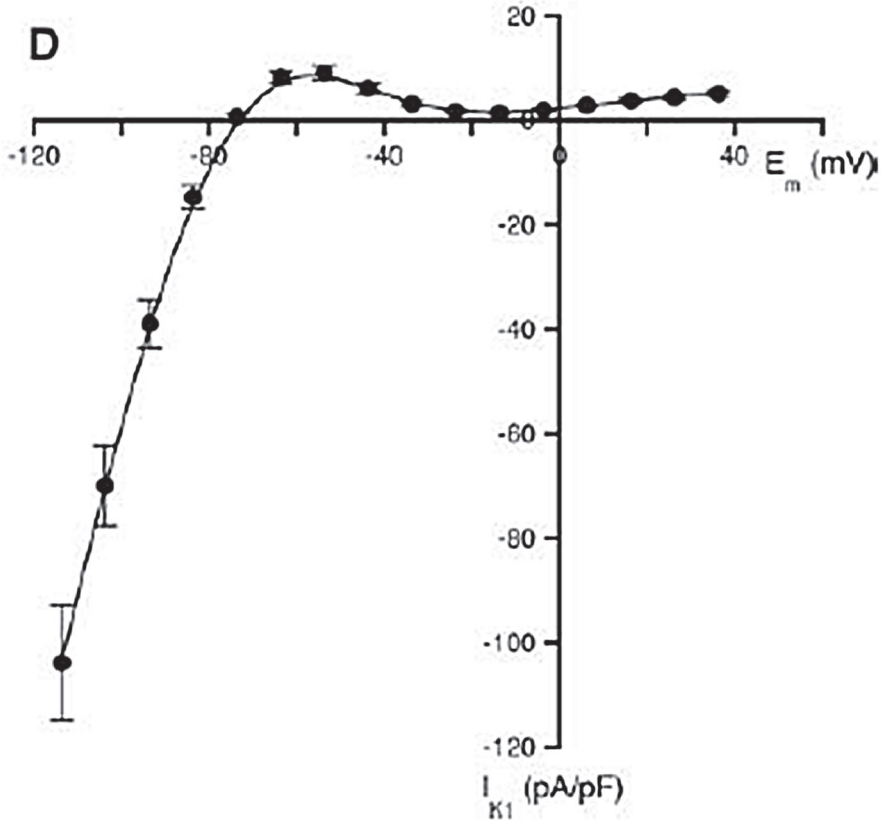

Figure 3. Current-voltage relationship of the typical I_{K1} measured in HEK293 cells stable expressing $K_{IR}2.1$.

Xiao *et al.*, 2003), which is present in cell membrane. This interaction stabilizes the channel in open conformation.

Inward rectifier potassium channels conduct inward currents at potentials more negative than the potassium reversal potential according to Ohm`s law. With shifting of the membrane potential to values positive to reversal potential for K^+ the current becomes much smaller (Fig 3). A small change in resting membrane potential is giving large changes in $K_{IR}2.x$ channel conductance. Thus I_{K1} maintains resting membrane potential. The rectification of the channel is also important for maintaining the plateau phase. It is generally accepted that $K_{IR}2.x$ channels are not conducting during the plateau phase at all and that this channel is not contributing to the repolarization until the membrane potential becomes more negative (Dhamoon and Jalife, 2005). However, some experiments in

dog right ventricular papillary muscle are showing prolongation of AP already during plateau phase after application of the specific I_{K1} blocker Ba^{+} (Lengyel *et al.*, 2004). The mechanism of the inward rectification of K^{+} channels is the voltage-dependent blockade of outward K^{+} currents by both intracellular Mg^{2+} (Matsuda *et al.*, 1987; Vandenberg, 1987) and positively charged polyamines (Ficker *et al.*, 1994; Lopatin *et al.*, 1994).

The only known specific I_{K1} blocker is Ba^{2+}. Unfortunately application of barium ions to animals is toxic and affecting several organ systems. A few case reports about barium intoxication in humans show also cardiac arrhythmias (Johnson and VanTassell, 1991), but a detailed study of I_{K1} role in cardiac arrhythmias is not possible due to lack of a specific blocker applicable *in vivo*. The potential importance of this channel in cardiac arrhythmias can be derived from genetic diseases interfering with mutation in $K_{IR}2.x$ proteins. Andersen-Tawil syndrome (LQT7) is, amongst other symptoms, accompanied by long QT syndrome with TdP arrhythmias and sudden cardiac death (Tristani-Firouzi *et al.*, 2002). This is indicative of the importance of I_{K1} for the cardiac repolarization reserve. Therefore further extensive research is necessary to asses in detail what the relation between I_{K1} and cardiac arrhythmias is. For this, finding of a specific I_{K1} blocker applicable *in vivo* would be a logical and crucial first step.

Two different binding sites have been identified for binding of polyamines (spermine, spermidine). D172 in the M2 transmembrane domain and E224 and E299 in the cytoplasmic C-terminal region (Fig 2A) were pointed out as the aminoacids important for the binding of polyamines (Stanfield *et al.*, 1994; Wible *et al.*, 1994; Taglialatela *et al.*, 1995; Yang *et al.*, 1995b; Kubo and Murata, 2001). Very recently, the antimalarial drug chloroquine was identified as an I_{K1} blocker (Rodríguez-Menchaca *et al.*, 2008). However, this drug is a multichannel blocker with quite low sensitivity for I_{K1} compared to other channels. The residues important for its binding, E224, E299, F254 and D259 are located in cytoplasmic C-terminus and largely correspond to the same region of binding as polyamines. Thus this region could be a target of interest in development of a specific I_{K1} blocker.

Cardiac safety assessment

In the past decades, many drugs were withdrawn from the market because of their potential to induce TdP (Redfern *et al.*, 2003). This adverse effect does not occur only in cardiovascular drugs but in a wide spectrum of structurally and functionally different drugs. One part of the evaluation of the cardiac toxicity of new drug candidates therefore concerns testing the proarrhythmic potential

of these compounds. For instance, the current strategy of the U.S. Food and Drug Administration (FDA) is based on the thorough QT/QTc study in healthy volunteers (ICH Guideline E14, 2005). If the QTc prolongation is less than 5 ms, the drug is approved as safe. A prolongation of more than 20 ms discards the drug from the approval process. If the QTc prolongation is 5 to 20 ms, additional verification of cardiac safety is required (ICH Guideline S7B, 2005).

On the other hand, the pharmaceutical industry is trying to identify unsafe drugs in earlier stages of drug development to lower the cost of development. I_{Kr} is generally accepted as the main suspected target of drugs inducing TdP and thus a hERG assay is often used to determine the hERG blocking potency of the drug candidate.

The weakness of this current approach of cardiac drug safety testing is in three important aspects. First aspect is that correlation between QT prolongation and proarrhythmic potential is not always predictive (Ahmad and Dorian, 2007). There are drugs prolonging QT without inducing TdP (Table 2.; Antzelevitch, 2007). Experiments with a torsadogenic I_{Kr} blocker d-sotalol show increased QT interval far before an occurrence of TdP and QT prolongation is present also in animals that did not experienced TdP arrhythmia (Thomsen *et al.*, 2004). Therefore, in our opinion, there is a need for another surrogate marker, which will correlate with arrhythmogenic outcome better.

Secondly, focus on one current - I_{Kr} is limiting the specificity of the testing systems. It has been shown in preparations with decreased repolarization reserve that the block of I_{K1} or I_{Ks} is proarrhythmic as well (Biliczki *et al.*, 2002; Burashnikov and Antzelevitch, 2002; Vos *et al.*, 2001). The decreased repolarization reserve has been described in several models of cardiac diseases. Under these circumstances, the drugs affecting ancillary currents could have a proarrhythmic potential too.

	IKr block	QT prolongation	TdP
Almokalant	+	+	+
Amiodarone	+	+	-
Moxifloxacin	+	+	-
Ranolazine	+	±	-
Haloperidol	+	-	-
DPI 201-106	-	+	+

Table 2. Examples of poor correlation between IKr block, QT prolongation and TdP arrhythmia.

The third weakness of the current cardiac safety assessment is the fact, that only acute effects of the drug on hERG channel are tested. An increasing number of drugs is identified to have an effect on channel protein trafficking, decreasing the total current available in the membrane and thus reducing the repolarization reserve (Cordes *et al.*, 2005; Kuryshev *et al.*, 2005; Rajamani *et*

al., 2006; Sun *et al.*, 2006; Guo *et al.*, 2007; Wang *et al.*, 2007; van der Heyden *et al.*, 2008). This chronic effect of drugs on cardiac repolarization is not tested at all.

Models of cardiac arrhythmias and predicting markers

In general there are three different possibilities of preclinical testing of drugs for arrhythmogenic potential. Cultured cells are used in hERG assays. As already mentioned, there is no clear correlation between hERG block and proarrhythmic endpoint and this assay suffers from high number of false positive as well as false negative outcomes. Measurements in primary cultures of disaggregated cardiac cells are also not very convincing. Damage of ion channels and changes in channel expression during isolation and storage lead to high variation in electrophysiological parameters (Saint and Chung, 1999). The freshly isolated cardiomyocytes could be the favorable alternative still suffering from damages caused by isolation, but not that caused by storage or culture artifacts.

Other *in vitro* models are isolated tissues or hearts. Isolated Purkinje fibers, Langendorff perfused hearts, papillary muscles or wedge preparations have generally good sensitivity and specificity (Eckardt *et al.*, 2002; Valentine *et al.*, 2004; Aiba *et al.*, 2005; Joshi *et al.*, 2004; Champeroux *et al.*, 2005; Lengyel *et al.*, 2004). Disadvantage of these methods is low throughput and technical complexity.

In vivo TdP arrhythmia models would seem most likely to predict arrhythmias in humans. The *in vivo* models can be subdivided into conscious and anesthetized animals. There are not much data available from conscious animals. In fact three models were introduced. AV block combined with hypokalemia is producing TdP-like polymorphic arrhythmias in dogs (Chezalviel *et al.*, 1995). Carlsson *et al.* (1993) found that infusion of APD prolonging agents such as almokalant or dofetilide was associated with the induction of TdP in conscious rabbits. Nevertheless after anesthesia of these rabbits inducibility was lost. The TdP arrhythmias in anesthetized rabbits were present only if animal was pretreated with α_1 agonist such as methoxamine (Carlsson *et al.*, 1993). The chronic AV block dog model was introduced by Vos *et al.* (1995) and is well discriminating the proarrhythmic effects of various hERG blockers (Chiba *et al.*, 2001). The important limitations of animal models are high cost and time consumption.

As already mentioned, the clinical incidence of TdP even after treatment with potent torsadogenic drug is low. Although the incidence of TdP in animal

models developed for testing of this arrhythmia is higher, the outcome never reaches 100%. The same holds true for *in vitro* models. Thus, all testing assays do not evaluate intrinsic torsadogenicity, but look at surrogate markers suspected to be linked to TdP arrhythmia. The markers used are hERG blocking effect (Roden, 2004), prolongation of APD/QT, triangulation of APD, dispersion of APD (TRIaD; Hondeghem, 2008) and beat-to-beat variability of APD/QT (Thomsen *et al.*, 2004).

Scope of the thesis

This thesis is addressing two important repolarizing currents – I_{Kr} and I_{K1}. The role of I_{Kr} in arrhythmias is well described. A large number of drugs are interacting with this channel and it is critical for pharmaceutical industry to identify chemical structures responsible for the binding. In chapter 2, the structure-function relationship between the hERG channel and a number of dofetilide analogues is described to specify structural features responsible for the hERG toxicity.

The role of I_{K1} in arrhythmias is poorly studied. The main reason for that is lack of a specific I_{K1} blocker, which can be used *in vivo*. In chapter 3, we identified pentamidine as a specific blocker of I_{K1}. Pentamidine is not an ideal I_{K1} blocker and its use *in vivo* has some limitations (low affinity, effect on protein trafficking). In chapter 4, we have used pentamidine as starting point and studied the effect of different pentamidine analogues on I_{K1} channel to screen for the best candidate for development of a specific I_{K1} blocker.

An increasing number of drugs are identified to interact with the protein trafficking process. This potentially adverse effect of the drugs is not evaluated in cardiac safety assessment. We have addressed this issue in chapter 5, where we studied the chronic effect of pentamidine on $K_{IR}2.1$ and hERG trafficking and some of the possibilities to avert this.

Focus of the regulatory authorities on hERG block and QT prolongation during drug approval process is becoming obsolete. New testing models are needed. In chapter 6 the sensitivity and specificity of different *in vivo* and *in vitro* models that can be used for testing of proarrhythmic potential of new compounds are compared and discussed.

Chapter 2

Exploring Chemical Substructures Essential for hERG K^+ Channel Blockade by Synthesis and Biological Evaluation of Dofetilide Analogues

Shagufta, Guo D, Klaasse E, de Vries H, Brussee J, Nalos L, Rook MB, Vos MA, van der Heyden MAG, IJzerman AP.

ChemMedChem. 2009 Oct;4(10):1722-32.

In this study we followed a new approach to analyze molecular substructures required for hERG channel blockade. We designed and synthesized 40 analogues of dofetilide (**1**), a potent hERG potassium channel blocker, and established structure–activity relationships (SAR) for their interaction with this important cardiotoxicity-related off-target. Structural modifications to dofetilide were made by diversifying the substituents on the phenyl rings and the protonated nitrogen and by varying the carbon chain length. The analogues were evaluated in a radioligand binding assay and SAR data were derived with the aim to specify structural features that give rise to hERG toxicity

Introduction

The human ether-a-go-go-related gene (hERG) encodes the rapidly acting delayed rectifier potassium current channel (I_{Kr}), which is the main protein involved in phase three repolarization of the cardiac action potential. The effects on heart rhythm by class III antiarrythmic drugs is due to their interaction with this hERG potassium channel resulting in prolongation of the QT interval. However, nonantiarrythmic drugs and their metabolites may also cause prolongation of the QT interval in the electrocardiogram, which increases risk for torsade de pointes, a ventricular arrhythmia causing syncope, ventricular fibrillation and sudden death.(Sanguinetti and Tristani-Firouzi, 2006; Wilke *et al.*, 2007; Recanatini *et al.*, 2005) In recent years, this type of cardiac toxicity has become a major pharmacological safety concern for the pharmaceutical industry and health regulatory agencies (Valentin *et al.*, 2008).A number of drugs were withdrawn from the market or failed in late-stage clinical trials because cardiac arrhythmia was a side effect of treatment (Recanatini *et al.*, 2008). Therefore understanding drug–hERG channel interaction at a molecular level is important and of general interest for rational drug design.

A tremendous research effort has been undertaken in both the pharmaceutical industry and academia to understand the structural requirements for binding to the hERG potassium channel in order to avoid potential toxicity. Thus, in silico methods in particular have emerged as an important approach for the prediction of hERG blockade in available series of compounds (Stansfeld *et al.*, 2007; Pearlstein *et al.*, 2003a; Cavalli *et al.*, 2002; Ekins *et al.*, 2006; Kramer *et al.*, 2008; Thai *et al.*, 2008; Pearlstein *et al.*, 2003b; Cianchetta *et al.*, 2005; Choe *et al.*, 2006; Shamovsky *et al.*, 2008; Aronov, 2006; Farid *et al.*, 2006). However, fundamentally these in silico models are training-set dependent

and therefore nongeneric. More traditionally, series of compounds designed for a given therapeutic target, are also screened for additional hERG activity. Once established, this unwanted activity is then 'synthesized out' in the next series of compounds, if at all possible (Yoshizumi *et al.*, 2008; McCauley *et al.*, 2004; Matasi *et al.*, 2005; Friesen *et al.*, 2003; Slee *et al.*, 2008; Meyers *et al.*, 2007.; Kawai *et al.*, 2007; Fraley *et al.*, 2004; Su *et al.*, 2007; Price *et al.*, 2006; Bilodeau *et al.*, 2004; Dinges *et al.*, 2007; Zhang *et al.*, 2005a; Sisko *et al.*, 2006; Mukaiyama *et al.*, 2008; Judd *et al.*, 2007; Iyengar *et al.*, 2009). Notably, this approach has provided important information regarding the molecular characteristics of hERG channel blockers. In this study we take a different approach by assuming that design and synthesis of compounds primarily for the hERG channel as the main target can afford more precise structure–activity relationships (SAR) and can facilitate the discovery of chemical alerts for hERG potassium channel toxicity.

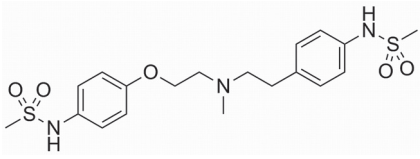

Dofetilide (**1**)

Dofetilide (**1**) (Cross *et al.*, 1990) was selected as the lead scaffold from which hERG channel inhibitors can be developed. It is a member of a methanesulphonanilide class of antiarrhythmic drugs with high affinity for the hERG channel (Singleton *et al.*, 2007; Snyders and Chaudhary, 1996; Diaz *et al.*, 2004). Its protonated nitrogen, phenyl rings and methanesulphonamide group are hypothesized to form a π-cation interaction with Tyr 652, π–π interaction with Phe 656 and hydrogen bonds with the OH groups of Thr 623, Ser 624, Ser 649 and Tyr 652 of the inner pore region of the hERG channel, respectively. Therefore, we have considered substituents of the phenyl rings and the protonated nitrogen as main structural features to be varied in the development of dofetilide analogues. Substitution of the phenyl ring can be diversified to discover the nature and position of substituents required for interaction with the hERG channel. Substituents at the nitrogen can be varied to modulate the basicity of the molecule (pK_a), among other properties, and to analyze its consequences for the interaction with the hERG channel. Evidence in literature also revealed that the spacing between the basic nitrogen and the aromatic group(s) is important to cover the separation between the Phe 656 and Tyr 652 side chains in the pore region (Pearlstein *et al.*, 2003a; Pearlstein *et al.*, 2003b). Thus any change in chain length connecting the phenyl rings with the nitrogen atom in dofetilide may have important consequences in hERG-channel binding also. Therefore, we also synthesized a number of analogues with varying

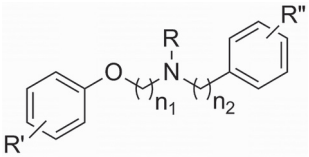

40 Dofetilide analogues

carbon chain lengths between the phenyl rings and the nitrogen atom. In total, 40 analogues of dofetilide (**1**) were synthesized. We analyzed the hERG-channel binding characteristics of these compounds, and identified SAR in order to recognize the basic structural features required for hERG activity.

2 Results and Discussion

Chemistry

The phenyl-substituted analogues were synthesized following the synthetic approach reported by Liu et al. for the preparation of *p*-methylsulfonamido phenethylamine analogues (Liu *et al.*, 2002).The preparation of phenyl ring-substituted analogues **30–45**, based on the Topliss scheme (Topliss, 1972), involved a three-step synthesis (Scheme 1). Phenols **2–7** were reacted with

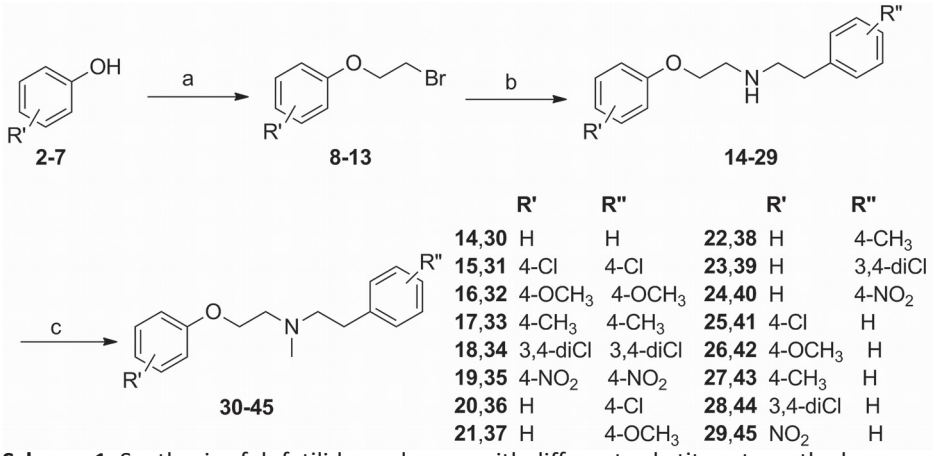

	R'	R"		R'	R"
14,**30**	H	H	**22**,**38**	H	4-CH_3
15,**31**	4-Cl	4-Cl	**23**,**39**	H	3,4-diCl
16,**32**	4-OCH_3	4-OCH_3	**24**,**40**	H	4-NO_2
17,**33**	4-CH_3	4-CH_3	**25**,**41**	4-Cl	H
18,**34**	3,4-diCl	3,4-diCl	**26**,**42**	4-OCH_3	H
19,**35**	4-NO_2	4-NO_2	**27**,**43**	4-CH_3	H
20,**36**	H	4-Cl	**28**,**44**	3,4-diCl	H
21,**37**	H	4-OCH_3	**29**,**45**	NO_2	H

Scheme 1. Synthesis of dofetilide analogues with different substituents on the benzene ring (**30–45**). *Reagents and conditions:* a) 1,2-dibromoethane, NaOH, TBAB, EtOH, reflux; b) phenethylamine or 4-substituted phenethylamine, K_2CO_3, CH_3CN, RT; c) 1. HCOOH, HCHO, reflux; 2. ethanolic HCl.

1,2-dibromoethane in ethanol with NaOH and tetrabutylammonium bromide (TBAB) to give the brominated intermediates **8–13**. Substitution of **8–13** with the corresponding phenethylamines in acetonitrile and in the presence of K_2CO_3 afforded the secondary amines **14–29** as key intermediates. The final step was the N-methylation of **14–29**, which was performed in a straightforward Eschweiler–Clarke reaction using formaldehyde and formic acid to afford compounds **30–45**. The products were subsequently converted to their hydrochloride salts by means

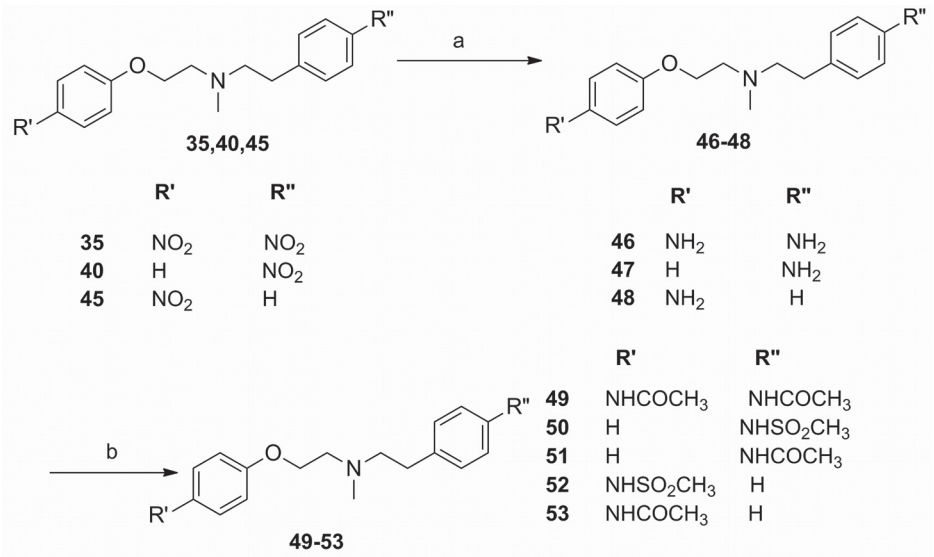

Scheme 2. Synthesis of the amine-, acetamide- and sulphonamide-substituted analogues **46–53**. *Reagents and conditions*: a) 1. Fe, CH_3COOH, THF, H_2O, reflux; 2. ethanolic HCl; b) 1. MsCl or AcCl, Et_3N, CH_2Cl_2, 0°C; 2. ethanolic HCl

of ethanolic HCl (see the Experimental Section and Supporting Information for details).

The amine-, acetamide- and sulphonamide-substituted analogues **46–53** were synthesized according to the route depicted in Scheme 2. The nitro groups of **35**, **40** and **45** were reduced to amines using Fe and acetic acid in water and THF in good yields. Amines **46–48** were converted to their hydrochloride salts before

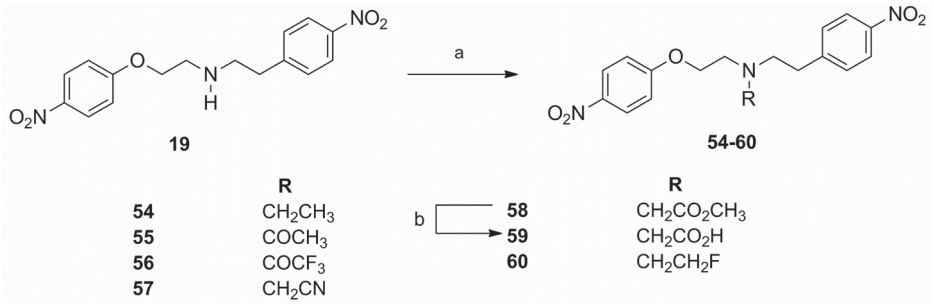

Scheme 3. Synthesis of aliphatic N-substituted analogues **54–60**. Reagents and conditions: **54**; a) 1. CH_3CH_2I, K_2CO_3, DMF, RT; 2. ethanolic HCl. **55**; a) CH_3COCl, Et_3N, CH_2Cl_2, 0 °C→RT. **56**; a) $(CF_3CO)_2O$, Et_3N, CH_2Cl_2, 0 °C→RT. **57**; a) $BrCH_2CN$, DIPEA, CH_3CN, 0 °C→RT. **58**; a) $BrCH_2CO_2CH_3$, K_2CO_3, DMF, 0 °C→RT. **59**; b) NaOH, dioxane, 60 °C. **60**; a) 1. $BrCH_2CH_2OH$, K_2CO_3, EtOH, reflux; 2. DAST, CH_2Cl_2, −60→15 °C; 3. ethanolic HCl.

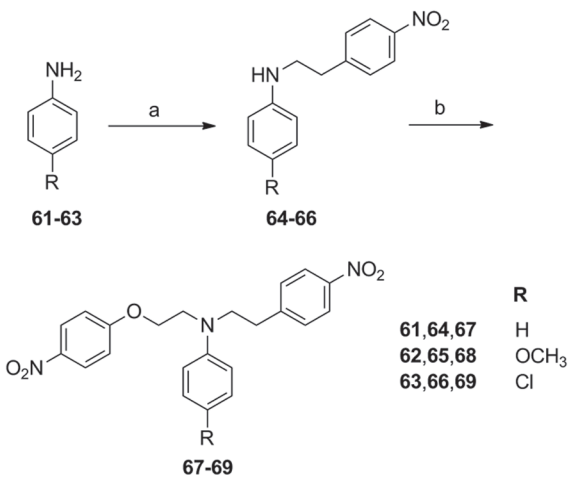

Scheme 4. Synthesis of aromatic N-substituted analogues **67–69**. *Reagents and conditions:* a) 1-(2-bromoethyl)-4-nitrobenzene, KI, CH_3CN, MW, 110 °C, 30 min; b) 1-(2-bromoethoxy)-4-nitrobenzene, KI, CH_3CN, MW, 170 °C, 1 h.

biological evaluation. Compounds **49–53** were synthesized from the free amines **46–48**. Reaction with methanesulphonyl chloride (MsCl) or acetyl chloride (AcCl) in the presence of triethylamine gave the desired methanesulphonamides **50** and **52** and the acetamides **49**, **51** and **53**, respectively. Compounds **50–53** were converted to their solid hydrochloride forms using ethanolic HCl.

Aliphatic N-substituted analogues **54–60** were synthesized following the route shown in Scheme 3. The secondary nitrogen of **19** was alkylated with the corresponding alkyl halide or acyl halide in the presence of a suitable base and solvent to afford the required products **54–58**. Acid **59** was prepared as its hydrochloride salt from **58** by ester hydrolysis in the presence of NaOH and dioxane and subsequent acidification with dilute HCl. Compound **60** was synthesized from **19** in two steps via alkylation of the secondary nitrogen with 2-bromoethanol in the presence of K_2CO_3 followed by fluorination of the hydroxy group using diethylaminosulfur trifluoride (DAST) in dichloromethane. Compounds **54** and **60** were viscous oils and were converted to their hydrochloride salts for biological evaluation.

Aromatic N-substituted analogues **67–69** were synthesized via the general procedure shown in Scheme 4. Microwave irradiation of the appropriate anilines **61–63** with 1-(2-bromoethyl)-4-nitrobenzene and a catalytic amount of KI in acetonitrile at 110 °C for 30 min provided the intermediates **64–66**. Reaction of the secondary aromatic amines **64–66** with 1-(2-bromoethoxy)-4-nitrobenzene in the presence of KI in acetonitrile, under microwave-assisted heating to 170 °C for 1 h, provided the final products **67–69**.

Analogues with varying chain lengths (**77–81**) were prepared following the same reaction conditions (see Scheme 5) as described for **30–45** in Scheme 1. Commercially available 4-nitrophenol (**7**) was alkylated with the corresponding

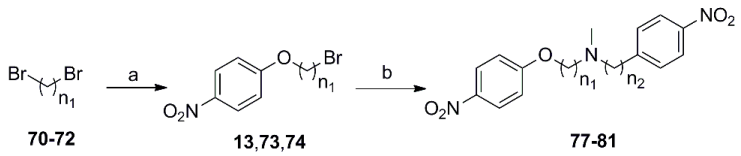

70-72 13,73,74 77-81

	n_1	n_2		n_1	n_2
70,**13**	2	-	**77**	2	1
71,**73**	3	-	**78**	3	1
72,**74**	4	-	**79**	3	2
75	-	1	**80**	4	1
76	-	2	**81**	4	2

Scheme 5. Synthesis of analogues with varying carbon chain lengths (**77–81**). *Reagents and conditions:* a) **7**, NaOH, TBAB, EtOH, reflux; b) 1. **75** or **76**, K_2CO_3, CH_3CN, RT; 2. HCOOH, HCHO, reflux; 3. ethanolic HCl.

dibromo alkanes **70–72** to afford the intermediates **13**, **73** and **74**. Further reaction of **13**, **73** and **74** with the subsequent amines (**75** and **76**) provided the secondary amines, which were used in their crude forms for further methylation of the nitrogen using formaldehyde and formic acid to provide the final products **77–81**. Compounds **77**, **79** and **81** were converted to their hydrochloride salts whereas **78** and **80** were used as free bases for biological testing.

Biology

Chiu *et al.*, 2004 described the use of 5 mm KCl in the incubation buffer when measuring the specific binding of [^{3}H]astemizole to membranes from HEK293 cells stably expressing the hERG channel. During optimization of the radioligand binding assay, this concentration was found to be far from optimal. In our hands, the optimal window between total and nonspecific binding was only reached at a concentration of 60 mm KCl or higher (results not shown). Increasing concentrations of dofetilide (**1**) displaced specific [^{3}H]astemizole binding, yielding two affinity sites, one with higher affinity (4.1±0.9 nM) and the other with lower affinity (29±10 μM) (Figure 1).

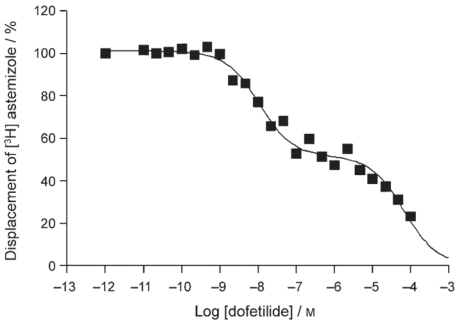

Figure 1. Displacement of specific [^{3}H] astemizole binding to HEK293 membranes expressing the hERG K^+ channel by dofetilide (**1**), showing two affinity sites.

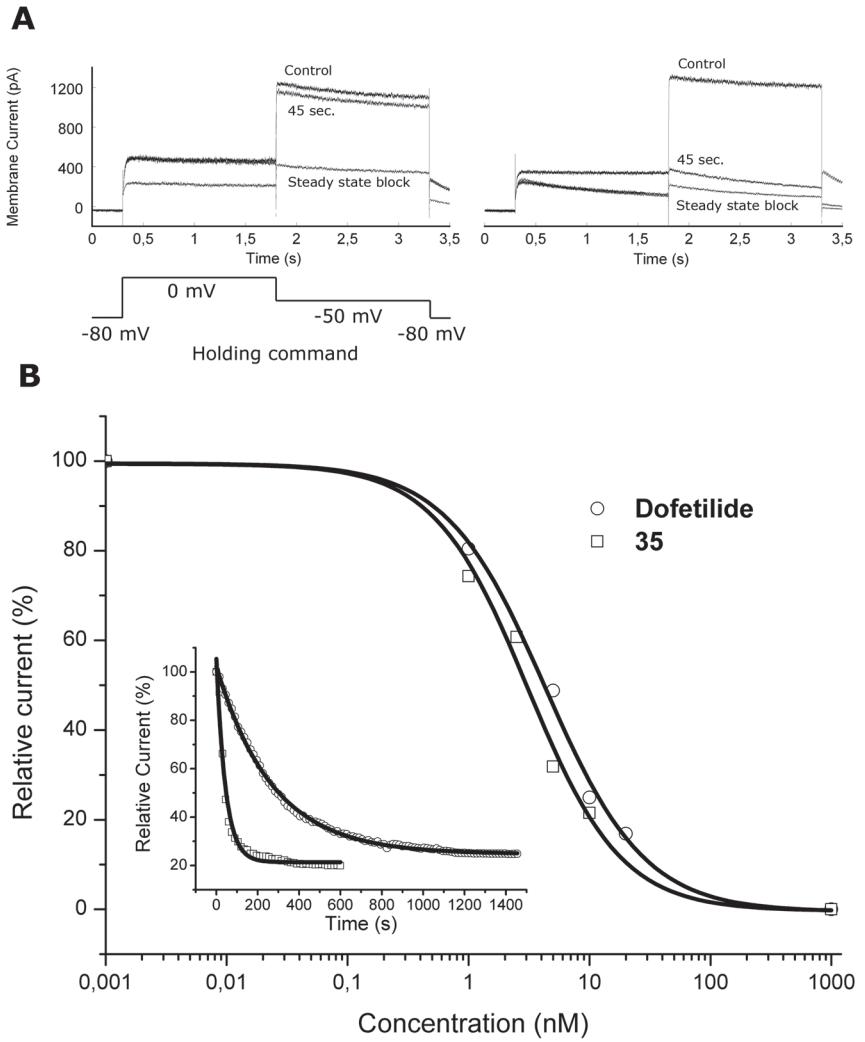

Figure 2. Concentration-dependent blockade of the hERG current by dofetilide (**1**) and analogue **35** with standard short tail protocol. a) Examples of original hERG current traces of control, 10 nM dofetilide (**1**) (left panel) and 10 nM **35** (right panel) at 45 s following application and at steady state. b) IC_{50} curve for dofetilide (**1**; ○) and **35** (□) derived from multiple measurements and fitted using the Hill equation. Each point represents at least four independent measurements. Inset: time-dependent I_{Kr} block for dofetilide (**1**; ○) and **35** (□) at 10 nM, average of four independent measurements. Drug infusion was started at t=0.

In an electrophysiological patch clamp assay (Witchel *et al.*, 2002; Brown, 2004; Weerapura *et al.*, 2002) on the same HEK293 cells stably expressing the channel, dofetilide (**1**) also displayed nanomolar affinity as a functional blocker of the hERG current (Figure 2). The concentration-dependent response of **1** with the standard short tail patch clamp protocol yielded an IC_{50} value of 4.3±0.7 nM, which is comparable to the K_i value found for the high affinity site (4.1±0.9 nM). Therefore, to reliably determine the high-affinity site K_i values, all dofetilide analogues were tested at 12 different concentrations at least.

Structure–Activity Relationships

Ring substituents

Thorough search of the literature on the hERG potassium channel indicates that structural modifications to the aromatic rings of a drug have a significant effect on hERG activity. Incorporation of electron-withdrawing or removal of electron-donating groups can disrupt the π-stacking interactions between aromatic residues (Phe 656 and Tyr 652) of the pore cavity and aromatic moieties of the drug, and can thus affect the hERG activity (Pearlstein *et al.*, 2003b; Jamieson *et al.*, 2006).To further study this effect and to specify the chemical groups essential for hERG blockade, we synthesized 24 dofetilide analogues (**30–53**) and evaluated them in a radioligand binding assay (Table 1). Initially the effect of substituents on both phenyl rings was investigated in **30–35**, **46** and **49**. Deletion of the methanesulphonamide moiety on both phenyl rings (**30** vs **1**) virtually abolishes hERG channel affinity; replacement of methanesulphonamide with different groups (Cl, **31**; OCH_3, **32**; CH_3, **33**; 3,4-diCl, **34**; NO_2, **35**) affects affinity for the hERG channel in the following way. Analogues **31** (R′, R″=4-Cl), **33** (R′, R″=4-CH_3) and **35** (R′, R″=4-NO_2) are equally active (K_i=4.2, 5.1, and 5.7 nM, respectively), **34** (R′, R″=3,4-diCl) is more active (K_i=0.31 nM) whereas **32** (R′, R″=4-OCH_3) does not recognize the dofetilide binding site very well (K_i=399 nM). The only exceptions to this group of analogues are **46** (R′, R″=4-NH_2) and **49** (R′, R″=4-$NHCOCH_3$) that, like the unsubstituted derivative **30**, have reduced affinity and displace the radioligand by only 39% and 34%, respectively, at a final concentration of 10 μM. These results indicate that for high hERG channel affinity a 3,4-diCl group as R′ and R″ is optimal.

Next, SAR studies were carried out to investigate the effect of substituents on either the phenyl or the phenoxy ring. Analogues **36–40** (R′=H, R″=4-Cl, 4-OCH_3, 4-CH_3, 3,4-diCl, 4-NO_2) and **50** (R′=H, R″=4-$NHSO_2CH_3$), containing substituents only on the phenyl ring, have decreased affinity compared to the

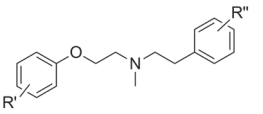

Compd	R′	R′′	K_i [nM] or displacement [%][a]	n
1	4-$NHSO_2CH_3$	4-$NHSO_2CH_3$	4.1±0.9	3
30	H	H	37 %	3
31	4-Cl	4-Cl	4.2±1.6	3
32	4-OCH_3	4-OCH_3	399±64	4
33	4-CH_3	4-CH_3	5.1±4.7	4
34	3,4-diCl	3,4-diCl	0.31±0.28	3
35	4-NO_2	4-NO_2	5.7±3.0	3
36	H	4-Cl	15±6.2	3
37	H	4-OCH_3	8.0±7.8	3
38	H	4-CH_3	1.1±1.1	3
39	H	3,4-diCl	13±12	3
40	H	4-NO_2	23±12	3
41	4-Cl	H	3.1±1.9	4
42	4-OCH_3	H	3.3±2.0	4
43	4-CH_3	H	7.9±7.2	4
44	3,4-diCl	H	2.4±2.2	4
45	4-NO_2	H	3.1±1.9	3
46	4-NH_2	4-NH_2	39 %	3
47	H	4-NH_2	51 %	3
48	4-NH_2	H	44 %	3
49	4-$NHCOCH_3$	4-$NHCOCH_3$	34 %	3
50	H	4-$NHSO_2CH_3$	162±52	3
51	H	4-$NHCOCH_3$	41 %	3
52	4-$NHSO_2CH_3$	H	54±24	3
53	4-$NHCOCH_3$	H	20 %	3

Table 1. Binding affinities of dofetilide analogues **30–53** with varied phenyl ring substituents in radioligand binding assay of hERG K^+ channel. [a] K_i values ±SEM or displacement [%] at 10 μM (n=3) of specific [^{3}H]astemizole binding to membranes of HEK293 cells stably expressing the hERG K^+ channel.

parent compound **1** (K_i=15, 8.0, 13, 23, and 162 nM, respectively) except for **38** (R′=H, R″=4-CH_3), which exhibited a strong interaction with the hERG channel (K_i=1.1 nM). Analogue **47** (R′=H, R″=4-NH_2) demonstrated only 51% displacement of the radioligand and thus behaves in the same way as analogue **46** bearing NH_2 on both rings. Analogue **51** (R′=H and R″=4-$NHCOCH_3$) does not bind to the hERG channel very well, showing only 41% displacement of the radioligand. A comparison of these analogues (**36–40** and **50**) with compounds **1** and **30–35** shows that except for OCH_3 and CH_3, the single substitutions (Cl, 3,4-diCl, NO_2 and $NHSO_2CH_3$) decrease the affinity, with the latter substituent ($NHSO_2CH_3$) exhibiting the most profound effect (K_i=162 nM).

Analogues **41–45** and **52** (R′=4-Cl, 4-OCH_3, 4-CH_3, 3,4-diCl, 4-NO_2 and 4-$NHSO_2CH_3$, R″=H) with substituents on the phenoxy rather than the phenyl ring show affinities comparable to **1** (K_i=3.1, 3.3, 7.9, 2.4 and 3.1 nM) except for **52** (K_i=54 nM). Similarly to **46** and **49**, analogues **48** and **53** bearing NH_2 and $NHCOCH_3$ groups on the phenoxy ring show decreased hERG affinity and displace only 44% and 20% of the radioligand, respectively. This indicates that the acetamide substituent, whether on one phenyl ring or on both, is detrimental to hERG channel affinity. Likewise, an amino group is not well accommodated when present on one or both phenyl rings.

In general, substituents on the aromatic rings are favorable for hERG channel affinity. In case of dofetilide analogues, lipophilic or electron-withdrawing substituents on the phenoxy ring tend to be more favorable for hERG channel affinity compared to these substituents on both or on one phenyl ring. Reduction in hERG activity was observed with polar and bulky groups such as NH_2, $NHSO_2CH_3$ and $NHCOCH_3$ groups. Interestingly, compounds bearing a $NHSO_2CH_3$ group exhibited much higher affinity than analogues bearing the isosteric substituent $NHCOCH_3$.

Substitution of the central nitrogen atom

Mutagenesis and homology modeling studies on the hERG channel described in the literature have revealed the importance of the basic nitrogen (pK_a) for π-cation interaction with the Tyr 652 residue (Mitcheson *et al.*, 2000; Pearlstein *et al.*, 2003b). A properly located phenyl ring or hydrophobic group at this position in the ligand can also interact with Tyr 652 via π–π or hydrophobic interactions (Pearlstein *et al.*, 2003b; Jamieson *et al.*, 2006). Considering these points, we synthesized and evaluated the binding affinities of aliphatic (**54–60**) and aromatic (**67–69**) N-substituted analogues (Table 2). A nitro substituent on both phenyl rings was used to take into account the high affinity and synthetic accessibility of analogue **35**. The unsubstituted analogue **19** displayed an affinity

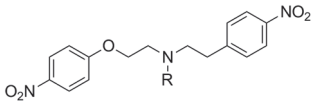

Compd	R	pK_a	K_i [nM] or displacement [%][a]	n
19	H	8.99	48±4.0	3
35	CH_3	9.27	5.7±3.0	3
54	CH_2CH_3	9.61	1.2±0.6	4
55	$COCH_3$	1.80	278±73	3
56	$COCF_3$	-4.95	162±13	3
57	CH_2CN	6.96	100±12	3
58	$CH_2CO_2CH_3$	6.20	30 %	3
59	CH_2CO_2H	10.00	116±110	3
60	CH_2CH_2F	7.63	3.1±1.0	3
67	C_6H_5	3.23	36 %	3
68	4- OCH_3-C_6H_4	3.84	42 %	3
69	4-Cl-C_6H_4	2.65	41 %	3

Table 2. Binding affinities and calculated pK_a of analogues **19**, **35**, **54–60** and **67--69** with different nitrogen substituents in radioligand binding assay of hERG K^+ channel. [a] K_i values ±SEM or displacement [%] at 10 μM (n=3) of specific [^{3}H]astemizole binding to membranes of HEK293 cells stably expressing the hERG K^+ channel.

of 48 nM (calculated pK_a ~8.99). N-Alkylation with CH_3 (**35**) and CH_2CH_3 (**54**) substituents increased the pK_a of the basic nitrogen (**35**, pK_a ~9.27; **54**, pK_a ~9.61) leading to an increased hERG affinity (**35**, K_i=6 nM; **54**, K_i=1.2 nM). Abolishing the basicity of the nitrogen by acylation (**55**, pK_a ~1.80; **56** pK_a =−4.95) resulted in decreased hERG affinity (K_i=278 and 162 nM, respectively). Lowering the pK_a in a less rigorous manner to ~6.96 (**57**, R=CH_2CN) still had an unfavorable, though less significant effect on the binding affinity (K_i=100 nM). Introduction of a CH_2COCH_3 group on the nitrogen (**58**) also caused a decrease in pK_a (~6.20) and this compound showed only 30 % displacement of the radioligand. Ester hydrolysis of **58** led to compound **59**, with a zwitterionic nature and a high calculated pK_a value (~10) for the nitrogen atom. This increase in pK_a was found to cause a twofold decrease in binding affinity (K_i=116 nM) in comparison to compound **19**. Interestingly, the presence of a negatively charged carboxylate group only had a limited effect on the affinity values, which is comparable to the results observed by Zhu *et al.*, 2006. Slight reduction in pK_a (~7.63)

through β-fluorination (**60**) also caused a slight reduction in affinity compared to compound **54** (K_i=3.1 nM). Introduction of a phenyl or a substituted-phenyl (4-OCH_3 or 4-Cl) ring on the nitrogen atom (**67–69**) appeared unfavorable for hERG channel affinity with radioligand displacement of only 36, 42 and 41 %, respectively, at 10 μM concentration.

These results explain the importance of the basic nitrogen atom for hERG channel activity. Analogues with aliphatic or acyl groups on the nitrogen (**19**, **35**, **54–58** and **60**) show increased activity with increasing pK_a. However, the presence of a polar and bulky group near the nitrogen atom decreases hERG affinity, as seen in compound **59**. In the same way, a decrease in pK_a in analogues **67–69** results in the reduction of hERG affinity, even though an aromatic ring is present on the nitrogen, which was hypothesized to form π–π interactions with Tyr 652 rather than π-cation interactions. The difference in activity between secondary and tertiary nitrogen analogues **19** and **35**, **54**, respectively is also noteworthy. Although these compounds have similar pK_a values, they exhibited a ~10- to 40-fold difference in affinity. From these results it appears that control of pK_a by varying the substituents on the nitrogen atom could be a sensible approach to reducing hERG activity, however, other important binding parameters such as lipophilicity and steric aspects must also be considered.

Varying chain length

In order to investigate the significance of the distance between the phenyl ring and the protonated nitrogen we synthesized analogues **77–81** with varying carbon chain lengths (n_1 and n_2). Analogue **35**, with n_1=n_2=2 and a NO_2 group on both phenyl rings, was again used as the reference compound. The results of the radioligand binding assay performed on analogues **77–81** are listed in Table 3. Analogue **77** (n_1=2, n_2=1) showed a 33-fold decrease in affinity (K_i=202 nM) compared with analogue **35**. Increasing the carbon chain length between the phenoxy and nitrogen (n_1=3 and 4) while keeping n_2=1 (**78**

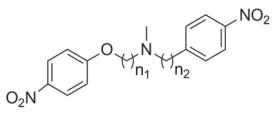

Compd	n_1	n_2	K_i [nM][a]	n
35	2	2	5.7±3.0	3
77	2	1	202±49	3
78	3	1	5.1±1.9	3
79	3	2	1.8±1.0	3
80	4	1	10.0±4.9	3
81	4	2	1.8±1.6	3

Table 3. Binding affinities of analogues **35** and **77–81** with varied carbon chain length in radioligand binding assay of hERG K^+ channel. [a] K_i values ±SEM (n=3) of specific [^{3}H]astemizole binding to membranes of HEK293 cells stably expressing the hERG K^+ channel.

and **80**) resulted in similar affinities (K_i=5.1 and 10.0 nM) in comparison to **35**. Analogue **79** (n_1=3 and n_2=2) showed an increase in binding affinity (K_i=1.8 nM). Fixing the chain length between the nitrogen and phenyl ring to two carbons in **81** (n_1=4, n_2=2) lead to high binding affinity (K_i=1.8 nM) indicating that the molecule is a good inhibitor of the hERG channel binding site.

These results indicate that the distance between the nitrogen and lipophilic groups (e.g., a phenyl ring as in dofetilide) in a ligand has a profound effect on hERG affinity. Fixing one of the carbon chain lengths (n_2 or n_1) in the dofetilide series, while increasing the length on the other side (n_1 or n_2) generally yields an increase in hERG channel affinity, suggesting that there is more available space in the binding pocket. Reducing the total chain length as in analogue **77** substantially decreases hERG channel affinity.

Patch clamp assay

An electrophysiological patch clamp assay (Witchel *et al.*, 2002; Brown, 2004) was used to measure and compare functional hERG current blockade by dofetilide (**1**) and analogue **35**. Experiments were performed on intact HEK293 cells stably expressing hERG channels. Two different protocols were used to assess differences in potency and kinetics of preferential drug binding to the open/inactivated state of hERG channels (Weerapura *et al.*, 2002). Dofetilide (**1**) and analogue **35** were tested at four different concentrations (**1**: 1, 5, 10, 20 nM; **35**: 1, 2.5, 5, 10 nM). Both compounds **1** and **35** blocked the hERG channel current with similar potencies but with different kinetics (Figure 2A and Table 4). The concentration-dependent response of **1** and **35** with the standard short tail protocol (STP) yielded an IC_{50} value of 4.3±0.7 nM for **1** and 3.1±0.6 nM for analogue **35** (Figure 2B), which is comparable to the K_i values found for the binding site (4.1±0.9 nM and 5.7±3.0 nM, respectively) determined in the radioligand binding assay. After drug application, the time required to reach the steady state of inhibition was shorter for analogue **35** (τ=45±12 s) compared to **1** (τ=287±93 s) ($p<0.05$) (Figure 2B inset).

Compd	IC_{50} [nM][a]	K_i [nM][b]	τ[c]
Dofetilide (**1**)	4.3±0.7	4.1±0.9	287±93
35	3.1±0.6	5.7±3.0	45±12

Table 4. Patch clamp IC_{50} values, K_i high-affinity site and τ values for dofetilide (**1**) and **35**. [a] IC_{50} values determined from Figure 2 by using standard short tail hERG protocol. [b] K_i values from Table 1. [c] τ of the rate of the block (s). Time required to reach 2/3 of maximal inhibition of hERG current.

Conclusions

A number of points should be considered to ensure reduced hERG channel affinity when designing long, flexible molecules with a protonated nitrogen in the center of the pharmacophore and aromatic rings on the periphery (Figure 3). Substituents on the aromatic rings should be avoided. If substituents are essential

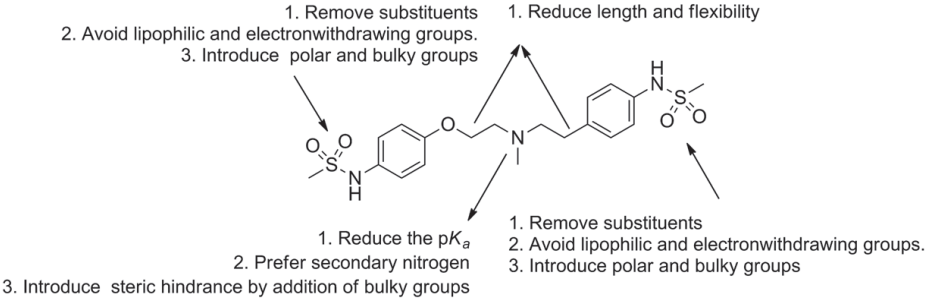

Figure 3. Proposed strategy to reduce the hERG activity of dofetilide (**1**).

for therapeutic targets then lipophilic and electron withdrawing groups should be evaded. Preference should be given to polar and bulky groups such as NH_2 and $NHCOCH_3$ in order to increase the steric hindrance around the aromatic ring(s). Among the polar groups, carbonamides are preferable in comparison to sulphonamides for reducing the hERG channel affinity. In order to reduce the hERG channel affinity of a compound with a protonated nitrogen, a first consideration is to reduce the pK_a by varying the substituents on the protonated nitrogen. One could also aim for a secondary rather than a tertiary nitrogen atom. Steric hindrance near the nitrogen atom by introducing polar and bulky groups such as an acid and/or a phenyl ring may also decrease hERG channel affinity. Preference should be given to a short and strained molecule if possible. A short distance between one of the lipophilic end groups and the central nitrogen atom reduces hERG channel affinity.

Dofetilide analogues described herein provide valuable information about the chemical features that can increase the hERG channel affinity of a molecule. This knowledge may be useful in designing novel therapeutics with low affinity for the hERG channel and consequently reduced cardiotoxicity.

Experimental Section

Chemistry

Material and Methods: All reagents were obtained from commercial sources and all solvents were of analytical grade. ^{1}H and ^{13}C NMR spectra were recorded on a Bruker AC 200 and Bruker AC 400 (^{1}H NMR, 200 MHz and 400 MHz; ^{13}C NMR, 50 MHz and 100 MHz) spectrometer with TMS as an internal standard. Chemical shifts are reported in δ (ppm) and the following abbreviations are used; s=singlet, d=doublet, dd=double doublet, t=triplet, m=multiplet, br=broad and Ar=aromatic. Melting points were measured on a Büchi melting point apparatus and are uncorrected. The value stated for each compound is the initial temperature at which the compound begins to melt. Elemental analyses were performed by Leiden Institute of Chemistry and are within 0.4% of theoretical values unless otherwise stated. Reactions were routinely monitored by TLC using Merck silica gel F254 plates. Microwave reactions were performed on an Emrys Optimizer (Biotage AB). Wattage was automatically adjusted to maintain the desired temperature. The pK_a values were calculated using a structure-based calculation plugin provided by Chemaxon.

For general procedures only a representative compound is fully described. Characterization data for all other final compounds can be found in the Supporting Information. Further experimental details of synthesis and characterization of precursors and intermediates are also given in Supporting Information.

General procedure for the synthesis of compounds 30–45

A 36% formaldehyde solution in H_2O (13.56 mmol, 4.7 equiv) and formic acid (17.89 mmol, 6.2 equiv, 88%) were added to the secondary amine **14–29** (2.89 mmol, 1 equiv) and the resulting mixture was refluxed for 4–5 h. The mixture was cooled and adjusted to pH 14 with aq NaOH (20%). The mixture was extracted with EtOAc (2×) and the combined organic layers were washed with brine, dried (Na_2SO_4), filtered and concentrated. Purification by column chromatography on SiO_2 (EtOAc/petroleum ether (PE), 80:20) followed by hydrochloride salt formation using ethanolic HCl and recrystallization from absolute EtOH and Et_2O mixture afforded the desired product **30–45**.

Methyl-phenyl-(2-phenoxyethyl)amine hydrochloride (30): Prepared from **14**. White crystalline solid (66%): mp: 145 °C; ^{1}H NMR (CD_3OD,

400 MHz): δ=7.30–7.24 (m, 7H, ArH), 7.03–6.98 (m, 3H, ArH), 4.39 (t, 2H, J=4.8 Hz, OCH_2), 3.69 (br s, 2H, CH_2N), 3.49 (br s, 2H, NCH_2), 3.13 (t, 2H, J=4.8 Hz, CH_2Ar), 3.04 ppm (s, 3H, NCH_3); ^{13}C NMR (CD_3OD, 100 MHz): δ=159.0, 137.4, 130.7, 130.0, 129.8, 128.3, 122.9, 115.7, 63.1, 58.8, 56.2, 41.8, 31.2 ppm; Anal. calcd for $C_{17}H_{22}ClNO$: C 69.98, H 7.55, N 4.80, found: C 70.01, H 7.09, N 4.87.

General procedure for the synthesis of compounds 46–48

A solution of nitro compound **35**, **40** or **45** (3.33 mmol, 1 equiv, as free base) and AcOH (1 mL) in H_2O (1 mL) and THF (10 mL) was refluxed for 15 min and then treated with Fe (17.91 mmol, 5.4 equiv). The reaction mixture was subsequently refluxed for 5–6 h until no starting material was visible by TLC. The reaction mixture was allowed to cool at RT and concentrated. The residue was washed with EtOAc (3×20 mL) and filtered. The filtrate was washed with a saturated aq $NaHCO_3$, H_2O and brine, dried (Na_2SO_4), filtered and concentrated. Purification by column chromatography on SiO_2 (CH_3OH/CH_2Cl_2, 1:9) afforded the amino product as a viscous oil. These compounds were used without further purification in the synthesis of subsequent compounds. However, they were converted to their hydrochloride salt using ethanolic HCl and further recrystallized from absolute EtOH and Et_2O before being evaluated biologically.

Methyl-[2-(4-aminophenoxy)ethyl]-[2-(4-aminophenyl)ethyl]-amine tris hydrochloride (46): Prepared from **35** using AcOH (2 mL), H_2O (2 mL), THF (10 mL) and Fe (35.81 mmol, 10.8 equiv). Brown hygroscopic solid (57%): mp: 121 °C; ^1H NMR (CD_3OD, 200 MHz): δ=7.54 (d, 2H, J=8.0 Hz, ArH), 7.40 (d, 4H, J=8.7 Hz, ArH), 7.20 (d, 2H, J=8.7 Hz, ArH), 4.47 (t, 2H, J=5.1 Hz, OCH_2), 3.81–3.51 (m, 4H, CH_2NCH_2), 3.30–3.18 (m, 2H, CH_2Ar), 3.07 ppm (s, 3H, NCH_3); ^{13}C NMR (CD_3OD, 50 MHz): δ=159.1, 138.6, 131.6, 130.7, 125.3, 124.4, 117.0, 63.5, 58.2, 55.8, 41.2, 30.4 ppm; Anal. calcd for $C_{17}H_{26}C_{l3}N_3O$•$1.5H_2O$: C 48.41, H 6.93, N 9.96, found: C 48.53, H 7.12, N 9.88.

General procedure for the synthesis of compounds 49–53

MsCl or AcCl (2.22 mmol, 1 equiv) was added dropwise to an ice-cold solution of amine **46–48** (2.22 mmol, 1 equiv, as free base) and Et_3N (3.33 mmol, 1.5 equiv) in CH_2Cl_2 (10 mL). The reaction mixture was stirred at RT overnight, filtered and concentrated. Purification by column chromatography on SiO_2

(CH_3OH/CH_2Cl_2, 5:95 or 10:90) afforded the pure product. Compounds **50–53** were obtained as viscous oils so they were converted to their hydrochloride salt using ethanolic HCl followed by recrystallization from absolute EtOH and Et_2O, whereas compound **49** was solid so it was used as such for biological evaluation.

N-[4-(2-{[2-(4-Acetylaminophenyl)ethyl]-methyl-amino}-ethoxy) phenyl]-acetamide (49): Prepared from **46** using Et_3N (6.67 mmol, 3 equiv) and AcCl (4.44 mmol, 2 equiv). Creamy white solid (60 %): mp: 166 °C; ^{1}H NMR (CD_3OD, 200 MHz): δ=7.46–7.40 (m, 4 H, ArH), 7.15 (d, 2 H, J=8.8 Hz, ArH), 6.87 (d, 2 H, J=9.5 Hz, ArH), 4.07 (t, 2 H, J=5.1 Hz, OCH_2), 2.86 (t, 2 H, J=5.1 Hz, CH_2N), 2.81–2.66 (br s, 4 H, NCH_2, CH_2Ar), 2.40 (s, 3 H, NCH_3), 2.09 (s, 3 H, $NHCOCH_3$), 2.08 ppm (s, 3 H, $NHCOCH_3$); ^{13}C NMR (CD_3OD, 50 MHz): δ=171.2, 171.1, 156.6, 137.6, 136.9, 132.8, 129.7, 122.7, 121.1, 115.1, 66.8, 60.5, 56.6, 42.6, 33.2, 23.4, 23.2 ppm; Anal. calcd for $C_{21}H_{27}N_3O_3$: C 68.27, H 7.37, N 11.37, found: C 67.80, H 7.72, N 11.30.

Ethyl-[2-(4-nitrophenoxy)ethyl]-[2-(4-nitrophenyl)ethyl]-amine hydrochloride (54): A solution of **19** (1.1 mmol, 1 equiv) in DMF (3 mL) was treated with K_2CO_3 (3.27 mmol, 3 equiv) and ethyl bromide (1.31 mmol, 1.2 equiv), and the reaction mixture was stirred at RT overnight. After addition of H_2O and EtOAc, the aqueous phase was washed with EtOAc (2×). The combined organic layers were successively washed with H_2O and brine, dried ($MgSO_4$), filtered and concentrated. The crude oil was purified by silica gel chromatography (EtOAc/PE, 7:3). The HCl salt was then prepared by treatment with ethanolic HCl and concentration in vacuo. Recrystallization from absolute EtOH and Et_2O gave the HCl salt of **54** as creamy white crystalline solid (61 %): mp: 146 °C; ^{1}H NMR (CD_3OD, 400 MHz): δ=8.29–8.23 (m, 4 H, ArH), 7.63 (d, 2 H, J=8.8 Hz, ArH), 7.23 (d, 2 H, J=9.2 Hz, ArH), 4.59 (t, 2 H, J=4.8 Hz, OCH_2), 3.86–3.83 (m, 2 H, CH_2N), 3.63–3.59 (m, 2 H, NCH_2), 3.55–3.50 (m, 2 H, CH_2Ar), 3.35–3.31 (m, 2 H, NCH_2CH_3), 1.48 ppm (t, 3 H, J=7.2 Hz, NCH_2CH_3); ^{13}C NMR (CD_3OD, 100 MHz): δ=164.6, 149.3, 146.0, 144.3, 131.9, 127.6, 125.6, 116.8, 64.9, 55.4, 53.4, 51.1, 31.4, 9.90 ppm; Anal. calcd for $C_{18}H_{22}ClN_3O_5$: C 54.62, H 5.60, N 10.62; found: C 53.84, H 5.84, N 10.46.

N-[2-(4-Nitrophenoxy)ethyl]-N-[2-(4-nitrophenyl)ethyl]-acetamide (55): A solution of **19** (1.1 mmol, 1 equiv) in CH_2Cl_2 (5 mL) was treated with Et_3N (1.63 mmol, 1.5 equiv) and AcCl (1.31 mmol, 1.2 equiv) at 0 °C, and the reaction mixture was stirred at RT overnight. The solvent was evaporated and the crude product preabsorbed on silica. Purification by column chromatography

(EtOAc/PE, 6:4) afforded **55** as a white crystalline solid (79%): mp: 103 °C; ^{1}H NMR (CDCl3, 400 MHz): δ=8.18–8.11 (m, 2H, ArH), 7.41–7.39 (m, 2H, ArH), 6.97–6.91 (m, 2H, ArH), 4.27–4.14 (m, 2H, OCH_2), 3.76–3.69 (m, 4H, CH_2NCH_2), 3.08–3.07 (m, 2H, CH_2Ar), 2.24–2.00 ppm (m, 3H, $NCOCH_3$); ^{13}C NMR ($CDCl_3$, 100 MHz): δ=171, 163.7, 163.2, 147, 146, 142.1, 141.8, 129.9, 126.1, 124.2, 123.9, 114.6, 114.5, 67.2, 66.8, 51.8, 48.6, 48.2, 46.2, 35.5, 34.0, 22.1, 21.5 ppm; Anal. calcd for $C_{18}H_{19}N_3O_6$: C 57.91, H 5.13, N 11.25, found: C 58.29, H 5.33, N 11.33.

Trifluoro-N-[2-(4-nitrophenoxy)ethyl]-N-[2-(4-nitrophenyl)ethyl]-acetamide (56): A solution of **19** (1.1 mmol, 1 equiv) in CH_2Cl_2 (5 mL) was treated with Et_3N (1.63 mmol, 1.5 equiv) and trifluoroacetic anhydride (1.31 mmol, 1.2 equiv) at 0 °C, and the reaction mixture was stirred at RT overnight. The solvent was evaporated and the crude product preabsorbed on silica. Purification by column chromatography (EtOAc/PE, 4:6) afforded **56** as white crystalline solid (75%): mp: 95 °C; ^{1}H NMR ($CDCl_3$, 400 MHz): δ=8.24–8.18 (m, 4H, ArH), 7.41–7.39 (m, 2H, ArH), 6.92–6.96 (m, 2H, ArH), 4.34–4.18 (m, 2H, OCH_2), 3.90–3.77 (m, 4H, CH_2NCH_2), 3.14–3.07 ppm (m, 2H, CH_2Ar); ^{13}C NMR ($CDCl_3$, 100 MHz): δ=169.1, 163.2, 162.9, 147.3, 147.1, 146.0, 144.8, 142.3, 142.1, 129.9, 126.2, 124.3, 124.1, 114.6, 67.4, 65.9, 50.6, 50.2, 47.5, 35.6, 33.0 ppm; Anal. calcd for $C_{18}H_{16}F_3N_3O_6$: C 50.59, H 3.77, N 9.83, found: C 50.60, H 4.06, N 9.89.

2,2,2-{[2-(4-Nitrophenoxy)ethyl]-[2-(4-nitrophenyl)ethyl]-amino}-acetonitrile (57): A solution of **19** (1.1 mmol, 1 equiv) in CH_3CN (3 mL) was treated with N,N-diisopropylethyl amine (3.26 mmol, 3 equiv) and bromoacetonitrile (1.31 mmol, 1.2 equiv) at 0 °C, and the reaction mixture was stirred at RT overnight. The solvent was evaporated and the crude product preabsorbed on silica. Purification by column chromatography (EtOAc/PE, 4:6) afforded **57** as creamy white crystalline solid (77%): mp: 84 °C; ^{1}H NMR ($CDCl_3$, 400 MHz): δ=8.20 (d, 2H, , J=9.2 Hz, ArH), 8.13 (d, 2H, J=8.4 Hz, ArH), 7.37 (d, 2H, J=8.8 Hz, ArH), 6.92 (d, 2H, J=9.2 Hz, ArH), 4.12 (t, 2H, J=4.8 Hz, OCH_2), 3.77 (s, 2H, CH_2CN), 3.08 (t, 2H, J=4.8 Hz, CH_2N) 2.98 (t, 2H, J=6.4 Hz, NCH_2), 2.92 ppm (t, 2H, J=6.4 Hz, CH_2Ar); ^{13}C NMR ($CDCl_3$, 100 MHz): δ=163.2, 146.9, 146.7, 141.8, 129.5, 125.9, 123.7, 115.0, 114.4, 67.1, 55.5, 52.8, 42.9, 33.8 ppm; Anal. calcd for $C_{18}H_{18}N_4O_5$: C 58.37, H 4.90, N 15.13, found: C 59.59, H 5.26, N 15.20.

{[2-(4-Nitrophenoxy)ethyl]-[2-(4-nitrophenyl)ethyl]-amino}-acetic acid methyl ester (58): A solution of **19** (2.18 mmol, 1 equiv) in DMF (5 mL) was treated with K_2CO_3 (6.53 mmol, 3 equiv) and methylbromoacetate (2.61 mmol, 1.2 equiv) at 0 °C, and the reaction mixture was stirred at RT for 2 h. Upon completion, H_2O and EtOAc were added and the aqueous phase was washed with EtOAc (2×). The combined organic layers were successively washed with H_2O and brine, dried ($MgSO_4$), filtered and concentrated. Purification by column chromatography (EtOAc/PE, 4:6) afforded **58** as a yellow crystalline solid (66 %): mp: 74 °C; ^{1}H NMR ($CDCl_3$, 400 MHz): δ=8.20–8.10 (m, 4 H, ArH), 7.36 (d, 2 H, J=8.4 Hz, ArH), 6.90 (d, 2 H, J=8.8 Hz, ArH), 4.09–4.07 (m, 2 H, OCH_2), 3.69 (s, 3 H, CO_2CH_3), 3.54 (s, 2 H, $NCH_2CO_2CH_3$), 3.18–3.16 (m, 2 H, CH_2N) 3.06 (t, 2 H, J=7.2 Hz, NCH_2), 2.91–2.87 ppm (m, 2 H, CH_2Ar); ^{13}C NMR ($CDCl_3$, 100 MHz): δ=171.0, 163.5, 163.2, 147.8, 146.5, 141.6, 129.6, 125.9, 123.5, 114.3, 67.8, 56.1, 55.3, 53.0, 51.6, 34.6 ppm; Anal. calcd for $C_{19}H_{21}N_3O_7$: C 56.57, H 5.25, N 10.42, found: C 56.91, H 5.50, N 10.47.

{[2-(4-Nitrophenoxy)ethyl]-[2-(4-nitrophenyl)ethyl]-amino}-acetic acid hydrochloride (59): A solution of **58** (0.25 mmol) in dioxane (2 mL) was treated with aq NaOH (0.5 mL, 1 m). The reaction mixture was heated to 60 °C for 1 h. Upon completion, the reaction mixture was acidified with aq HCl (0.2 m). The aqueous phase was extracted with EtOAc (2×) and the combined organic layers were successively washed with H_2O and brine, dried ($MgSO_4$), filtered and concentrated to give the HCl salt of **59** as brown solid (66 %): mp: 87 °C; ^{1}H NMR (CD_3OD, 400 MHz): δ=8.13–8.07 (m, 4 H, ArH), 7.49 (d, 2 H, J=8.4 Hz, ArH), 7.08–7.02 (m, 2 H, ArH), 4.47 (t, 2 H, J=4.4 Hz, OCH_2), 4.23 (s, 2 H, NCH_2CO_2H), 3.81 (t, 2 H, J=4.4 Hz, CH_2N) 3.61–3.56 (m, 2 H, NCH_2), 3.20–3.18 ppm (m, 2 H, CH_2Ar); ^{13}C NMR ($CDCl_3$, 100 MHz): δ=169.0, 163.9, 148.7, 145.4, 143.7, 131.3, 126.9, 125.0, 116.1, 64.9, 57.4, 55.8, 55.3, 31.2 ppm; Anal. calcd for $C_{18}H_{20}ClN_3O_7$: C 50.77, H 4.73, N 9.86, found: C 49.91, H 5.39, N 9.67.

(2-Fluoroethyl)-[2-(4-nitrophenoxy)ethyl]-[2-(4-nitrophenyl)ethyl]-amino hydrochloride (60): A solution of **19** (1.36 mmol, 1 equiv) in EtOH (5 mL) was treated with K_2CO_3 (4.08 mmol, 3 equiv) and 2-bromoethanol (2.72 mmol, 2 equiv) and the reaction mixture was refluxed for 48 h. Upon completion, K_2CO_3 was filtered off and the reaction mixture was concentrated and purified by silica gel chromatography (CH_3OH/EtOAc, 5:95) to give 2-{[2-(4-nitrophenoxy) ethyl]-[2-(4-nitrophenyl)ethyl]-amino}-ethanol as a colorless viscous oil. A solution of this intermediate (1.07 mmol, 1 equiv) in CH_2Cl_2 (5 mL) at −65 °C was treated dropwise with a solution of DAST (1.6 mmol, 1.5 equiv) in CH_2Cl_2

(2 mL) with vigorous stirring under an argon atmosphere. The reaction mixture was gradually allowed to warm to 15 °C overnight. It was then cooled to −40 °C and poured in portions into ice-cold saturated aq $NaHCO_3$ and the product was extracted with CH_2Cl_2. The combined organic extracts were washed with H_2O, dried (Na_2SO_4), filtered and concentrated. The crude oil was purified by silica gel chromatography (EtOAc/PE, 4:6). The HCl salt was prepared by treatment with ethanolic HCl and concentration in vacuo. Recrystallization from absolute EtOH and Et_2O gave the HCl salt of **60** as white crystalline solid (57 %): mp: 113 °C; ^{1}H NMR ($CDCl_3$/CD_3OD, 400 MHz): δ=8.27–8.18 (m, 4 H, ArH), 7.49 (d, 2 H, J=8 Hz, ArH), 7.06 (d, 2 H, J=8.4 Hz, ArH), 5.13–5.01 (m, 2 H, NCH_2CH_2F), 4.66 (br s, 2 H, OCH_2), 3.87–3.78 (m, 2 H, CH_2N), 3.61–3.54 (m, 4 H, NCH_2, CH_2Ar), 3.41–3.37 ppm (m, 2 H, NCH_2CH_2F); ^{13}C NMR ($CDCl_3$+CD_3OD, 100 MHz): δ=162.2, 147.4, 143.5, 142.5, 130.0, 126.2, 124.3, 114.9, 79.5, 63.5, 55.2, 53.6, 53.4, 52.8, 29.8 ppm; Anal. calcd for $C_{18}H_{21}ClFN_3O_5$: C 52.24, H 5.12, N 10.15, found: C 51.12, H 5.62, N 10.21.

General procedure for the synthesis of compounds 67–69

A solution of secondary amine **64–66** (1 mmol, 1 equiv) in CH_3CN (3 mL) in a microwave vial was treated with **13** (1 mmol, 1 equiv) and KI (0.1 mmol, 0.1 equiv). The vial was sealed and heated in a microwave at 170 °C for 1 h. The cooled reaction mixture was diluted with CH_2Cl_2 and washed with saturated aq $NaHCO_3$, H_2O, brine, dried (Na_2SO_4), filtered and concentrated. Purification by column chromatography on SiO_2 (EtOAc/PE, 2:8) afforded the secondary amines **67–69**.

[2-(4-Nitrophenoxy)ethyl]-[2-(4-nitrophenyl)ethyl]-phenyl-amine (67): Prepared from **64**. Yellow solid (66 %): mp: 95 °C; ^{1}H NMR ($CDCl_3$, 400 MHz): δ=8.16–8.13 (m, 4 H, ArH), 7.37–7.25 (m, 4 H, ArH), 6.88–6.76 (m, 5 H, ArH), 4.10 (t, 2 H, J=5.6 Hz, OCH_2), 3.73–3.66 (m, 4 H, CH_2NCH_2), 3.04 ppm (t, 2 H, J=7.2 Hz, CH_2Ar); ^{13}C NMR ($CDCl_3$, 100 MHz): δ=163.5, 147.4, 146.6, 141.7, 129.7, 125.9, 123.8, 117.3, 114.3, 112.4, 66.2, 53.1, 50.8, 33.5 ppm; Anal. calcd for $C_{22}H_{21}N_3O_5$: C 64.86, H 5.20, N 10.31, found: C 65.14, H 5.40, 10.42.

General procedure for the synthesis of compounds 77–81

Final compounds **77–81** were prepared in the same manner as compound **35**.

Methyl-(4-nitrobenzyl)-[2-(4-nitrophenoxy)ethyl]-amine hydrochloride (77): Prepared from **13** and **75**. Light yellow crystalline solid (67 %): mp: 163 °C; ^{1}H NMR ($(CD_3)_2CO$, 400 MHz, free base): δ=8.22–8.17 (m, 4 H, ArH), 7.66 (d, 2 H, J=8.8 Hz, ArH), 7.17–7.13 (m, 2 H, ArH), 4.34 (t, 2 H, J=6 Hz, OCH_2), 3.80 (s, 2 H, CH_2Ar), 2.93 (t, 2 H, J=5.6 Hz, CH_2N), 2.38 ppm (s, 3 H, NCH_3); ^{13}C NMR ($(CD_3)_2CO$, 100 MHz, free base): δ=164.8, 148.5, 147.8, 142.1, 130.1, 126.4, 123.9, 115.5, 67.9, 62.0, 56.3, 43.0 ppm; Anal. calcd for $C_{16}H_{18}ClN_3O_5$: C 52.25, H 4.93, N 11.43, found: C 52.31, H 4.91, N 1.63.

Biological assays

Radioligand binding assay

The [^{3}H]astemizole radioligand binding assay for the hERG K^+ channel was performed as described by Chiu *et al.*, 2004 with minor modifications. In short, membrane aliquots containing 10 μg (hERG/HEK293) protein were incubated in a total volume of 100 μL of 10 mm HEPES, 130 mm NaCl, 60 mm KCl, 0.8 mm $MgCl_2$, 1 mm Na EGTA, 10 mm Glucose, 0.1 % BSA, pH 7.4 at 25 °C for 1 h. Displacement experiments were routinely performed using 12 concentrations of cold ligand in the presence of 1.5–2.0 nM [^{3}H]astemizole. Nonspecific binding was determined in the presence of 10 μM astemizole. Incubations were terminated by dilution with ice-cold wash-buffer, containing 25 mm TrisHCl, 130 mm NaCl, 60 mm KCl, 0.8 mm $MgCl_2$, 0.05 mm $CaCl_2$ and 0.05 % BSA (pH 7.4). Separation of bound from free radioligand was performed by rapid filtration through Whatman GF/B filters using a Brandel harvester. Filters were subsequently washed with ice-cold wash-buffer (6×2 mL). Filter-bound radioactivity was measured by scintillation spectrometry (LKB Wallac, 1219 Rackbeta) after addition of Packard Emulsifier Safe (3.5 mL). The results were analyzed using GraphPad Prism (version 5).

Patch clamp assay

HEK293 cells stably expressing hERG were cultured on 11 mm glass coverslips and placed in a temperature controlled perfusion chamber (Cell Microcontrols, Norfolk, USA) at 37 °C. Voltage clamp measurements of hERG-

mediated ion currents were performed in the whole cell patch clamp mode using a HEKA EPC-10 Double Plus amplifier controlled by PatchMaster 2.20 software (HEKA Elektronik, Lambrecht/Pfalz, Germany). All patch clamp experiments were corrected for 14.2 mV liquid junction potential and patch pipette series resistance was compensated for>70 %. Data were analyzed using FitMaster (HEKA, Germany) and Kaleidagraph (Synergy Software, Reading, USA) software.

Bath perfusion and patch pipette filling solutions had the following composition (values given in mmol L^{-1}): Tyrode bath solution: NaCl, 130; KCl, 5.4; $CaCl_2$, 1; $MgCl_2$, 1; glucose, 6; $NaHCO_3$, 17.5; HEPES, 10 (pH 7.2, NaOH). Patch pipette solution: potassium gluconate, 125; KCl, 10; HEPES, 5; EGTA, 5; $MgCl_2$, 2; $CaCl_2$, 0.6; Na_2ATP, 4 (pH 7.20, KOH).

Patch pipettes were made using a Sutter P-2000 micropipette puller (Sutter Instrument Company, Novato, USA) and had resistances of ~2.5 MΩ when fire polished and filled with pipette solution.

At baseline, a "long" tail current protocol (LTP) was run first, followed by a "short" tail current protocol (STP), both under control conditions. Perfusion of Tyrode solution containing various concentrations of dofetilide (**1**) or **35** was started 45 s after the beginning of the STP. After a steady-state level of hERG current inhibition was reached, running the LTP again finished the experiment. Four dofetilide (**1**) concentrations (1, 5, 10 and 20 nM) and four concentrations of **35** (1, 2.5, 5 and 10 nM) were tested.

Short tail current protocol (STP): Cells were depolarized to 0 mV from a holding potential −80 mV for 1500 ms, allowing activation and inactivation of hERG current. Cells were then repolarized to a test potential of −50 mV for 1500 ms allowing the ensuing hERG tail current to deactivate. This voltage clamp protocol was repeated every 15 s. The peak amplitude of hERG tail current was measured during the repolarizing pulse at −50 mV before and during exposure of dofetilide (**1**) or **35** (Figure 2A).

Further experimental details of long tail current protocol, results and figures of long and short tail current protocols are given in Supporting Information.

Acknowledgements

This study was financially supported by the Dutch Top Institute Pharma, project number D2–201.

Chapter 3

The anti-protozoal drug pentamidine blocks $K_{IR}2.x$-mediated inward rectifier current by entering the cytoplasmic pore region of the channel.

de Boer TP, Nalos L, Stary A, Kok B, Houtman MJC, Antoons G, van Veen TAB, Beekman JDM, de Groot BL, Opthof T, Rook MB, Vos MA, van der Heyden MAG.

Br J Pharmacol. 2010 Apr;159(7):1532-41.

Background and purpose: Pentamidine is a drug used in treatment of protozoal infections. Pentamidine treatment may cause sudden cardiac death by provoking cardiac arrhythmias associated with QTc prolongation and U-wave alterations. This proarrhythmic effect was linked to hERG trafficking inhibition but not to acute block of ion channels contributing to the action potential. Because the U-wave has been linked to the cardiac inward rectifier current (I_{K1}) we examined the action and mechanism of pentamidine-mediated I_{K1} block.
Experimental approach: Patch clamp measurements of I_{K1} were performed on cultured adult canine ventricular cardiomyocytes, $K_{IR}2.1$-HEK293 cells and $K_{IR}2.x$ inside-out patches. Pentamidine binding to cytoplasmic amino acid residues of $K_{IR}2.1$ channels was performed by molecular modelling.
Key results: Pentamidine application (24 h) decreased I_{K1} in cultured canine cardiomyocytes and $K_{IR}2.1$-HEK293 cells under whole cell clamp conditions. Pentamidine inhibited I_{K1} in $K_{IR}2.1$-HEK293 cells 10 minutes after application. When applied to the cytoplasmic side under inside-out patch clamp conditions, pentamidine block of I_{K1} was acute (IC_{50}=0.17 μM). Molecular computer modeling predicted pentamidine-channel interactions in the cytoplasmic pore region of $K_{IR}2.1$ at amino acids E224, D259 and E299. Mutation of these conserved residues to alanine reduced pentamidine block of I_{K1}. Block was independent of the presence of spermine. $K_{IR}2.2$ and $K_{IR}2.3$ based I_{K1} was also sensitive to pentamidine blockade.
Conclusions and Implications: Pentamidine inhibits cardiac I_{K1} by interacting with three negatively charged amino acids in the cytoplasmic pore region. Our findings may provide new insights for development of specific I_{K1} blocking compounds.

Introduction

The ventricular cardiac action potential (AP) has a long plateau and repolarization phase, essential for contractility and recovery of excitability. Between subsequent APs, there is a constant resting membrane potential based on potent inward rectifier current (I_{K1}). In mammals, the KCNJ2 and KCNJ12 gene products $K_{IR}2.1$ and $K_{IR}2.2$ constitute the main determinants of I_{K1} in the ventricle (Dhamoon and Jalife, 2005). In addition, $K_{IR}2.3$ encoded by the KCNJ4 gene contributes to cardiac I_{K1}. Inhibition of endogenous I_{K1} by dominant negative $K_{IR}2.1$ expression in the working ventricular myocardium of guinea pigs induces ectopic pacemaker activity (Miake *et al.*, 2002). In

humans, loss-of-function mutations in $K_{IR}2.1$ correlates with Andersen-Tawil syndrome (ATS1) characterized by ventricular arrhythmias, periodic paralysis and dysmorphic features (Plaster *et al.*, 2001; Tristani-Firouzi *et al.*, 2002). ATS1 is associated with the appearance of more prominent U waves (Zhang *et al.*, 2005b; Nagase *et al.*, 2007).

Acquired ion channel dysfunction, either by loss or gain of function, may result in a wide variety of cardiac arrhythmias (Murphy and Dargie 2007; Kannankeril and Roden, 2007). The culprit ion current involved is often the $K_v11.1$ (hERG) based rapid component of the delayed rectifier current (I_{Kr}). Unfortunately, non-cardiac drugs may affect this current but many other currents as well. Recently, the widely used antimalarial drug chloroquine and the estrogen receptor antagonist tamoxifen were demonstrated to inhibit $K_{IR}2.1$ based I_{K1} by blocking the ion channel pore from the cytoplasmic side or by interfering in the $K_{IR}2.1$-PIP2 interaction, respectively (Rodríguez-Menchaca *et al.*, 2008; Ponce-Balbuena *et al.*, 2009).

Pentamidine belongs to the diamine family used for treatment of pathogenic protozoic infections causing human African trypanosomis (sleeping sickness), visceral Leishmaniasis (Bray *et al.*, 2003) and opportunistic pathogenic infections causing candidiasis and pneumonia in immunocompromised individuals, like HIV-positive patients (Sands *et al.*, 1985; Goa and Campoli-Richards, 1987). Clinically, pentamidine has been associated with QTc prolongation, U-wave amplitude increase, U-wave alternans and Torsade de Pointes arrhythmias with and without electrolyte abnormalities (Bibler *et al.*, 1988; Mitchell *et al.*, 1989; Gonzalez *et al.*, 1991; Quadrel *et al.*, 1992; Eisenhauer *et al.*, 1994; Girgis *et al.*, 1997). Recently, pentamidine has been shown to reduce I_{Kr} and to prolong the AP, because it hampers transport of the $K_v11.1$ ion channel protein towards the sarcolemma (Cordes *et al.*, 2005; Kuryshev *et al.*, 2005). Although this might explain QTc prolongation, U-wave alterations remain unexplained. Given the similarity between alterations in U-wave morphology under conditions of KCNJ2 mutations and pentamidine administration, we have assessed whether pentamidine affects the inward rectifier current and its mode of action at the molecular level.

We demonstrate that i) pentamidine inhibits I_{K1} in isolated adult ventricular cardiac myocytes at clinical concentrations; that ii) it produces acute block of $K_{IR}2.x$ based I_{K1} by plugging the pore region from the cytoplasmic side; that iii) acidic amino acids E224, D259 and E299 of $K_{IR}2.1$ are directly involved in pentamidine mediated outward I_{K1} block.

Methods

Cell culture

The investigation conformed to the Guide for the Care and Use of Laboratory Animals published by the US National Institutes of Health (NIH Publication No. 85-23, revised 1996) and was approved by the institutional committee for animal experiments. Left ventricular myocytes from adult dogs were isolated and GFP-tagged $K_{IR}2.1$ (nomenclature according to Alexander *et al.*, 2008) HEK293 (HEK-KWGF) cells were generated and cultured as described previously (De Boer *et al.*, 2006a,b). In inside-out experiments, HEK293T cells were transfected with 20 ng KCNJx cDNA and 6 ng EGFP per cm2 and used within 48 hours. Mouse KCNJ2, KCNJ12 and KCNJ4 pCXN2 expression constructs and human wildtype, E224A, F254A, D259A and E299A mutant KCNJ2 constructs have been described previously (Rodríguez-Menchaca *et al.*, 2008; Ishihara and Ehara, 2004).

Pentamidine

Pentamidine-isethionate (Pentacarinat® 300, Sanofi Aventis) was dissolved in water at a pentamidine concentration of 0.1 M, sterilized by filtration (0.22 μm), aliquoted and stored at -20°C until use.

Western blotting

Cells were lysed in RIPA buffer (20 mM Tris-HCl, pH 7.4, 150 mM NaCl, 10 mM Na_2HPO_4, 1% (v/v) Triton X-100, 1% (w/v) Na-deoxycholate, 0.1% (w/v) SDS, 1 mM EDTA, 50 mM NaF, 2 mM PMSF and 14 μg/ml aprotinin). Lysates were clarified by centrifugation at 14000xg for 10' at 4ºC and mixed with loading buffer. Twenty-five micrograms of proteins were separated by 10% SDS-PAGE and blotted onto nitrocellulose membrane (Bio-Rad, Veenendaal, Netherlands). Protein transfer was assessed by Ponceau S staining (Sigma, St Louis, USA). After blocking with 5% non-fat milk, blots were incubated with $K_{IR}2.1$ (Cat. no. sc-28633; Santa Cruz Biotechnology, Santa Cruz, CA, USA) and Cadherin (Cat. no. C1821; Sigma) antibodies for adult cardiomyocytes, or GFP antibody (Cat. no. sc-9996; Santa Cruz Biotechnology) for HEK-KWGF cells. Finally, peroxidase-conjugated secondary antibody (Jackson ImmunoResearch, West Grove, PA, USA) was applied. Standard ECL procedure was used as final detection (Amersham Bioscience, Buckinghamshire, UK). ImageQuant TL software (Amersham) was used for signal quantification.

Electrophysiology

Patch clamp measurements were done using a HEKA EPC-10 Double Plus amplifier controlled by PatchMaster 2.10 software (HEKA, Lambrecht/Pfalz, Germany). Voltage clamp measurements of whole cell I_{K1} were performed by applying 1 second test pulses ranging between -120 and +40 mV, with 10 mV increments, from a holding potential of -40 mV and with minimal series resistance compensation of 70%. Steady state current at the end of the pulse was normalized to cell capacitance and plotted versus test potential. Inside-out patch-clamp measurement of I_{K1} were done in absence of Mg^{2+} as described previously (Ishihara and Ehara, 2004). Excised membrane patches were placed close to the inflow region of the recording chamber, and experiments were started after inward rectification due to endogenous polyamines had disappeared as completely as possible. Currents were elicited using a ramp protocol, from -100 to 100 mV in 5 seconds, starting at a holding potential of -40 mV. Recorded current traces were normalized to the holding current at -40 mV obtained from the control traces. After recording control traces, excised membrane patches were exposed to bath solution containing spermine and/or pentamidine. For determination of IC_{50}, each excised membrane patch was exposed to a series of pentamidine concentrations. Fractional block of outward I_{K1} was calculated using current level at +50 mV, and values obtained with experimental solutions were divided by corresponding values from the previously recorded control trace. Patch pipettes were made with a Sutter P-2000 puller (Sutter Instrument, Novato, CA, USA) and had resistances of 2-3 MΩ. Extracellular solution for whole cell I_{K1} measurements contained (in mmol/L-1): NaCl 140, KCl 5.4, $CaCl_2$ 1, $MgCl_2$ 1, glucose 6, $NaHCO_3$ 17.5, HEPES 15, pH 7.4/NaOH. Pipette solution contained potassium gluconate 125, KCl 10, HEPES 5, EGTA 5, $MgCl_2$ 2, $CaCl_2$ 0.6, Na_2ATP 4, pH 7.20/KOH. Inside-out experiments were done with a bath solution containing: KCl 125, EDTA (2K) 4, K_2HPO_4 7.2, KH_2PO_4 2.8, pH 7.20/KOH. Pipette solution contained KCl 145, $CaCl_2$ 1, HEPES 5, pH 7.40/KOH.

Molecular modeling and ligand docking

Pentamidine was docked into the crystal structure of the cytoplasmic $K_{IR}2.1$ domain (pdb identifier: 1U4F) (Pegan *et al.*, 2005). Drug coordinates were obtained from the ZINC database (Irwin and Shoichet, 2005). FlexX (version 1.20.1) in Sybyl8.0 (Tripos International, St. Louis, MI, USA) was used to randomly dock pentamidine (n=100) into the cytoplasmic cavity of $K_{IR}2.1$ using default parameters. Ligand partial charges were calculated with

the Gasteiger–Hückel method. Modeling was visualized with Pymol software (Delano Scientific). Modelling, docking and visualization were performed on a Linux 4 Intel Core2 Quad workstation, SUSE Linux 10.2 operating system.

Statistics

Group averages are presented as mean ± standard error of mean and were tested for significance using Student's t-test (two groups) or an ANOVA test with a Holm's post-hoc test when more than two groups were involved. Analysis was done using Kaleidagraph 4.0 (Synergy Software, Reading, PA, USA) with the significance level at $p < 0.05$.

Results

Pentamidine inhibits cardiac I_{K1}.

Based on the findings of pentamidine-associated U-wave alterations in patients and a correlation between the U-wave and I_{K1}, we hypothesized that pentamidine might inhibit I_{K1} in cardiac myocytes. Fig. 1 and Table 1 show that pentamidine treatment at 10 μM for a period of 24 h inhibited the inward and outward components of I_{K1} by 62% and 73% respectively in adult canine ventricular myocytes (Fig. 1A and 1B, Table 1). 1 μM pentamidine appeared to yield mild inhibition, but this inhibitory effect did not reach significance, even when the period of application was prolonged from 24 to 48 h. Furthermore, pentamidine substantially changed the kinetics of the inward component; the time to 90% of maximal activity increased almost 30-fold (Table 1). $K_{IR}2.1$

	Adult Dog Cardiomyocytes		HEK-KWGF		
	control	10 μM	control	1 μM	10 μM
Max. outward current (pA/pF)	0.30±0.04 (6)	0.08±0.02 (6)	29.0±8.0 (6)	1.6±1.1 (9)	-9.4±7.2 (6)
Max. inward current (pA/pF)	-13.3±1.2 (6)	-5.1±0.1 (6)	-482±128 (6)	-162.9±59.0 (6)	42.0±19.0 (6)
90% max. current rise time (ms)	22.0±0.4 (6)	541±85 (6)	2.6±0.2 (6)	ND	727±36 (5)

Table 1. Twenty-four hours pentamidine treatment on I_{K1} characteristics. P<0.05 for all treatments vs control. Number of experiments are indicated between brackets. ND, not determined.

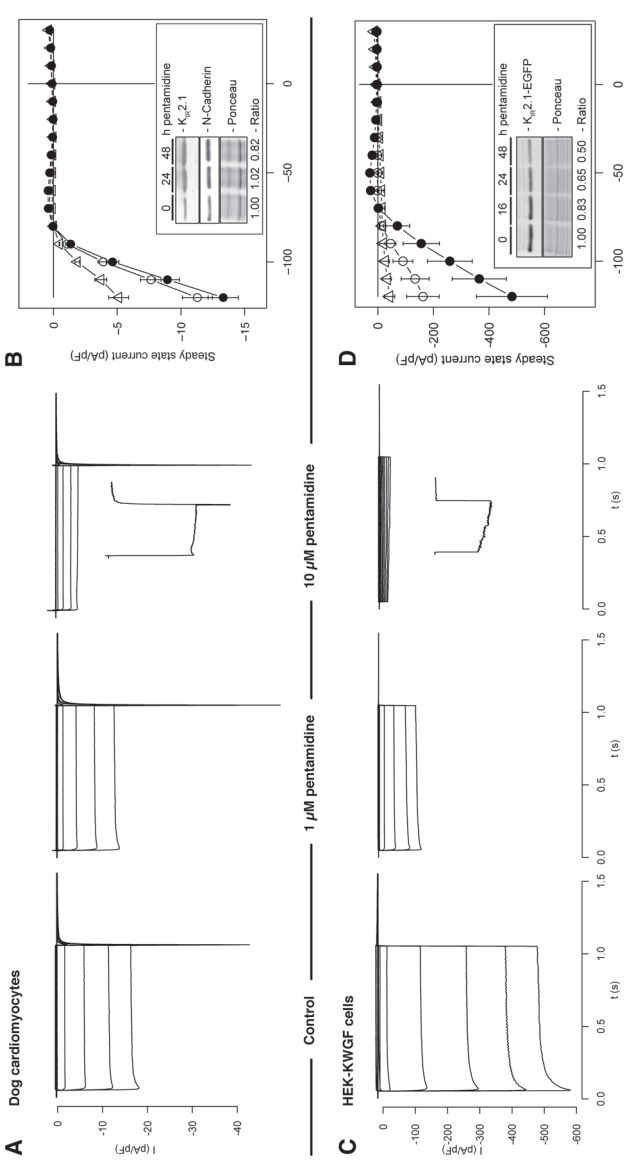

Figure 1. Pentamidine inhibits I_{K1} in cultured cardiomyocytes. Treatment for 24 h with pentamidine decreased I_{K1} densities in cultured adult dog cardiomyocytes (A, B) and HEK-KWGF cells (C, D). Besides reduced current levels, also inward current activation was slowed as can be seen with 10 μM pentamidine in dog cardiomyocytes, and more pronounced with HEK-KWGF cells (see insets depicting currents evoked by a step to -120 mV). Solid circles: control; open circles: 1 μM pentamidine; triangles: 10μM pentamidine. (B, inset), Representative image (N=2) of $K_{IR}2.1$ expression in cultured adult cardiomyocytes in time (hours) following pentamidine treatment (10 μM) as determined by western blot, N-Cadherin and Ponceau staining serve as loading control for quantification. (D, inset), Representative image (N=3) of $K_{IR}2.1$-GFP expression in HEK-KWGF cells after pentamidine treatment (10 μM) as determined by western blot, Ponceau staining serves as loading control for quantification.

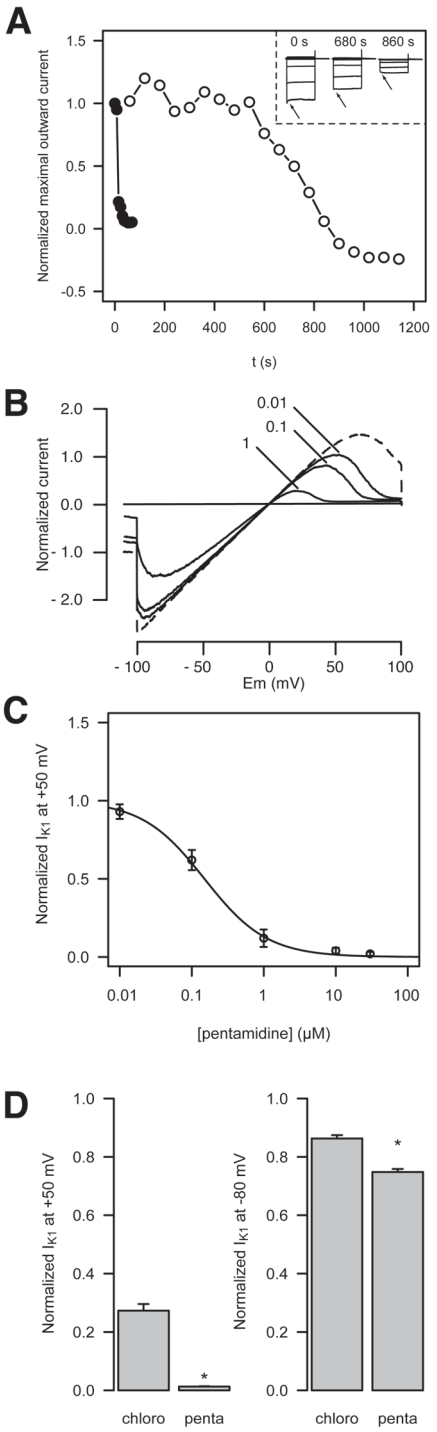

Figure 2. Pentamidine dose response relationship for $K_{IR}2.1$ mediated I_{K1}. Typical recordings demonstrating a much slower developing pentamidine (10 µM) induced I_{K1} block in whole cell (open symbols) compared to inside-out recordings (solid symbols). Inset: Current traces during drug application in the whole cell configuration display altered channel kinetics (arrows). Control cells displayed no rundown for at least 20 minutes (A). Typical inside-out recording depicting inhibition of I_{K1} with increasing concentrations of pentamidine, demonstrating strongest effects on outward current. Dashed trace is the control recording (B). Average concentration-response curve for I_{K1} recorded in the inside-out configuration (n=11) (C). Comparison of the inhibitory effect of chloroquine and pentamidine (both 1 µM) measured in inside-out experiments. Pentamidine has a significantly stronger blocking effect at equal concentration, particularly for outward currents (D).

protein expression levels as assessed by western blot revealed no decrease at 24 h and 18% decrease at 48 h of 10 μM pentamidine incubation.

Cardiac I_{K1} is mainly determined by $K_{IR}2.1$ protein. Therefore we analyzed whether $K_{IR}2.1$ based I_{K1} density is sensitive to pentamidine in HEK293 cells stably expressing GFP-tagged $K_{IR}2.1$ (HEK-KWGF). Under these conditions the effects of pentamidine were even stronger. Even 1 μM pentamidine applied for 24 h reduced the inward (66%) and outward component of I_{K1} (94%) with virtually complete blockade at 10 μM pentamidine (Fig. 1C and 1D, Table 1). At the protein level a 17%, 35% and 50% inhibition in expression levels was found at 16, 24 and 48 h of incubation with 10 μM pentamidine, respectively.

Pentamidine acutely blocks I_{K1} channels when applied from the cytoplasmic side.

To further explore the time relationship between pentamidine application and I_{K1} block, the drug was infused during continuous I_{K1} measurement. Fig. 2A shows that acute application of 10 μM pentamidine decreased I_{K1} after 10 minutes in HEK-KWGF cells in the whole cell patch mode (open circles). Altered opening kinetics of the inward component was seen from that time point on (inset). This effect was slow, because pentamidine acts from the cytoplasmic side of the ion channel as can be appreciated from the data in the inside-out patch configuration (Fig. 2A filled circles), resulting in an IC_{50} of 0.17 ± 0.04 μM and a Hill-coefficient of -0.87 ± 0.10 (n=11) (Fig. 2B and 2C).

We next compared pentamidine mediated block with that of chloroquine that also inhibits the I_{K1} ion channel acutely with an IC_{50} of 1.1 ± 0.2 μM (Rodríguez-Menchaca *et al.*, 2008). Fig. 2D shows the block of I_{K1} by 1 μM pentamidine and by 1 μM chloroquine. Chloroquine outward current block was 70%, pentamidine caused a 95% block. Although inward current was less affected by both drugs, pentamidine was again more potent than chloroquine. No additive effects were seen when applying the two drugs together (not shown).

Direct pentamidine block depends on negatively charged residues in the $K_{IR}2.1$ cytoplasmic pore region. Since the direct effects of pentamidine on $K_{IR}2.1$ based I_{K1} reflect those observed for chloroquine (Rodríguez-Menchaca *et al.*, 2008), we next assessed whether pentamidine is also able to enter the cytoplasmic pore region and with which amino acids it interacts. Molecular modeling was used to examine potential physical interaction sites of the $K_{IR}2.1$ channel with pentamidine. Fig. 3B and 3C show the preferential orientation of pentamidine within the cytoplasmic cavity. Pentamidine adopts a u-shaped

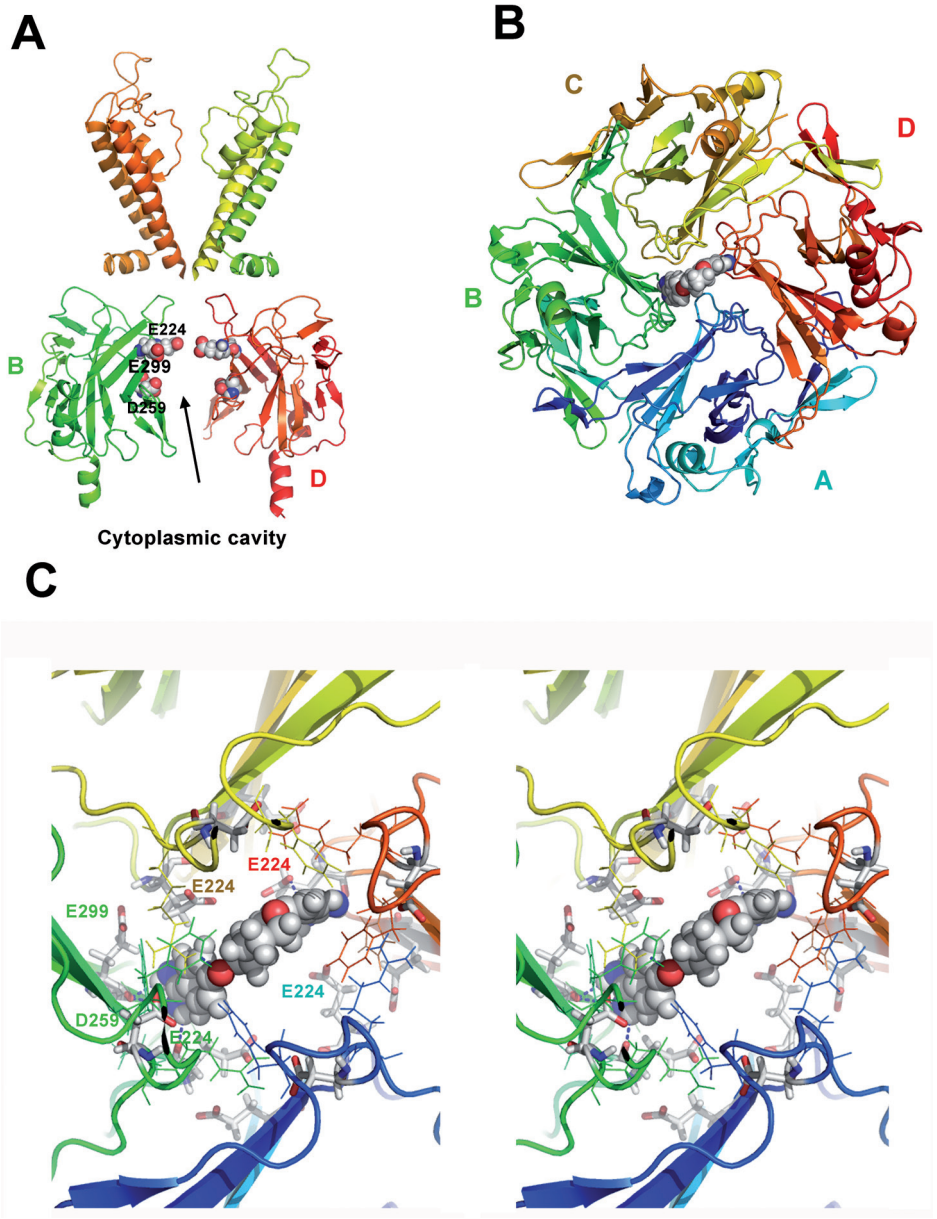

Figure 3. Docking of pentamidine within the $K_{IR}2.1$ cytoplasmic domain. Side view of 2 $K_{IR}2.1$ domains. The transmembrane regions (homology model of $K_{IR}2.1$, unpublished) and cytoplasmic domain (1U4F, crystal structure) with acidic residues E224, D259, E299 important for pentamidine block, highlighted (A). Bottom view of the preferential orientation of pentamidine in the cytoplasmic pore domain (B). Stereo view of the cytoplasmic pore domain with pentamidine plugging the pore. Residues are colored according to domains (A=blue, B=green, C=orange, D=red) (C). All Figures were prepared using the program PyMol (Delano Scientific).

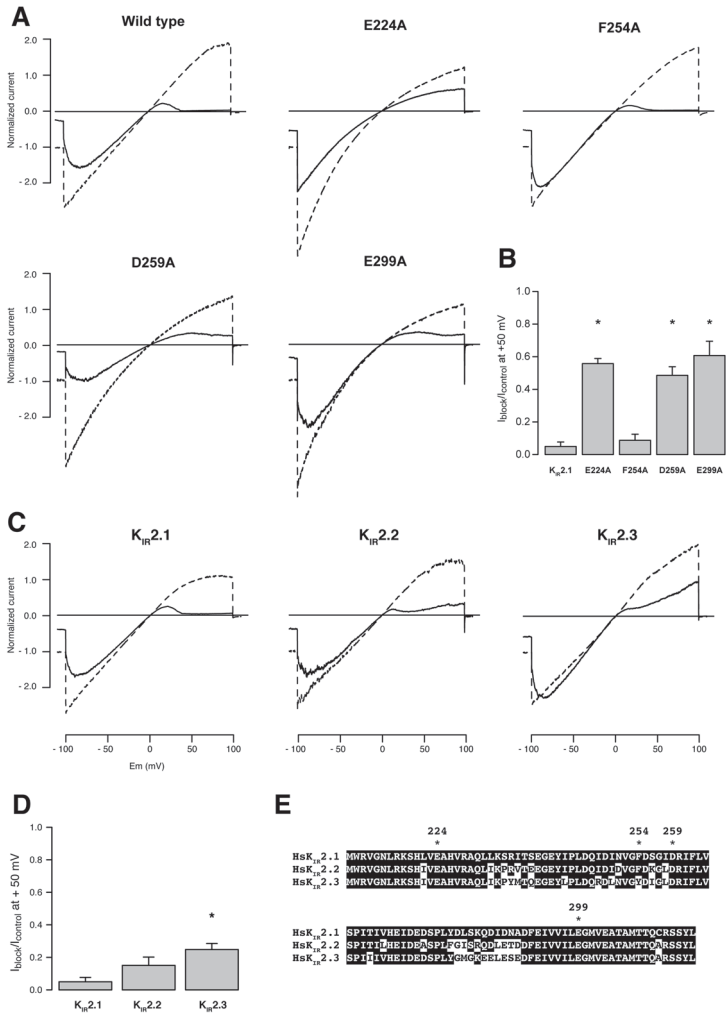

Figure 4. Pentamidine interacts with specific residues lining the $K_{IR}2.1$ channels pore region. Inside-out recordings of I_{K1} based on human $K_{IR}2.1$ in absence (dashed line) and presence of 1 μM pentamidine (solid line). Depicted are recordings from Alanine substitution mutants that demonstrate loss of normal pentamidine block of outward current when residues E224, D259 and E299 are mutated (A). Plot of average residual I_{K1} (at 50 mV) for the mutants depicted in A, normalized to control current levels (B). Inside-out recordings of I_{K1} based on mouse $K_{IR}2.1$, -2.2 and -2.3 in the absence (dashed) and presence of 1 μM pentamidine (solid line), showing reduced pentamidine sensitivity of channels composed of $K_{IR}2.2$ and $K_{IR}2.3$ tetramers (C, D). Amino acid alignment of cytoplasmic pore region of human $K_{IR}2.1$, -2.2 and -2.3. Amino acid residues mutations tested for pentamidine block are indicated by asterisks. Murine sequences in this region are identical to the human forms (not shown). F254 is not conserved in $K_{IR}2.3$. Identical residues are indicated in white lettering and black shading (E).

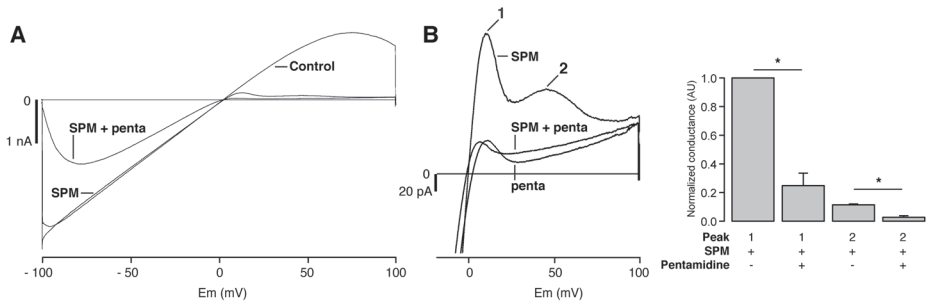

Figure 5. Pentamidine block is independent of spermine. Inside-out recording of mouse $K_{IR}2.1$ based I_{K1} in the absence of spermine and pentamidine (control), in the presence of 0.1 μM spermine (SPM) or with the combination of 1 μM pentamidine and spermine (SPM + penta) (A). Enlargement of panel A illustrates that outward I_{K1} block by 1 μM pentamidine is not different when pentamidine is added in the presence or absence of 0.1 μM spermine (averaged traces of 3, 3 and 4 patches, respectively) (B, left panel). The numbered peaks correspond with Mode 1 and 2 block of I_{K1} channels by spermine (Ishihara et al., 2004). Conductance of these peaks was significantly diminished by pentamidine, especially Mode 2 block seems sensitive to pentamidine. Values were normalized using the Mode 1 conductance recorded in presence of spermine for each recording (B, right panel).

binding conformation and favorable interactions with residues E224, D259 and E299 are predicted. The carboxylate oxygen atoms of E224 from two opposing subunits form hydrogen bonds with the protons of the amino moiety of the benzamidine rings from pentamidine. Hydrogen bonds are also formed between the backbone oxygen of E299 and 2 nitrogen atoms of pentamidine. Furthermore, the carboxylate oxygen of D259 from subunit B interacts favorably with the amino group of one of the benzamidine rings.

Using inside-out patches, Fig. 4A ('wildtype') and Fig. 4B ('$K_{IR}2.1$') show that wildtype human $K_{IR}2.1$ I_{K1} channels are effectively blocked (95%) by 1 μM pentamidine. The mutation E224A, D259A and E299A all significantly diminish this outward current block to about 50%, whereas the F254A mutation did not affect outward block, in contrast to its effect on chloroquine-mediated block (Rodríguez-Menchaca *et al.*, 2008).

In the heart, I_{K1} ion channels are formed by either homo- or heterotetramers of $K_{IR}2.1$, $K_{IR}2.2$ and $K_{IR}2.3$. We therefore assessed the effect of acute pentamidine block on homotetramers of murine $K_{IR}2.2$ and $K_{IR}2.3$ using the inside-out voltage clamp configuration. Fig. 4C and 4D shows that pentamidine sensitivity is significant reduced for $K_{IR}2.3$ compared to $K_{IR}2.1$. $K_{IR}2.2$ sensitivity for pentamidine block is in between that of $K_{IR}2.1$ and $K_{IR}2.3$ channels. Amino-acid alignment of the cytoplasmic pore region from $K_{IR}2.1$, 2.2 and 2.3 reveals

complete identity for E224, D259 en E299 (Fig. 4E). By and large, we conclude that cardiac I_{K1}, irrespective of its underlying molecular determinants, displays pentamidine mediated acute block.

Inward rectification of I_{K1} ion channels is accomplished by the binding of polyamines inside the cytoplasmic and transmembrane regions of the pore (Lu, 2004). Negative charged amino acids E224, D259 and E299 in the cytoplasmic region of the pore are likely to attribute the polyamine induced rectification (Fujiwara and Kubo 2006; Tai *et al.*, 2009). To assess whether pentamidine block is affected by the presence of polyamines, pentamidine was applied in the presence of spermine. With low concentrations of spermine (0.1 μM), the outward component of I_{K1} displayed in a bi-phasic block (Fig. 5A,B), presumably due to transmembrane region (peak 1) and cytoplasmic region (peak 2) spermine interaction (Ishihara and Ehara, 2004; Ishihara and Yan, 2007). Co-application of pentamidine largely inhibited the cytoplasmic spermine binding region (peak 2), leaving the transmembrane region relatively unaffected (Fig. 5). These results indicate that pentamidine enters and blocks the I_{K1} channel pore, but most likely does not penetrate as far as spermine. Thus, pentamidine-mediated I_{K1} block is not dependent on the presence of the polyamine spermine.

Discussion and conclusions

K_{IR}2.x ion channel blockers.

Very few acute K_{IR}2.1 ion channel blocking drugs for which the mode of action has been resolved have been described today. Tamoxifen, 4-hydroxy-tamoxifen and raloxifene mediated block is voltage-independent and has been suggested to act by interference of the K_{IR}2.1-PIP2 interaction, outside of the pore region (Ponce-Balbuena *et al.*, 2009). Chloroquine was found to inhibit the K_{IR}2.1 based I_{K1} channel in a voltage dependent mode by plugging the cytoplasmic pore region (Rodríguez-Menchaca *et al.*, 2008). We observed voltage-dependent pentamidine block, i.e. the outward component of I_{K1} was more strongly affected than the inward component, and altered kinetics with respect to maximum current rise time upon hyperpolarization. In addition, our molecular docking simulations identified a binding site for pentamidine in the cytoplasmic pore domain of K_{IR}2.1. The binding site is flanked by negatively charged residues E224, D259 and E229 which is in agreement with our alanine substitution results. Therefore, our data suggest that pentamidine block acts by the drug plugging the conduction pore similarly as has been suggested for chloroquine (Rodríguez-Menchaca *et al.*, 2008). Both drugs seem to

interact primarily with $K_{IR}2.1$ by electrostatic interactions. Our modeling on the closed state $K_{IR}2.1$ model did not provide evidence for drug interaction in the transmembrane cavity. Due to the lack of a working open state model, we cannot rule out the possibility of direct interaction of pentamidine with the transmembrane cavity for an open channel, which would result in drug-channel interaction at additional amino acid residues. The somewhat different behavior of the inward component compared to the outward component in the different mutants with respect to pentamidine block may be indicative for this suggestion.

Of the above mentioned drugs only pentamidine displays specificity towards I_{K1}, while chloroquine, tamoxifen and raloxifene block additional cardiac ion channels (White, 2007; He *et al.*, 2003; Liu *et al.*, 1998; Liu *et al.*, 2007; Liew *et al.*, 2004). However, pentamidine is known to affect cardiac I_{Kr} non-acutely by interfering in forward trafficking of hERG mediated channels (Cordes *et al.*, 2005; Kuryshev *et al.*, 2005). With respect to $K_{IR}2.1$, we observed a decrease in protein expression levels at a relatively slow timescale and after the time point on which direct channel block is evident. Expression level decrease occurred faster in HEK-KWGF cells compared to adult cardiomyocytes, which may be explained by differences in $K_{IR}2.1$ half-life in the ectopic expression system compared to native $K_{IR}2.1$ expressing cells. However, a difference in pentamidine uptake, which is transporter dependent (Ming *et al.*, 2009) could also account for the observed differences in timing.

Clinical use and pharmacology of pentamidine.

The second-line drug pentamidine is widely used, and advocated, in treatment of diverse forms of Leishmaniasis (WHO estimation of 12 million infections worldwide, 1.5-2 million new cases each year) and Human African Trypanosomis (WHO estimation 70 thousand infections) (Lai A Fat *et al.*, 2002; Werbovetz, 2006). In the western world it has been used for the treatment of P. carinii pneumonia in HIV-positive patients but prescription is decreasing due to improved control of the primary infection in this patient group. Nevertheless, pentamidine use may increase due to import (Zeegelaar *et al.*, 2005) and northward spreading (Dujardin *et al.*, 2008) of Leishmaniasis in the western world, and in developing countries due to Leishmaniasis becoming resistant to first-line medication (Croft *et al.*, 2006). Intravenous application of clinical doses (4 mgkg-1) results in plasma levels of 1.5-5 μM (Sands *et al.*, 1985; Goa and Campoli-Richards, 1987; Lidman *et al.*, 1994), comparable with the concentrations used in our *in vitro* experiments and in studies on $K_v11.1$ (hERG) (Cordes *et al.*, 2005; Kuryshev *et al.*, 2005). Although pentamidine directly interacts with the I_{K1} channel, block in the whole cell configuration occurs only

after a short lag-time of 10 minutes, suggesting a relatively slow entrance of pentamidine into the cell. Indeed, pentamidine uptake in mammalian cells was defined recently as an organic cation transporter dependent process (Ming *et al.*, 2009). In mice, rats and humans, pentamidine accumulates in tissues with a strong preference for liver and kidney while brain tissue remains virtually devoid of the drug (Waalkes *et al.*, 1970; Waldman *et al.*, 1973; Donnelly *et al.*, 1988). Neurons, like cardiac myocytes, express high levels of functional $K_{IR}2.x$ ion channels. The absence of pentamidine in brain tissue may explain the absence of strong neurological disorders during pentamidine therapy.

Experimental use of pentamidine and future perspectives.

In contrast to several other ion currents like I_{Kr} and I_{Ks}, the contribution of I_{K1} to repolarization redundancy, known as repolarization reserve (Roden, 1998b) has not been studied extensively *in vivo*. This is mainly due to the limited availability of specific I_{K1} inhibitors applicable to large animal models. The specific I_{K1} inhibitor barium is of limited use in *in vivo* studies due to reported lethality mainly caused by respiratory arrest (Roza and Berman, 1971). The I_{K1} pore blockers chloroquine (Rodríguez-Menchaca *et al.*, 2008) and pentamidine in principle may serve as alternatives for experimental use of Ba^{2+}. Disadvantages of chloroquine are its effects on protein degradation (Jansen *et al.*, 2008) and direct block of other cardiac ion channels (White, 2007). Pentamidine on the other hand may be used as a direct I_{K1} blocker, but long-term application may lead to "trafficking" defects of $K_v11.1$ and $K_{IR}2.1$ channel proteins also. Recently, pentamidine infusion in dogs was reported to induce mild QT(c) prolongation, which was speculated by the authors to be caused by unexpected rapid I_{Kr} channel trafficking defects (Yokoyama *et al.*, 2009). Based on our results described here, we hypothesize that the mild QT(c) prolongation in sinus rhythm (Yokoyama *et al.*, 2009) and chronic AV block (our unpublished observations) dogs is caused by acute I_{K1} block.

A potential clinical use for specific I_{K1} blockers can be found in gain-of-function mutations in the KCNJ2 gene resulting in exacerbation of $K_{IR}2.1$ based I_{K1} associated with atrial fibrillation (Xia *et al.*, 2005; Zhang *et al.*, 2005c; Ehrlich, 2008). As elegantly shown by El Harchi *et al.* (2009) mutant channels are susceptible for chloroquine inhibition presenting new opportunities for drug based treatments (El Harchi *et al.*, 2009).

Irrespective of the application of I_{K1} blocking drugs, target specificity is strongly required. Therefore, the molecular modeling studies on chloroquine (Rodríguez-Menchaca *et al.*, 2008) and pentamidine (this study) interaction with the $K_{IR}2.1$ based I_{K1} channel, may promote further development of more

specific I_{K1} channel blockers, applicable for both *in vivo* experimentation and therapeutic use.

Acknowledgements

We would like to thank Dr. J. Miyazaki and Dr. Y. Kurachi (Osaka University, Japan), Dr. L. Jan (University of California San Francisco, USA) and Dr. K. Ishihara (Saga University, Japan) for providing us with the pCXN2 and KCNJ2, -4 and -12 constructs; Dr. Tristani-Firouzi (University of Utah School of Medicine, USA) for pore mutation constructs; This work was support by a grant from Top Institute Pharma, (D2-101), Leiden, The Netherlands (L.N., A.S.).

Conflict of interest

The authors state no conflict of interest.

Chapter 4

Evaluation of pentamidine analogues for efficient and specific I_{K1} inhibition. A preliminary study.

Nalos L, Stary-Weinzinger A, de Boer TP, Varkevisser R, Linder T, Houtman MJC, de Kort P, Waasdorp M, Peschar M, Rook MB, Vos MA, van der Heyden MAG.

In excitable cells, $K_{IR}2.x$ ion channel carried inward rectifier current (I_{K1}) sets the negative and stable resting membrane potential, and potentiates the final phase of action potential repolarization. Loss- or gain-of-function mutations are correlated with severe cardiac arrhythmias, while pathological cardiac remodeling affects normal expression levels of $K_{IR}2.x$ protein. Currently, no specific I_{K1} inhibitor for *in vivo* application is available which severely hampers studies on the precise role of I_{K1} in normal cardiac physiology and pathophysiology. We found previously that the diamine antiprotozoal drug pentamidine (P) inhibits I_{K1} by plugging the cytoplasmic pore region of the channel. We hypothesize that P can be used as a lead compound to further develop more efficient and specific I_{K1} inhibitors.
We now analyzed 7 pentamidine analogues (PA-1 to PA-7) for their I_{K1} blocking potency at a single concentration using inside-out patch clamp. PA-6 demonstrated highest blocking efficiency and was tested further. Modeling indicated that PA-6 had less electrostatic, but more lipophilic interactions with the cytoplasmic channel pore. This resulted in a higher channel affinity for PA-6 (ΔG -44.1 kJ/Mol) than for the parent component P (ΔG -31.7 kJ/Mol). PA-6 (200 nM) inhibited I_{K1} in isolated cardiac myocytes (>90%) and prolonged action potential duration of normal canine adult atrial (28.6%) and ventricular (19.4%) cardiomyocytes. In contrast to P, PA-6 increased $K_{IR}2.1$ expression levels (2.1 fold at 48 h) and mature $K_v11.1$ was not affected. We conclude that small modifications in P alters $K_{IR}2.1$ blocking characteristics, and found one analogue to inhibit $K_{IR}2.1$ more efficiently without causing ion channel trafficking defects of $K_v11.1$.

Introduction

Resting membrane potential and stability in working myocytes strongly results from activity of the cardiac inward rectifier current (Lopatin and Nichols, 2001; Dhamoon and Jalife, 2005). I_{K1} activity contributes also to final phase three repolarization. Experimental I_{K1} perturbation, either by $BaCl_2$ infusion, overexpression of dominant negative channels or null-mutation, results in diverse electrical phenotypes (reviewed in De Boer *et al.*, 2010a). Loss- or gain-of function mutations in patients have been associated with Andersen-Tawil Syndrome 1, congenital atrial fibrillation and catecholamine polymorphic ventricular fibrillation (reviewed in Anamunwo *et al.*, 2010). Finally, atrial fibrillation and heart failure associated electrical remodeling affect expression levels of the I_{K1} channel proteins (Dobrev *et al.*, 2002; Gaborit *et al.*, 2005;

Girmatsion *et al.*, 2009; Soltysinska *et al.*, 2009). Many of the cardiac I_{K1} functions have not been assessed in detail in large animal models due to the absence of a specific I_{K1} inhibitor. Barium ions at a low concentration is often used in *in vitro* or *ex vivo* experiments to produce a relatively specific I_{K1} block, however, this ion cannot be used in animals due to many non-cardiac effects resulting in premature death (reviewed in De Boer *et al.*, 2010a).

Recently, we described a dual mechanism by which the diamine anti-protozoal drug pentamidine (P) (Sands *et al.*, 1985) inhibits I_{K1} (De Boer *et al.*, 2010b, Nalos *et al.*, 2011a). P was able to interact with cytoplasmic pore regions of the $K_{IR}2.x$ based ion channel. It adopted a U-shaped conformation and interacted with three acidic amino acid residues (De Boer *et al.*, 2010b) and thereby blocked I_{K1} at an IC_{50} of 0.17 μM when measured in the inside-out orientation of the patch-clamp technique. When applied from the outside of the cell however, much higher concentrations of P were required to reach similar levels of inhibition in HEK293 cells. Besides direct channel block, P also resulted in a decrease in $K_{IR}2.1$ protein expression, thereby reducing the amount of plasma membrane localized ion channels (Nalos *et al.*, 2011a). Previous studies performed by others and confirmed by us, demonstrated that P also affected maturation of the $K_v11.1$ ion channel protein, the alpha-subunit of the delayed rectifier current I_{Kr} (Cordes *et al.*, 2005; Kuryshev *et al.*, 2005; Nalos *et al.*, 2011a). This would complicate long term assessment of I_{K1} involvement in cardiac electrophysiology *in vivo* when using P as a research tool. Moreover, its I_{Kr} blocking capacity has been associated with altered electrophysiological properties and TdP arrhythmias in patients by various authors (Bibler *et al.*, 1988; Mitchell *et al.*, 1989; Gonzalez *et al.*, 1991; Quadrel *et al.*, 1992; Eisenhauer *et al.*, 1994; Girgis *et al.*, 1997).

We proposed P as a lead compound for the development of improved I_{K1} blocking drugs (Van der Heyden and Sánchez-Chapula, 2011), that can be defined by I_{K1} inhibiting capacity at low nanomolar IC_{50} values without affecting trafficking and/or expression of $K_{IR}2.x$ and other ion channel proteins, and no direct block of additional cardiac ion current channels. In efforts to optimize P for its original purpose, i.e. antiprotozoal activity, a large number of pentamidine analogues (PAs) has been synthesized (Paine *et al.*, 2010). Here, we analyzed seven PAs for their I_{K1} blocking capacity. One compound that provided block at a nanomolar concentration in the whole cell orientation was further analyzed for its molecular interaction with the channel, its potential to block I_{K1} in isolated adult cardiomyocytes, its influence on action potential duration and potential interference with $K_{IR}2.1$ and $K_v11.1$ ion channel trafficking.

Materials and methods

Compounds

Pentamidine-isethionate (Pentacarinat® 300, Sanofi Aventis, Gouda, The Netherlands) was dissolved in water at a P concentration of 0.1 M, sterilized by filtration (0.22 μm), aliquoted, and stored at -20°C until use. PAs (PA-1 to PA-7) were kindly provided by Dr. R. Tidwell (University of North Carolina at Chapel Hill, USA), and dissolved in water (PA-1 to PA-6) or DMSO (PA-7) at

Code	Tidwell code	chemical structure
P	(pentamidine)	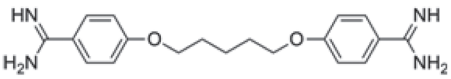
PA-1	(6MAA025)	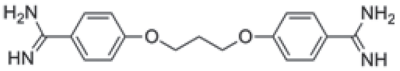
PA-2	(1KAO045)	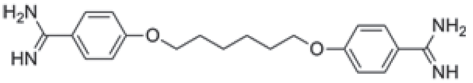
PA-3	(21DAP023)	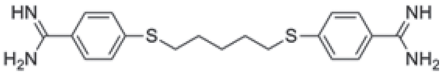
PA-4	(9SMB070)	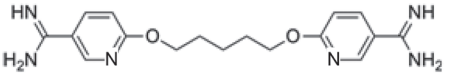
PA-5	(14SMB098)	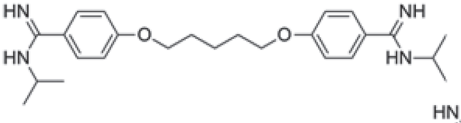
PA-6	(2EVK008)	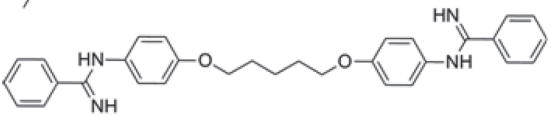
PA-7	(5MAA089)	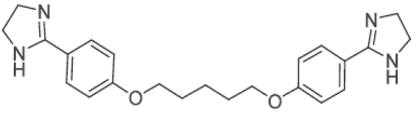

Table 1.

25 mM or the highest concentration below this depending on solubility, with a minimum of 1 mM. With respect to lead compound P, PA-1 to PA-3 are modified in the linker between the two phenyl groups, PA-4 bares modifications in the phenyl groups, PA-5 to PA-7 contain modifications in the amidine groups (for chemical structures see Table 1).

Cells

The investigation conformed to the Guide for the Care and Use of Laboratory Animals published by the US National Institutes of Health (NIH Publication No. 85-23, revised 1996) and was approved by the institutional committee for animal experiments. Left ventricular cardiomyocytes from adult healthy dogs were isolated and cultured as described previously (Volders *et al.*, 1999; De Boer *et al.*, 2006a; Nalos *et al.*, 2011b). Left atrial cardiomyocytes were isolated following an identical procedure, but cells were harvested from the free wall of the left atrium. Normal rabbit adult left ventricular cardiomyocytes were isolated as described previously (Nalos *et al.*, 2011b). GFP-tagged $K_{IR}2.1$ HEK293 (HEK-KWGF) cells were generated and cultured as described previously (De Boer *et al.*, 2006b). HEK-hERG cells were obtained from C. January (Zhou *et al.*, 1998). In time course experiments, cell incubation procedures were identical as described previously (Nalos *et al.*, 2011a).

Electrophysiology

Whole cell patch clamp I_{K1} measurements were done using a HEKA EPC-10 Double Plus amplifier controlled by PatchMaster 2.10 software (HEKA, Lambrecht/Pfalz, Germany) using pulse-protocols as described earlier (De Boer *et al.*, 2010b). Action potentials were triggered in whole-cell current clamp mode with 2 ms current injections at a cycle length of 2000 ms and recorded with PClamp9 software (Molecular Devices, Sunnyvale, CA, USA), as described previously (Oros *et al.*, 2010).

Inside-out patch clamp measurements were performed essentially identical as described before using a ramp protocol from -100 to 100 mV in 5s from a holding potential of -40 mV. (De Boer *et al.*, 2010b).

Molecular modeling and ligand docking

P and PAs were created with ChemBioDraw Ultra 12.0 (Cambridge Soft, MA 02140, USA) and subsequently processed with Open Babel 2.3 to generate 3D coordinates. The crystallographic coordinates of the cytoplasmic domain

of $K_{IR}2.1$ was downloaded from the pdb-database (PDB ID: 1U4F). FlexX version 1.3 (BioSolveIT GmbH, St. Augustin, Germany) was used for docking. The binding site was specified using the carboxylic acids of three Glu224 residues and the sphere center of the binding site was placed in the middle of the cavity. The radius of the binding site was set to 20 Å. Default settings of FlexX were applied for protonation and torsion angles. The ChemScore scoring function of FlexX was applied and the top 10 docking solutions were saved for analysis.

Western blot

Cell lysates were prepared in buffer D (20 mM HEPES pH7.6, 125 mM NaCl, 10% (v/v) glycerol, 1 mM EDTA, 1 mM EGTA, 1 mM dithiothreitol, 1% Triton X-100). Preparation, protein detection, quantification and analysis of western blots were performed identical as described before (Nalos *et al.*, 2011a).

Statistics

Group averages are presented as mean ± standard deviation. Differences between group averages were tested using Student's t-test in case of two groups or using a one-way ANOVA with a post-hoc test (Holm-Sidak) in the case of more than two groups. Differences were considered statistically significant if $p<0.05$. All analyses were carried out using KaleidaGraph 4.1 (Synergy Software, Reading, PA, USA).

Results and discussion

Since lead compound P blocks $K_{IR}2.1$ carried I_{K1} by entering the cytoplasmic pore region from the cytoplasmic side at an IC_{50} of ~0.17 µM with respect to the outward current component at +50 mV in the inside-out orientation (De Boer *et al.*, 2010b), we tested PA-1 to PA-7 under identical conditions (Figure 1A, B) at a concentration of 0.20 µM. As expected, outward current inhibition by P (51.8%) was near the IC_{50} value, while inward component (at -80 mV) was less strongly inhibited (13.4%), demonstrating the voltage-dependent behavior of P on $K_{IR}2.1$ ion channel block. Next analogues with modifications in the linker between the two phenyl groups were tested. Shortening by 2 carbon atoms (PA-1) decreased inhibiting potential of the outward component (13.1%). Lengthening by 1 carbon atom (PA-2) slightly increased the inhibition potential (24.6% and 60.3% for inward and outward component, respectively). Changing the linker

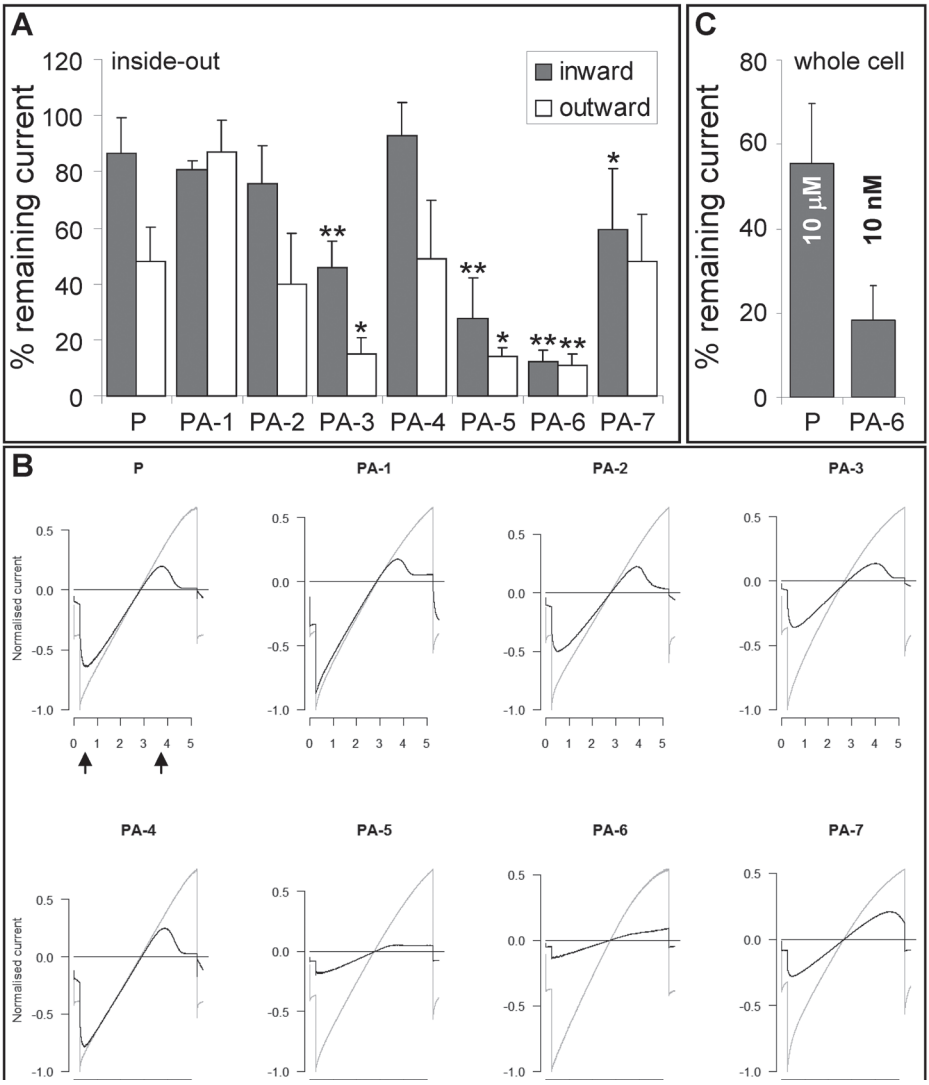

Figure 1. Inhibition of $K_{IR}2.1$ carried I_{K1} by pentamidine and its analogs. (A) $K_{IR}2.1$ channels in the inside-out orientations were treated with P and PA-1 to PA-7 at a concentration of 200 nM. Block of inward (gray bars, at -80 mV) and outward (white bars, at +50 mV) current is depicted. (B) Complete normalized steady state recordings of $K_{IR}2.1$ channels in the inside-out orientation under control (gray) and compound treated (black) conditions. Black arrows indicate time points used for determination of inward and outward current as depicted in A. Note, current measurements in inside-out mode are performed using symmetrical high potassium concentration on both sides of the membrane. (C) HEK-KWGF cells were treated with 10 µM P or 10 nM PA-6. Semi-acute (< 10 min) inhibition of outward current in the whole cell orientation at -65 mV is depicted. ** indicates $p<0.01$, * indicates $p<0.05$ (P vs. PA, n=5).

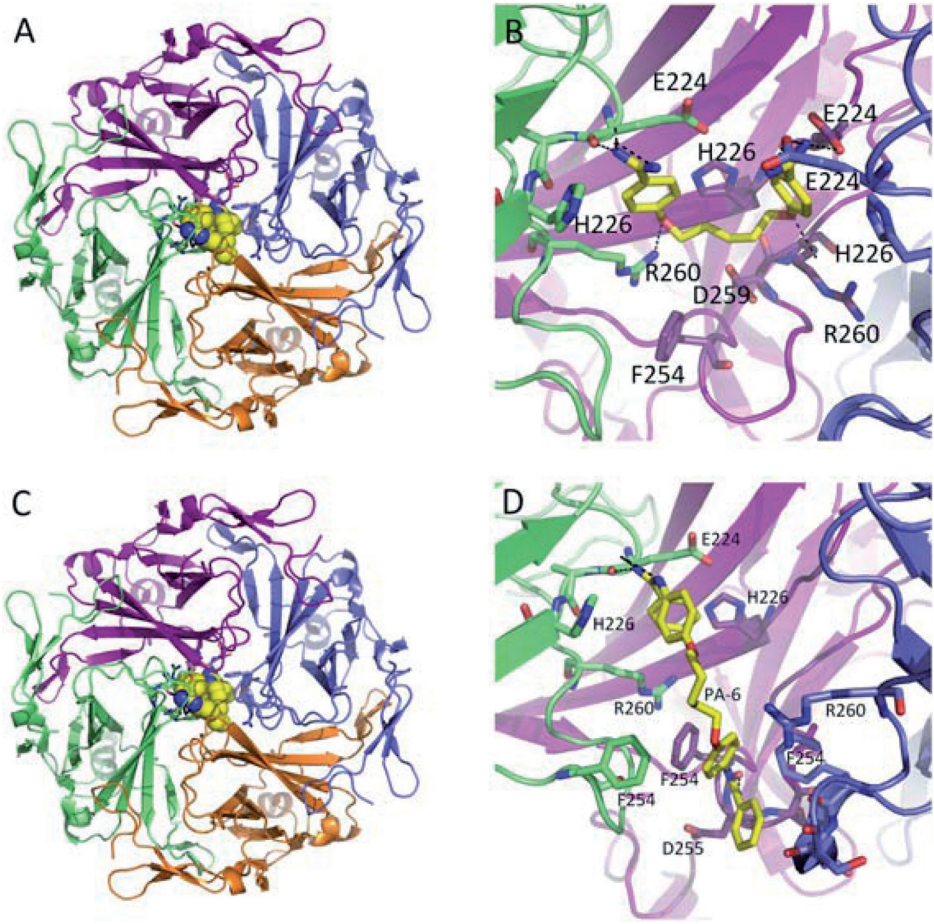

Figure 2. Pentamidine and PA-6 interactions with the cytoplasmic domain of $K_{IR}2.1$. (A, C) Top view of the four intracellular domains of $K_{IR}2.1$ shown as differently colored ribbons; P and PA-6 are shown as yellow spheres. (B) Lowest energy binding mode of P in U-shaped conformation, as has been shown previously (De Boer *et al.*, 2010b). (D) Lowest energy binding pose of PA-6, which is oriented longitudinal in the cytoplasmic cavity. Amino acids within 4 Å of the compounds are depicted as sticks. Black dashed lines denote hydrogen bonds.

oxygen into sulfur (PA-3) significantly potentiated inhibition capacity of inward (54.3%) and outward (85.1%) current. Inserting nitrogens in the aromatic rings (PA-4) did not change block (7.1% and 51.1% for inward and outward current, respectively) compared to P. On the other hand, modification in the amidine groups displayed largest effects on current when compared to P. Substitution of hydrogen for isopropyl (PA-5) potentiated inward (72.6%) and outward (85.8%) current inhibition. PA-6 with a phenyl-substituted alternative arrangement of the

amidine group also provided improved blocking capacity (87.9% and 89.2% for inward and outward current, respectively). However addition of imidazol moieties to the aromatic rings (PA-7) altered only inward blocking capacity significantly (40.5% and 52% for inward and outward inhibition, respectively). Furthermore, more subtle variations in voltage-dependent inhibition can be observed from the profiles of the complete traces (Figure 1B). For example, when compared to the unblocking characteristics of P upon hyperpolarisation, unblock of PA-1 is almost instantaneously; while hypolarisation-induced unblock of PA-4 takes an intermediate position between P and PA-1. Also, different profiles of voltage-dependency in outward-current block are evident. Our data demonstrate that specific and small modifications in the chemical structure of the compound alter blocking capacity. Interestingly, block by PA-6 appears voltage independent, although testing at lower concentrations is warranted.

For the remainder we focused on the most efficient blocking compound, PA-6. When applied to HEK-KWGF cells, stably expressing GFP-tagged murine $K_{IR}2.1$, P at a concentration of 10 μM inhibited outward current by ~45% (Figure 1C). In contrast, under the same conditions a 1000-fold lower concentration of PA-6 produced ~83% block. Correlated to the results obtained in the inside-out orientation, this greatly improved block of PA-6 compared to P in whole cell patch clamp might be caused by higher affinity for the channel, a reduction in non-specific cellular protein binding, different intracellular distribution, enhanced cell penetration or a combination of these factors.

Molecular modeling suggested that PA-6 adopts a different binding mode than P (Figure 2). While P interacted with the cytoplasmic domain of $K_{IR}2.1$ in a U-shaped conformation, PA-6 bound in a longitudinal conformation to the channel axis. This led to an increased number of lipophilic interactions (Table 2). In contrast, electrostatic interactions were slightly decreased for PA-6 compared to P. Table 2 lists calculated binding affinities and the number of lipophilic interactions for both compounds. In agreement with experimental data, the Chemscore scoring function in FlexX predicted stronger interactions for PA-6 (ΔG -44.1 kJ/Mol) than for P (ΔG -31.7 kJ/Mol). Despite the differences in binding orientations, both compounds physically occluded the cavity, thereby preventing ion conduction.

Compound	ΔG kJ/mol (Chemscore, FlexX)	HB IAs (E224, D259, E299)	lipophilic IAs
P	-31.7203	7	12
PA-6	-44.1031	6	19

Table 2. HB: hydrogen bonds; IAs: interactions

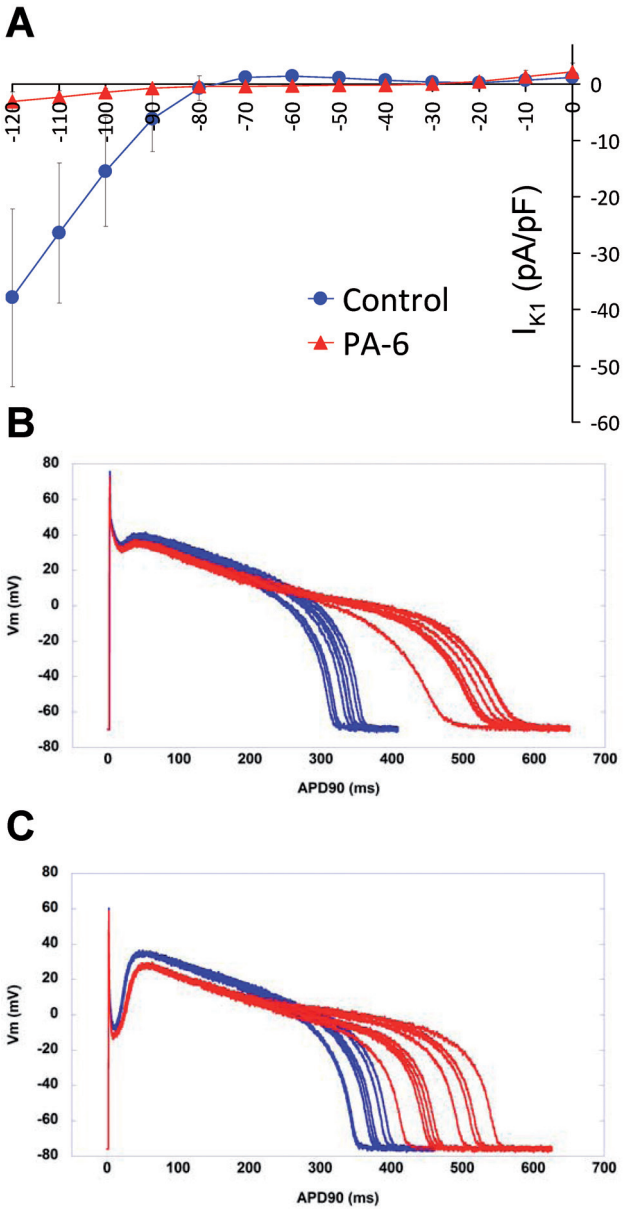

Figure 3. I_{K1} inhibition in isolated adult cardiomyocytes. (A) I-V curve of I_{K1} currents obtained from isolated canine adult ventricular cardiomyocytes under control (closed circles, blue) and PA-6 (200 nM) treated (closed triangles, red) conditions. (B,C) Action potential recordings from isolated canine adult atrial (B) and ventricular (C) cardiomyocytes under control (red) and PA-6 (200 nM) treated (blue) conditions. Cells were paced at 0.5 Hz.

To investigate whether PA-6 was also able to inhibit native I_{K1}, isolated canine adult ventricular cardiomyocytes were treated with 0.20 μM PA-6 acutely resulting in strong inward current inhibition (90.3±7.6% block at -120 mV), while the small outward current could not be reliably measured anymore (Figure 3A). Apparently, native I_{K1} which might be different from ectopic $K_{IR}2.1$-GFP expressed in HEK293 cells due to cellular environment, potential interaction with ancillary subunits and contribution of additional $K_{IR}2.x$ subunits, is also blocked efficient as seen for ectopic $K_{IR}2.1$ in HEK293 cells.

We next tested whether PA-6 would prolong action potential duration when added to isolated normal canine adult atrial and ventricular cardiomyocytes. As shown in Figure 3B and Table 3, PA-6 gave rise to an average action potential

Model/drug	Control		Drug	
	APD	STV	APD	STV
cAVB Dog Dofetilide	384±111	13.5±10.4	490±134	39.8±31.7
cAVB Dog PA-6	361±38	13.2±3.6	434±107	22.6±12.7
Rabbit $BaCl_2$	326±115	14.9±5.3	434±100	16.9±7.6

Table 3.

duration and short-term variability of the repolarization (STV) increase of 19.4±22.4% (p=0.06) and 63±52% (p=0.02) for ventricular (n=7) and 28.6±16.8% (p=0.10) and 121±13% (p<0.01) for atrial (n=3) cardiomyocytes, respectively. Remarkably, as PA-6 has profound effects on I_{K1} density, we did not observe changes in resting membrane potential (data not shown). These results are in accordance with our action potential measurements in adult rabbit ventricular cardiomyocytes treated with 50 μM $BaCl_2$. This prolonged action potential duration with 39±29% (p<0.05, n=7) and increased STV with 19%±39% (p=0.25, n=7; Table 3), while resting membrane potential was not changed significantly. Increasing $BaCl_2$ concentrations to 100 and 200 μM, further prolonged action potential duration and transient hyperpolarisation was observed following phase 3 repolarisation. We hypothesize that at resting membrane potential, background currents are relatively small which implies that residual amounts of functional I_{K1} channels are sufficient for keeping the resting membrane potential at normal levels. However, according to literature, resting membrane stability and cell excitability are more strongly affected by I_{K1} block. For example, action potential formation requires less depolarizing power, spontaneous activity becomes apparent, and final repolarization is accompanied by transient hyperpolarisation (Imoto *et al.*, 1987; Hirano and Hiraoka, 1988; Valenzuela and Vassalle, 1991).

Finally, we tested whether PA-6 at concentrations that strongly inhibit I_{K1} (50 and 100 nM), would inhibit $K_{IR}2.1$ expression and $K_v11.1$ maturation as seen previously for P (Nalos *et al.*, 2011a). In contrast to P that decreases $K_{IR}2.1$ protein levels upon prolonged incubation (1.00 vs. 0.53±0.15 and 0.42±0.05 for control, 24 and 48 h (n=2), respectively), PA-6 treatment resulted in an increase in $K_{IR}2.1$ expression (1.00 vs. 1.34±0.12 and 2.14±0.91 for control, 24 and 48 h (n=2), respectively) (Figure 4A). Although no mechanism has been described how an ion channel blocker is able to increase expression of the ion channel in an ectopic expression system, we envision that channel-inhibitor interaction may stabilize the channel and thereby prolong half-life or contribute to a more efficient trafficking towards the plasma membrane. This is in accordance with observations of congenital trafficking defects of $K_v11.1$ channels that can be rescued by one of its specific inhibitors such as E4031 (Balijepalli *et al.*, 2010). When applying PA-6 in *in vivo* studies we have to consider the opposing effect of direct channel block and increased channel expression. Several authors, including us, have shown that P inhibits maturation of $K_v11.1$ which results in less functional $K_v11.1$ at the plasma membrane (Kuryshev *et al.*, 2005; Cordes *et al.* 2005; Nalos *et al.*, 2011a). Compared to P, PA-6 does not interfere in $K_v11.1$ maturation (ratio mature/

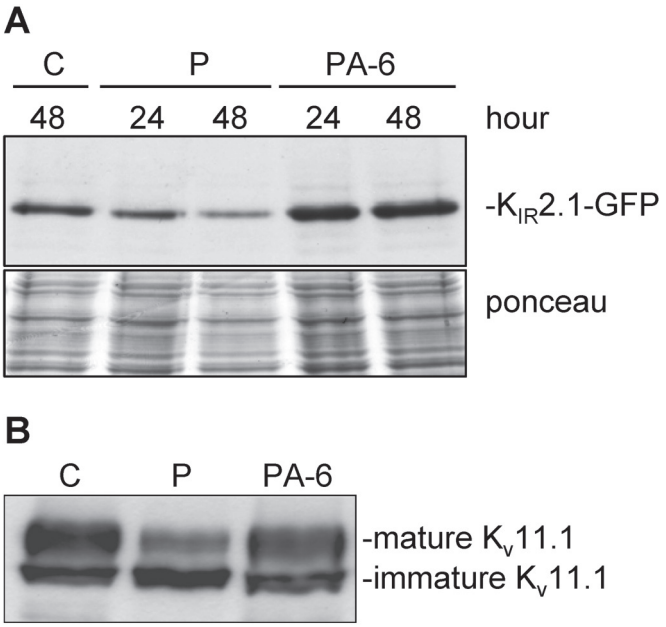

Figure 4. PA-6 enhances $K_{IR}2.1$ expression but does not interfere in $K_v11.1$ maturation. (A) HEK-KWGF cells treated for increasing time with 10 µM P display a time dependent decrease in $K_{IR}2.1$-GFP protein expression. Maximal $K_{IR}2.1$-GFP protein expression inhibition was seen after 48 h. In contrast, PA-6 (100 nM) resulted in a time-dependent increase in $K_{IR}2.1$-GFP protein expression. Maximum increase is seen after 48 h. Total protein staining (ponceau) of Western blots was used as loading control. (B) P (10 µM) decreases mature $K_v11.1$ and increases immature $K_v11.1$ expression. PA-6 (50 nM) does not affect the mature/immature ratio.

immature: 1.52±0.17 vs. 0.89±0.05 and 1.60±0.15 for control, P and PA-6 (n=2), respectively) (Figure 4B). Thus, compared to P, PA-6 at a concentration that strongly reduces I_{K1} does not interfere in protein trafficking that otherwise may result in decreased ion channel expression.

The 7 pentamidine analogues used in this study were originally designed to improve anti-protozoal activity. PA-6 has been studied in animal model of Trypanosomiasis infection (STIB900) (Bakunova *et al.*, 2004). In contrast to P, PA-6 performed worse as an antiprozoal compound (0/4 vs. 2/4 cured animals; survival 7 vs. >44.3 days after infection, for P and PA-6 respectively) when injected intraperitonally on 4 consecutive days from day 3 to day 6 postinfection at 20 mg/kg. Interestingly, infected animals left untreated expired between day 7 and 10, which was a few days later than animals treated with PA-6. Nevertheless, this study demonstrates that a the concentration used, PA-6 is not acutely lethal and would allow at least short time studies *in vivo* to determine a role for I_{K1} in the particular animal model under study.

As recently demonstrated by Noujaim *et al.*, (2010) another $K_{IR}2.1$ pore blocker, i.e. chloroquine, could be used as another lead compound. They focused on chloroquine specificity for $K_{IR}.x$ channels, and found that I_{K1} ($K_{IR}2.x$), I_{KACh} ($K_{IR}3.1$) and I_{KATP} ($K_{IR}6.2$) are all a target for chloroquine mediated block. However, in silico modeling subsequently demonstrated that the mode of drug-channel interaction differed considerable for the three channel types studied, which led to the conclusion that development of ion channel pharmacophores targeting specific members within the K_{IR} superfamily is a feasible approach.

In conclusion, we tested 7 different PAs for their I_{K1} inhibiting capacity that demonstrated that 1) blocking capacity of I_{K1} can be altered by small modifications in the chemical structure of the lead compound, and 2) PA-6 is a highly efficient I_{K1} blocker in ectopic expression systems and native cells, and shows no detrimental interference in $K_v11.1$ channel trafficking. Its ability to block other cardiac ion channels still needs to be investigated however.

Acknowledgements

We would like to thank Dr. R. Tidwell (University of North Carolina at Chapel Hill, USA) for providing PA-1 to PA-7, Dr. C.J. January (University of Wisconsin-Madison, USA) and Dr. A. IJzerman (LUMC, Netherlands) for HEK-hERG cells, Jet Beekman (UMCU, Netherlands) for providing canine cardiomyocytes, and Dr. T.P. de Boer for his assistance in preparing the manuscript. This work was supported by a grant from Top Institute Pharma, (D2-101), Leiden, The Netherlands (L.N.).

Chapter 5

Inhibition of lysosomal degradation rescues pentamidine-mediated decreases of K(IR)2.1 ion channel expression but not that of K(v)11.1.

Nalos L, de Boer TP, Houtman MJC, Rook MB, Vos MA, van der Heyden MAG.

Eur J Pharmacol. 2011 Feb 10;652(1-3):96-103.

The antiprotozoal drug pentamidine inhibits two types of cardiac rectifier potassium currents, which can precipitate life-threatening arrhythmias. Here, we use pentamidine as a tool to investigate whether a single drug affects trafficking of two structurally different potassium channels by identical or different mechanisms, and whether the adverse drug effect can be suppressed in a channel specific fashion. Whole cell patch clamp, Western blot, real time PCR, and confocal laser scanning microcopy were used to determine potassium current density, ion channel protein levels, mRNA expression levels, and subcellular localization, respectively.
We demonstrate that pentamidine inhibits delayed (I_{Kr}) and inward (I_{K1}) rectifier currents in cultured adult canine cardiomyocytes. In HEK293 cells, pentamidine inhibits functional K_v11.1 channels, responsible for I_{Kr}, by interfering at the level of full glycosylation, yielding a less mature form of K_v11.1 at the plasma membrane. In contrast, total K_{IR}2.1 expression levels, underlying I_{K1}, are strongly decreased, which cannot be explained from mRNA expression levels. No changes in molecular size of K_{IR}2.1 protein were observed, excluding interference in overt glycosylation. Remaining K_{IR}2.1 protein is mainly expressed at the plasma membrane. Inhibition of lysosomal protein degradation is able to partially rescue K_{IR}2.1 levels, but not those of K_v11.1.
We conclude that 1) a single drug can interfere in cardiac potassium channel trafficking in a subtype specific mode and 2) adverse drug effects can be corrected in a channel specific manner.

Introduction

The aromatic diamidine drug pentamidine is used as an antiprotozoal compound against diverse forms of Leishmaniasis and sleeping sickness (Sands *et al.*, 1985; Werbovetz, 2006). Pentamidine displays high toxicity, amongst which cardiotoxicity, that can precipitate Torsade de Pointes arrhythmias, is a potential life-threatening side effect (Sands *et al.*, 1985; Owens Jr, 2004). Torsade de Pointes elicited by pentamidine therapy might be caused by functional inhibition of delayed rectifier (I_{Kr}) (Cordes *et al.*, 2005; Kuryshev *et al.*, 2005) and inward rectifier (I_{K1}) (De Boer *et al.*, 2010b) repolarizing potassium currents. Inhibition of repolarizing current results in action potential lengthening and enhanced susceptibility to inward current (e.g. I_{CaL}) induced early after depolarizations (Roden, 2008). In general, drugs can target multiple ion channels, whereby the combined effect may be either pro-, anti-, or non-

arrhythmic (Antoons *et al.*, 2007). Drugs combining inhibition of multiple channels involved in repolarization are expected to display higher levels of pro-arrhythmia than channel specific drugs (Biliczki *et al.*, 2002). For a pro-arrhythmic drug, normalization of only one of its targets may render it safe. Pentamidine is a multi-target drug for which I_{Kr} inhibition takes place at the level of functional K_v11.1 (also known as hERG) protein expression (Cordes *et al.*, 2005; Kuryshev *et al.*, 2005), while I_{K1} inhibition results from a dual effect of direct I_{K1} channel block and decreased K_{IR}2.1 expression (De Boer *et al.*, 2010b).

Drugs affecting ion channel trafficking may pose an important arrhythmic risk (Van der Heyden *et al.*, 2008). Compared to direct channel block, the underlying mechanisms of affected trafficking, which include forward (towards the plasma membrane) and backward (removal from the plasma membrane) modes, are less well understood. In part, this is caused by the large lack of knowledge on normal cardiac potassium ion channel trafficking in general, and presumed differences in trafficking of potassium channel subtypes in particular. K_v11.1 belongs to the 6 transmembrane region family of voltage-gated potassium ion channels, has functional channels formed by tetramers, and is strongly expressed in the heart (Sanguinetti and Tristani-Firouzi, 2006). In contrast, the smaller K_{IR}2.1 channel belongs to the two transmembrane region family of potassium channels and is expressed in a large number of excitable tissues, e.g. muscle and neuronal cell types (De Boer *et al.*, 2010a). As for K_v11.1, the K_{IR}2.1 channel is assembled by tetramerization of its subunits.

In this study we used pentamidine as a tool that offers the opportunity to investigate whether a single drug affects trafficking of structurally different potassium channels by identical or different mechanisms. The goal of our investigation was to compare the effects of pentamidine on K_v11.1 and K_{IR}2.1 protein expression and, as proof-of-principle, to achieve channel specific suppression of adverse drug effects.

Materials and methods

Cell culture

The investigation conformed to the Guide for the Care and Use of Laboratory Animals published by the US National Institutes of Health (NIH Publication No. 85-23, revised 1996) and was approved by the institutional committee for animal experiments. Left ventricular cardiomyocytes from adult chronic complete atrioventricular block dogs were isolated and cultured as described previously (Volders *et al.*, 1999; De Boer *et al.*, 2006a). GFP-tagged

K_{IR}2.1 HEK293 (HEK-KWGF) cells were generated and cultured as described previously (De Boer *et al.*, 2006b). HEK-hERG cells were obtained from C. January (Zhou *et al.*, 1998). In pentamidine experiments, medium was replaced every 24 h. In time course experiments, cells were seeded and harvested on identical days. Different drug incubation times were achieved by replacing medium with drug containing medium at the appropriate time-point. At the same time, medium from control and previous initiated time points were refreshed with appropriate medium.

Pentamidine-isethionate (Pentacarinat® 300, Sanofi Aventis, Gouda, The Netherlands) was dissolved in water at a pentamidine concentration of 0.1 M, sterilized by filtration (0.22 μm), aliquoted, and stored at -20°C until use. Tunicamycin (Sigma-Aldrich, Zwijndrecht, The Netherlands) was dissolved in DMSO at a concentration of 10 mg/ml and used at 5 μg/ml in culture medium.

Electrophysiology

Patch clamp measurements were done using a HEKA EPC-10 Double Plus amplifier controlled by PatchMaster 2.10 software (HEKA, Lambrecht/ Pfalz, Germany). Voltage clamp measurements of whole cell I_{K1} were performed by applying 1 s test pulses ranging between -120 and +40 mV, in 10 mV increments, from a holding potential of -40 mV, and with series resistance compensation of at least 70%. Steady state current at the end of the pulse was normalized to cell capacitance and plotted versus test potential. I_{Kr} measurements were done using the method reported by Zhang (Zhang, 2006), which employs equimolar Cs^+ solutions and allows isolation and direct measurement of Cs^+-carried I_{Kr}. In contrast, I_{Kr} is conventionally measured by running an I_{Kr} voltage clamp protocol in the presence and absence of a strong I_{Kr} blocker, after which I_{Kr} is defined as the blocker-sensitive component. The alternative method was utilized to avoid potential interaction between the I_{Kr} blocker and pentamidine (which also is a documented I_{Kr} inhibitor). The specificity of this method is demonstrated by the experiment depicted in Fig. 1, done on freshly isolated dog cardiomyocytes. After a conditioning pulse to +50 mV, a tail current was elicited by return to the holding potential of -80 mV. This tail current was fully blocked by 1 μM dofetilide, a specific I_{Kr} blocker. Cultured cardiomyocytes were also tested, using the following protocol. From a holding potential of -80 mV, a 3s conditioning pulse to +20 mV was given, followed by a return to -80 mV. The return to holding potential elicited an I_{Kr} tail current, which was fitted with an exponential function in order to determine peak tail current. Peak tail currents were normalized to cell capacitance.

Patch pipettes were made with a Sutter P-2000 puller (Sutter Instrument, Novato, CA, USA) and had resistances of 2-3 MΩ. Extracellular solution for whole cell I_{K1} measurements contained (in mmol/L): NaCl 140, KCl 5.4, $CaCl_2$ 1, $MgCl_2$ 1, glucose 6, $NaHCO_3$ 17.5, HEPES 15, pH 7.4/NaOH. Pipette solution contained potassium gluconate 125, KCl 10, HEPES 5, EGTA 5, $MgCl_2$ 2, $CaCl_2$ 0.6, Na_2ATP 4, pH 7.20/KOH. Extracellular solution for I_{Kr} measurements contained CsCl 135, HEPES 10, glucose 10, and $MgCl_2$ 1, pH 7.20/CsOH. Pipette solution contained CsCl 135, EGTA 10, $MgCl_2$ 1, and HEPES 10, pH 7.20/CsOH.

Western blot

Cell lysates were prepared in RIPA buffer. Twenty µg protein lysate was mixed with Laemmli sample buffer and proteins were separated by 7% (K_v11.1) or 10% (K_{IR}2.1-EGFP) SDS-PAGE and subsequently electro-blotted onto nitrocellulose membrane (Biorad, Veenendaal, The Netherlands). Equal loading was confirmed by reversible Ponceau staining. K_{IR}2.1-EGFP was detected by monoclonal anti-GFP (cat. no. Sc-9996; Santa Cruz Biotechnology, Santa Cruz, CA, USA). K_v11.1 was detected by polyclonal anti-hK_v11.1 primary antibody (cat. no. APC-062; Alomone Labs, Jerusalem, Israel) and peroxidase-conjugated secondary antibody (Jackson ImmunoResearch, West Grove, PA, USA). Standard ECL procedure was used for final detection (GE Healthcare, Diegem, Belgium).

Real-time PCR

Total RNA was isolated using the Trizol (Invitrogen, Breda, The Netherlands) procedure and subsequently treated with DNAse I (Promega, Leiden, The Netherlands). First strand cDNA was prepared from 1 µg of RNA at 42 °C for 1 h with Superscript II reverse transcriptase (Invitrogen) using 250 pmol oligo-dT12-VN and 0.25 µg of random hexamers (Promega). For real-time PCR, target sequences were amplified on a LightCycler 1.5 system (Roche Diagnostics, Almere, The Netherlands) from first strand cDNA. Each PCR reaction contained 1 µl of LightCycler FastStart DNA master SYBR Green I mix (Roche), 0.5 µM primers, and 3 mM $MgCl_2$ in a total volume of 10 µl. The PCR program used consisted of pre-incubation (10 min at 95 °C), amplification (45 cycles of 10 s at 95 °C, 5 s at 60 °C (for GAPDH and β-Actin) or 62 °C (for K_{IR}2.1 and K_v11.1), and 10 s at 72 °C), and melting (5 s from 70 °C to 95 °C). The LinRegPCR method (Ramakers *et al.*, 2003) was used for quantification of the target amplicons relative to internal reference transcripts for GAPDH and

β-Actin. Primers are as follows: K_{IR}2.1, GCAGTCATGGCGAAGATGGCA (sense), TGCCCGGACATGAGCTTCCA (antisense); K_v11.1, ACCGCTGGACCATCCTGCATT (sense), TTCAGCAGGAAGGCAGCCGA (antisense); GAPDH, CCTGCCAAATATGATGACATCAAG (sense), GCCAAATTCGTTGTCATACCAGGA (antisense); β-Actin, GGTCATCACCATTGGCAATGAGCG (sense), CAGCACTGTGTTGGCGTACAGGTC (antisense).

Immunofluorescence and live-imaging microscopy

For immunofluorescence microscopy, HEK-KWGF or HEK-hERG cells cultured on 12mm Ø glass cover slips (Smethwick, Warley, UK) were fixed using 3% paraformaldehyde dissolved in PBS. After permeabilization with 0.5% Triton X-100 in PBS, cells were quenched with 50 mM glycine-PBS and blocked with NET-gel (150 mM NaCl, 5 mM EDTA, 50 mM Tris-HCl, pH 7.4, 0.05% Igepal, 0.25% gelatin, 0.02% NaN_3). Cells were then incubated overnight with either anti-GFP or anti-K_v11.1 primary antibody, for HEK-KWGF and HEK-hERG cells, respectively, followed by incubation with anti-mouse or anti-rabbit FITC conjugated secondary antibody (Jackson ImmunoResearch) for 2 h. Cover slips were mounted with Vectashield (Vector Laboratories Inc, Burlingame, CA, USA) and imaged using a 60x/1.40 NA Nikon PlanApo objective mounted on a Nikon Diaphot 300 microscope. Confocal images were made using a Nikon RCM 8000 confocal laser scanning unit with standardized settings for pinhole (1.5 µm confocality), PMT voltage (600 V) and Ar/Kr laser power (200 µW, 488 nm). Each acquired image was the result of 30 averaged frames acquired at 30 Hz.

For live-imaging of HEK-KWGF cells, cells were seeded on fluorodishes (WP1, Sarasota, Fl, USA), cultured for 24 h, and then incubated with 10 µM pentamidine for 24 h. Control cells were left untreated for 48 h after seeding. Cells treated with pentamidine for 6 h were first cultured for 42 h after seeding, and then treated with pentamidine for 6 h. Imaging was performed as described above for fixed cells.

Statistics

Group averages are presented as mean ± standard error of the mean. Differences between group averages were tested using Student's t-test in case of two groups or using a one-way ANOVA with a post-hoc test (Holm-Sidak) in the case of more than two groups. Differences were considered statistically

significant if $P < 0.05$. All analyses were carried out using KaleidaGraph 4.1 (Synergy Software, Reading, PA, USA).

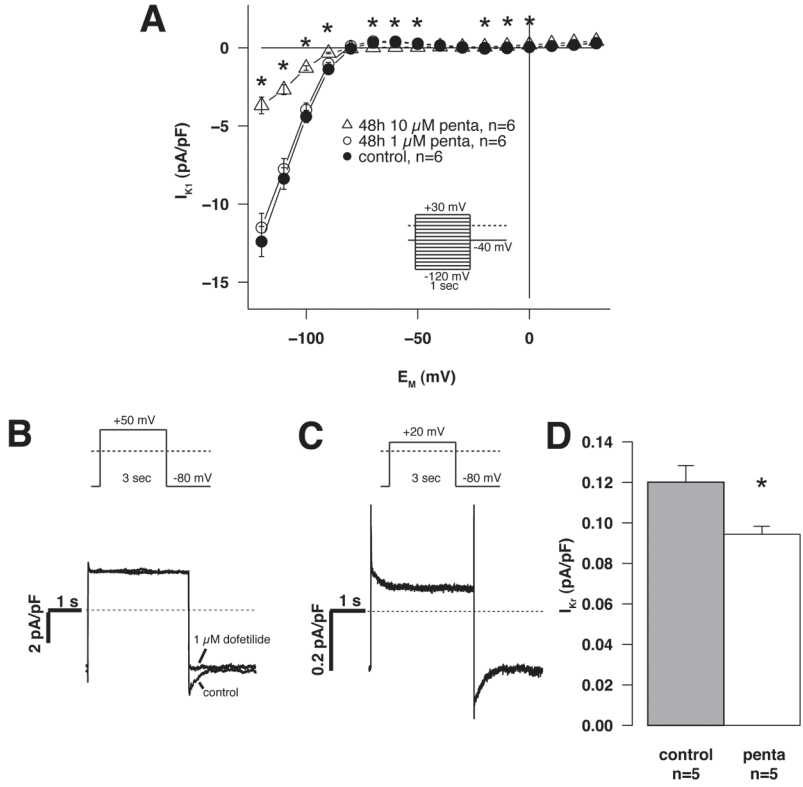

Figure 1. Inhibition of repolarising currents in cultured canine cardiomyocytes by long-term pentamidine exposure. (A) Plot depicting steady-state I_{K1} current density versus test potential, showing strong inhibition of I_{K1} by 10 µM, but not 1 µM pentamidine (48 h). * indicates a significant difference between control and 10 µM pentamidine current densities ($P<0.05$). (B) I_{Kr} measurement in freshly isolated canine cardiomyocyte, demonstrating the validity of the equimolar Cs^+ method. The tail current elicited by return to holding potential is fully blocked by the I_{Kr} blocker dofetilide. (C) Example of I_{Kr} measurement in cultured control canine cardiomyocyte using the equimolar Cs^+ method. No differences in tail current kinetics were observed between control and pentamidine exposed cells ($\tau = 0.26\pm0.03$ and 0.29 ± 0.04 s for control and pentamidine treated cells, respectively). (D) Bar plot showing decreased I_{Kr} tail current density after exposure to 10 µM pentamidine (48 h). * indicates $P<0.05$ (48 vs 0 h).

Results

We first determined the long term effects of a clinically relevant dose of pentamidine on potassium channel function in adult cardiomyocytes. Therefore, cultured isolated canine left ventricular cardiomyocytes were treated with

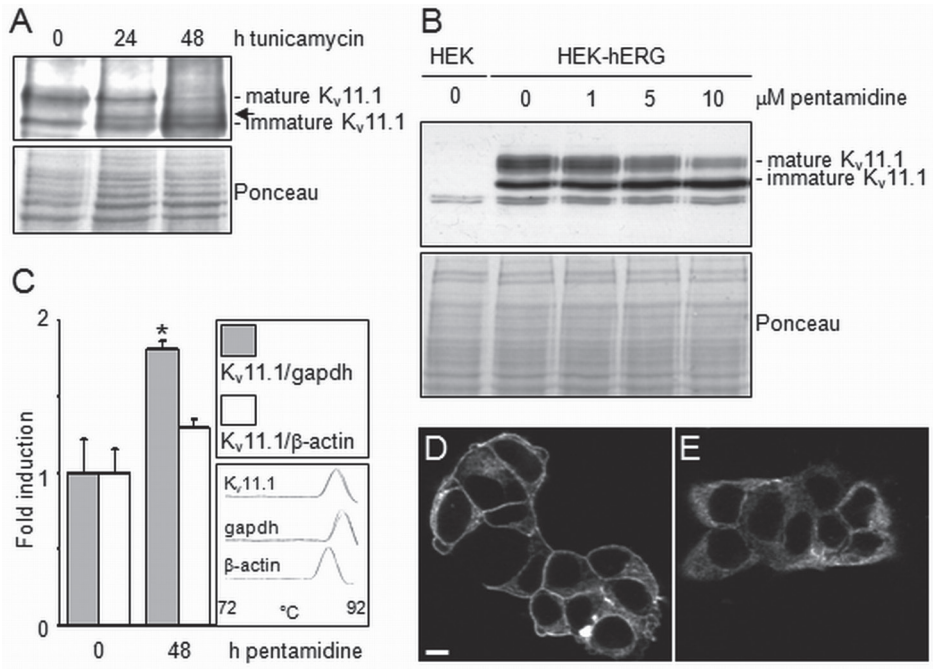

Figure 2. Pentamidine decreases mature K_v11.1 protein expression levels. (A) HEK-hERG cells treated with tunicamycin (5 μg/ml) for 24 and 48 h display progressive loss of mature K_v11.1. An intermediate form becomes visible upon treatment (arrow). Total protein staining (Ponceau) of Western blots was used as loading control. (B) HEK-hERG cells treated with increasing concentrations of pentamidine for 48 h display a concentration dependent decrease in mature K_v11.1 levels. Non-transfected HEK293 cell lysates were used as control. Total protein staining (Ponceau) of Western blots was used as loading control. (C) Real-time PCR reveals increased K_v11.1 mRNA levels when corrected for GAPDH expression (black bars), but no significant increase when corrected for β-actin (white bars). Expression in non-treated cells was indexed at 1.0; * indicates $P<0.05$ (48 vs 0 h). Melting curves for each product analyzed are shown to demonstrate amplification of a single product. (D) CLSM optical section of control HEK-hERG cells stained for K_v11.1 displays sharp demarcations at the edges and between individual cells, and diffuse cytoplasmic staining. Scale bar = 10 μm. (E) CLSM optical section of 10 μM pentamidine treated (24 h) HEK-hERG cells stained for K_v11.1, displaying diffuse cytoplasmic staining, but lacking sharp demarcations at the edges and between individual cells. Same magnification as in panel D.

pentamidine for 48 h. We observed a strong inhibition of I_{K1} after exposure for 48h to 10 μM pentamidine, but not with 1 μM (I_{K1} at -100 mV: -4.4 ± 0.4, -4.0 ± 0.4, and -1.3 ± 0.1 pA/pF for control, 1 μM, and 10 μM, respectively, see Figure 1A). Although current measurements were performed in absence of pentamidine, we detected altered current kinetics indicative of direct current block with 10 μM pentamidine (not shown, similar as in (De Boer *et al.*, 2010b)). We however cannot exclude protein downregulation contributing to reduced current levels in a 48 h timeframe (De Boer *et al.*, 2010). To measure I_{Kr} we applied the method reported by Zhang (2006) and first validated it using isolated canine cardiomyocytes. It was shown that the specific I_{Kr} blocker dofetilide completely inhibited the elicited tail current (Fig. 1B). Subsequently, pentamidine-induced inhibition of I_{Kr} was observed, be it to a smaller extent. 48 h exposure to 10 μM pentamidine significantly decreased the I_{Kr} tail current density from 0.120 ± 0.0082 to 0.094 ± 0.0039 pA/pF (Fig. 1C, D).

In HEK293 cells, K_v11.1 is expressed as a core N-glycosylated immature form (~135 kDa) and as a fully N-glycosylated mature form (~155 kDa) (Zhou *et al.*, 1998). Following treatment of our stably transfected HEK293 (HEK-hERG) cells with tunicamycin, a bacterial inhibitor of N-glycosylation, we observed loss of the mature form after 48 h, while an additional form, slightly larger than the immature form, was observed (Fig. 2B). In HEK-hERG cells it was observed that increased pentamidine concentrations of up to 10 μM for 48 h inhibited mature K_v11.1 protein levels (1.00, 0.83±0.02*, 0.57±0.07**, 0.47±0.05** for control, 1 μM, 5 μM, and 10 μM pentamidine, respectively; *P<0.05 and **P<0.01 vs control, N=3), while immature K_v11.1 levels showed a trend to increase (0.59±0.04, 0.58±0.08, 0.66±0.12, 0.81±0.13 for control, 1 μM, 5 μM, and 10 μM, respectively, as well as relative to control levels of the mature form), however did not reach significance (Fig. 2A). These data are indicative of interference in channel N-glycosylation, disturbed endoplasmic reticulum (ER) to Golgi transport, or both. To investigate whether pentamidine might interfere on the K_v11.1 mRNA level, quantitative PCR was performed. No apparent decrease in K_v11.1 mRNA levels was seen by real-time RT-PCR at the 48 h time point (Fig. 2C). Moreover, a significant increase in mRNA was observed when corrected for GAPDH, while a trend towards an increase was seen when corrected for β-actin. Finally, immunofluorescence microscopy revealed that K_v11.1 is expressed at the plasma membrane and diffusely in the cytoplasm in control cells (Fig. 2D). Upon pentamidine (10 μM) treatment for 24 h, plasma membrane expression was largely lost, while cytoplasmic staining appeared unaltered (Fig. 2E).

In insect Sf9 cells, Schwalbe *et al.* demonstrated that K_{IR}2.1 lacks N-glycosylation and is expressed as a single sized protein (Schwalbe *et al.*, 2002).

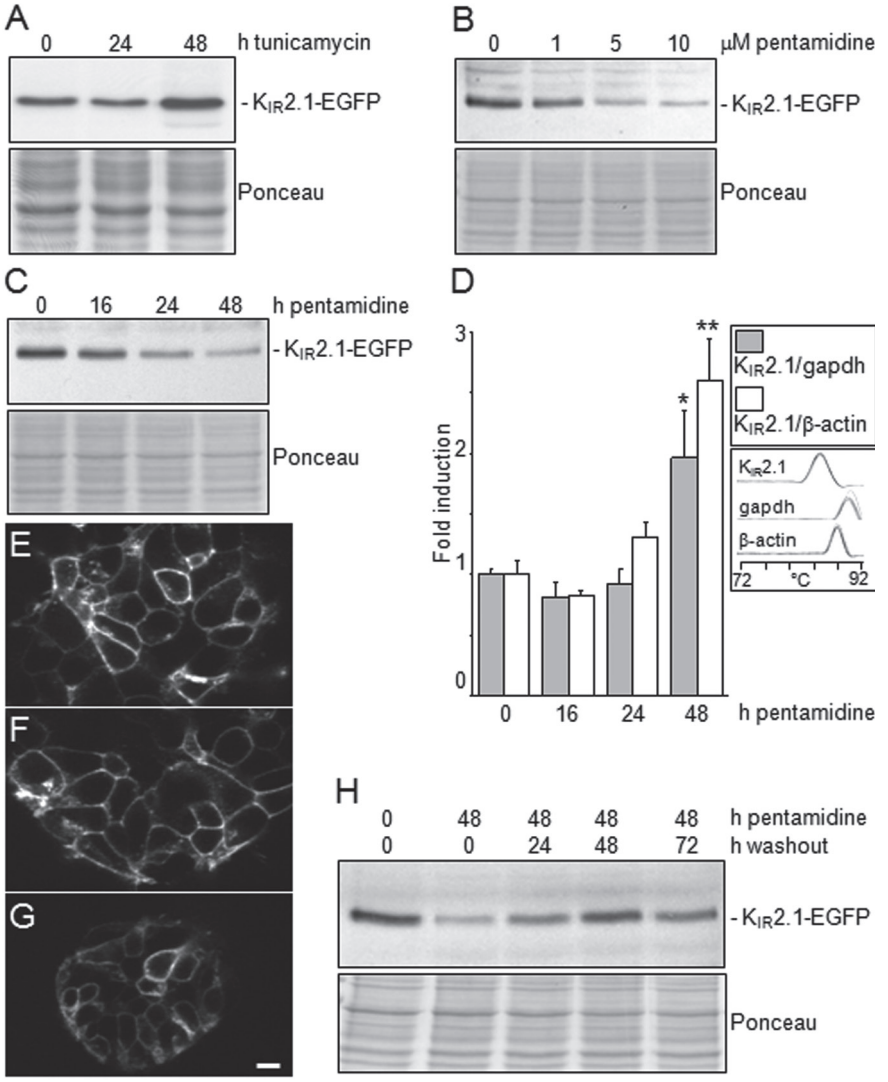

Figure 3. Pentamidine decreases $K_{IR}2.1$ protein expression levels. (A) HEK-KWGF cells treated with tunicamycin (5 µg/ml) for 24 and 48 h display no decrease in band intensity of the $K_{IR}2.1$-EGFP product. At 48 h, expression levels appear to increase. Total protein staining (Ponceau) of Western blots was used as loading control. (B) HEK-KWGF cells treated with increasing concentration of pentamidine for 48 h display decreased $K_{IR}2.1$-GFP protein expression. (C) HEK-KWGF cells treated for increasing time with 10 µM pentamidine display a time dependent decrease in $K_{IR}2.1$-GFP protein expression. Maximal $K_{IR}2.1$-GFP protein expression inhibition was seen after 48 h. (D) Real-time PCR reveals no significant change in $K_{IR}2.1$-GFP mRNA levels for 16 and 24 h time points, whereas a significant increase was observed at 48 h of treatment. $K_{IR}2.1$ mRNA

In HEK293 cells stably transfected with GFP-tagged $K_{IR}2.1$ (HEK-KWGF cells), the channel protein was present as a single band (Fig. 3A). In contrast to the $K_v11.1$ channel, tunicamycin treatment for up to 48 h did not decrease expression levels of the protein product, confirming in mammalian cells, previous data obtained from insect cells. Increasing concentrations of pentamidine decreased $K_{IR}2.1$-EGFP expression levels (1.00, 0.87±0.16, 0.42±0.05**, 0.33±0.05** for control, 1 μM, 5 μM and 10 μM pentamidine, respectively; **P<0.01 vs control, N=3), while no change in the size of the product was observed (Fig. 3B). A time course using 10 μM pentamidine indicated strongest inhibition at 48 h of treatment (1.00, 0.89±0.05, 0.61±0.06*, 0.46±0.10** for control, 16 h, 24 h and 48 h pentamidine, respectively; *P<0.05 and **P<0.01 vs control, N=3) (Fig. 3C). Decreased protein expression levels could not be explained by decreased $K_{IR}2.1$ mRNA levels as these remained similar for 24 h, while a significant increase was seen at 48 h (Fig. 3D). Confocal live imaging demonstrated that in control cells, $K_{IR}2.1$-EGFP is mainly expressed at the plasma membrane (Fig. 3E). Pentamidine treatment for 6 (Fig. 3F) or 24 h (Fig. 3G) did not alter this expression pattern; however expression levels were found to be decreased, such that it was necessary to adapt the image processing performed. Imaging did not reveal any intracellular accumulation of $K_{IR}2.1$-GFP at regions of the ER, Golgi apparatus, or endocytotic compartments. Since pentamidine in patients affects cardiac rhythm for several days following termination of medication (Quadrel *et al.*, 1992), we assessed the effect of wash-out of the drug. After an incubation period of 48 h with 10 μM pentamidine, it took a period of 24-48 h to restore original expression levels ((1.00, 0.43±0.13#, 0.85±0.20, 1.08±0.07, 0.78±0.10 for control, 48 h treatment, 24 h washout, 48 h washout, and 72 h washout, respectively; #P<0.1 vs control, N=3) (Fig. 3H), despite the presence of increased mRNA levels seen at 48 h of pentamidine treatment (Fig. 3D).

It has been shown that blockade of lysosomal degradation increases I_{K1} by augmenting functional $K_{IR}2.1$ protein levels (Jansen *et al.*, 2008). In this study, lysosomal inhibitors chloroquine, leupeptin, and NH_4Cl resulted in

levels were corrected for GAPDH (black bars) or β-actin (white bars). Expression in non-treated cells was indexed as 1.0; * indicates P<0.05 (48 vs 0, 16, and 24 h), ** indicates P<0.01 (48 vs 0, 16, and 24 h). (E) CLSM assisted live imaging of HEK-KWGF control cells displays mainly plasma membrane localized $K_{IR}2.1$-EGFP. (F, G) CLSM assisted live imaging of HEK-KWGF cells treated with 10 μM pentamidine for 6 (F) and 24 h (G) displays mainly plasma membrane localized $K_{IR}2.1$-EGFP. No intracellular accumulation was observed, although expression levels were decreased at 24 h. Scale bar = 10 μm (applies to panels E-G). (E) Pentamidine washout in HEK-KWGF restores original $K_{IR}2.1$-GFP expression levels after 24-48 h. Total protein staining (Ponceau) of Western blots was used as loading control.

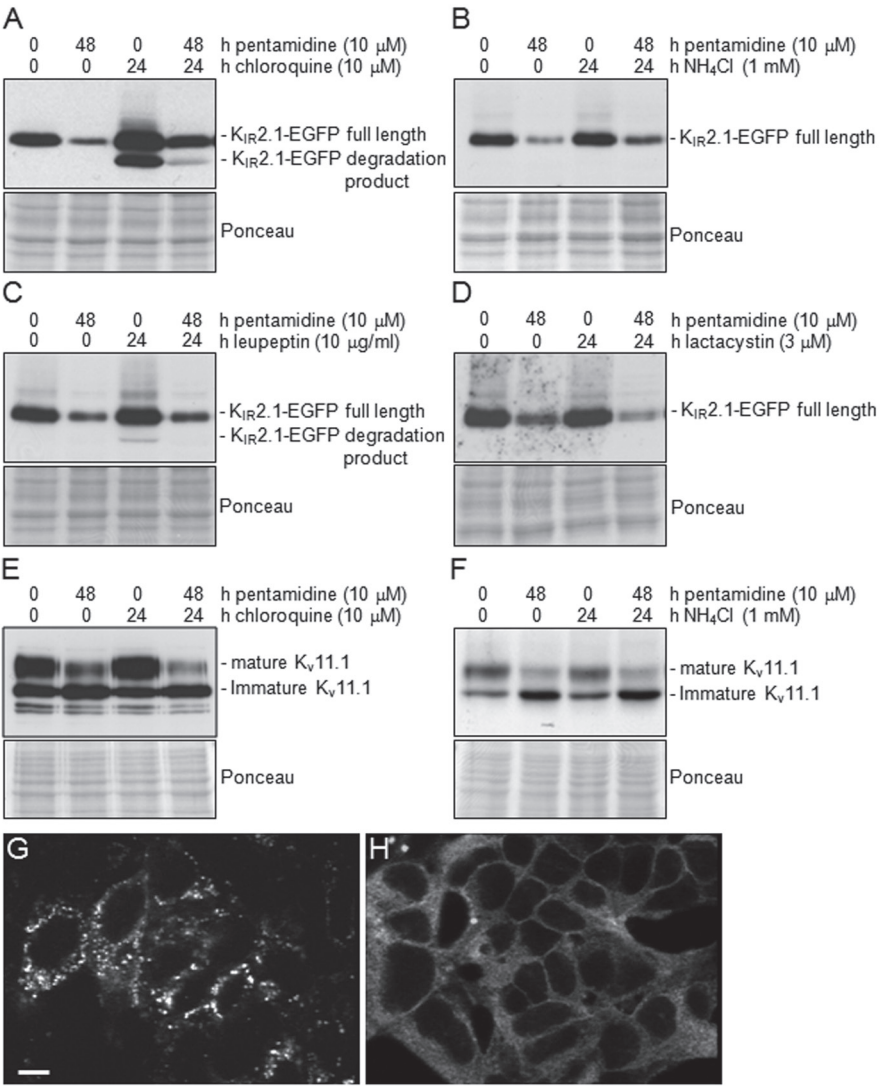

Figure 4. Inhibition of lysosomal degradation partially rescues K_{IR}2.1-GFP, but not mature K_v11.1 protein expression. (A, B, C) HEK-KWGF cells treated with 10 µM pentamidine for 24 h followed by 24 h of 10 µM pentamidine combined with lysosomal inhibitors chloroquine (10 µM; A), NH_4Cl (1 mM; B), or leupeptin (10 µg/ml; C). Control was left untreated for 48 h. Lysosomal inhibitor control was left untreated for 24 h followed by treatment with lysosomal inhibitors for 24 h. (D) HEK-KWGF cells treated with 10 µM pentamidine for 24 h followed by 24 h of 10 µM pentamidine combined with the proteasomal inhibitor lactacystin (3 µM). Control was left untreated for 48 h. Proteasomal inhibitor control was left untreated for 24 h followed by treatment with lactacystin inhibitors for 24 h. (E) HEK-hERG cells treated as in (A) display no

intracellular granular accumulation of $K_{IR}2.1$ in, what we presume, are lysosomes. Furthermore, upon Western blot analysis, chloroquine and leupeptin treatment yielded an additional protein product of a lower molecular weight, most likely a degradation product of the full length $K_{IR}2.1$-EGFP (Jansen *et al.*, 2008). In contrast, $K_v11.1$ is predominantly degraded via the proteasomal pathway under normal culture conditions (Gong *et al.*, 2005). To investigate whether pentamidine mediated decreases in $K_{IR}2.1$, but not that of $K_v11.1$, could be compensated by inhibiting lysosomal degradation, we treated HEK-KWGF cells with 10 µM pentamidine for 48 h and added the lysosomal inhibitor chloroquine during the last 24 h of the 48 h period. In the presence of chloroquine, original $K_{IR}2.1$-GFP expression levels were partially rescued (1.00, 0.40±0.11*, 0.84±0.18 for control, 48 h pentamidine, and 48 h pentamidine+24 h chloroquine, respectively, *P<0.05 vs control, N=3), despite the continuous presence of pentamidine (Fig. 4A). Furthermore, an extra band of lower molecular weight was present in the combination of pentamidine and chloroquine.

The less efficient blockers NH_4Cl (1.00, 0.30±0.04*, 0.43±0.11* for control, 48 h pentamidine, and 48 h pentamidine+24 h NH_4Cl, respectively, *P<0.05 vs control, N=2) (Fig. 4B) and leupeptin (1.00, 0.30±0.04*, 0.39±0.00* for control, 48 h pentamidine, and 48 h pentamidine+24 h leupeptin, respectively, *P<0.05 vs control, N=2) (Fig. 4C) also showed a trend towards rescue, but did not reach significance. In contrast, the proteasomal inhibitor lactacystin was completely unable to rescue pentamidine-mediated decreases in $K_{IR}2.1$-EGFP expression (1.00, 0.30±0.07*, 0.25±0.07* for control, 48 h pentamidine, and 48 h pentamidine+24 h lactacystin, respectively, *P<0.05 vs control, N=2) (Fig. 4E). As chloroquine was able to rescue $K_{IR}2.1$-EGFP levels, we next tested whether it was also able to rescue mature $K_v11.1$ expression. However, for this potassium channel, chloroquine was unable to rescue mature $K_v11.1$ expression levels in the presence of pentamidine (1.00, 0.28±0.04, 0.27±0.07, for control, 48 h pentamidine, and 48 h pentamidine+24 h chloroquine, respectively, *P<0.01 vs control, N=2) (Fig. 4E). Also NH_4Cl was unable to rescue mature $K_v11.1$ expression levels in the presence of pentamidine (1.00, 0.54±0.10, 0.45±0.15,

chloroquine mediated rescue of mature $K_v11.1$ expression. Total protein staining (Ponceau) of Western blots was used as loading control. (F) HEK-hERG cells treated as in (B) display no NH_4Cl mediated rescue of mature $K_v11.1$ expression. Total protein staining (Ponceau) of Western blots was used as loading control. (G) Immunostaining of HEK-KWGF cells treated with a combination of 10 µM pentamidine and 10 µM chloroquine for 24 h demonstrates intracellular accumulation of $K_{IR}2.1$-EGFP. Scale bar = 10 µm. (H) Immunostaining of HEK-hERG cells treated with a combination of 10 µM pentamidine and 10 µM chloroquine for 24 h demonstrates absence of intracellular accumulation of $K_v11.1$. Scale bar as in panel G.

for control, 48 h pentamidine, and 48 h pentamidine+24 h NH_4Cl, respectively, N=2) (Fig. 4F). Finally, co-application of pentamidine and chloroquine for 24 h resulted in intracellular accumulation of $K_{IR}2.1$-EGFP (Fig. 4G), presumably in lysosomes (Jansen *et al.*, 2008). In contrast, no intracellular accumulation was seen for $K_v11.1$ in HEK-hERG cells (Fig. 4H) and the expression pattern resembled that of 24 h pentamidine treatment (Fig. 2E).

Discussion

The ability of pentamidine to prolong QT-interval has been attributed to disturbed $K_v11.1$ trafficking (Kuryshev *et al.*, 2005; Cordes *et al.* 2005). In HEK-hERG cells, treatment with 10 μM pentamidine (48 h) resulted in a decrease of the mature form of $K_v11.1$ to 0.19 of control levels (1.00) (Cordes *et al.*, 2005). In our experiments with 10 μM pentamidine a lower extend of decrease was observed (0.43, average from experiments depicted in Figure 2B, 4E, 4F). Kuryshev and coworkers determined IC_{50} of mature $K_v11.1$ inhibition at 7.8 μM, which is in agreement with our experiments (0.57 with 5 μM and 0.47 with 10 μM pentamidine respectively). At the current level, Kuryshev *et al.* demonstrated less decrease in I_{Kr} in guinea-pig cardiomyocytes (0.65) than IK-$K_v11.1$ in HEK-hERG cells (0.35), which reflects our experiments in which I_{Kr} reduction in adult canine cardiomyocytes (0.78) was less than mature $K_v11.1$ reduction (0.43) in HEK-hERG cells. Hence, cardiomyocytes display less sensitivity towards pentamidine with respect to I_{Kr} than ectopically expressed $K_v11.1$ in HEK293 cells. Finally, maturation of Kv1.5 is not affected by pentamidine, which according to the authors depicts specificity of pentamidine for $K_v11.1$ (Kuryshev *et al.*, 2005). Here, we show that pentamidine inhibits expression of another potassium ion channel ($K_{IR}2.1$) although its underlying mechanism appears different.

Pentamidine has a wide variety of biological actions. Its antiprotozoal activity is thought to rely mainly on selective accumulation in the pathogen where it binds to AT sequences in the minor groove of kinetoplast DNA (Wilson *et al.*, 2008). In addition, pentamidine has been shown to interfere with pre-mRNA splicing (Warf *et al.*, 2009), tRNA function (Sun and Zhang, 2008), and RNA folding (Zhang *et al.*, 2002). We did not find a correlation between $K_v11.1$ and $K_{IR}2.1$ downregulation at the protein level and that of their mRNAs. Therefore, we conclude that pentamidine effects on these channels are not mediated by transcriptional interference. We, and others (Kuryshev *et al.*, 2005), demonstrated that pentamidine inhibits full N-glycosylation of $K_v11.1$, which may be either due to inappropriate trafficking from ER to Golgi or to direct interference of the glycosylation process in the Golgi itself. In addition, we

cannot rule out the possibility that core-glycosylation in the ER was disturbed. We are not aware of pentamidine affects on glycosylation of proteins other than K_v11.1.

For K_{IR}2.1, no N-glycosylation has been demonstrated (Schwalbe *et al.*, 2002) in insect cells, which is in agreement with our data in mammalian cells, showing presence of a single sized product only in HEK293 cells that are not affected by tunicamycin treatment, a bacterial inhibitor of N-glycosylation. We cannot exclude, however, that ER associated core-glycosylation was present in this channel that might be targeted by pentamidine. A reduction in K_{IR}2.1 protein following pentamidine may be due to translational interference, or to increased protein degradation via the lysosomal pathway. The latter would be consistent with tyrosine phosphatase inhibiting activity of pentamidine (Pathak *et al.*, 2002), as Tong and coworkers demonstrated that increasing tyrosine kinase activity, either by co-expression of v-Src or by PAO-mediated inhibition of tyrosine phosphatases, resulted in decreased K_{IR}2.1-mediated I_{K1} due to increased dynamin dependent internalization (Tong *et al.*, 2001). Also, pentamidine mediated increase in ER to lysosome trafficking, at the expense of ER to Golgi trafficking, is a possible mechanism that requires further experimentation.

For many mutation associated trafficking defects of ion channels, rescue of normal expression has been achieved by application of specific channel inhibitors (e.g. Zhou *et al.*, 1999; for a comprehensive review we refer to Balijepalli *et al.*, 2010). Whether rescue can also be achieved following acquired trafficking defects remains to be established. In addition to its action as an inhibitor of lysosomal degradation, chloroquine is also a direct K_{IR}2.1 blocker (Rodríguez-Menchaca *et al.*, 2008). This suggests that the observed chloroquine mediated rescue of K_{IR}2.1-EGFP expression could depend on direct chloroquine K_{IR}2.1-EGFP interaction, i.e. in the forward trafficking pathway, rather than on inhibiting lysosomal degradation of the protein. However, our observation that leupeptin and NH_4Cl also appear to mediate rescue (although no significant levels were reached in this study) and the fact that co-application of pentamidine and chloroquine results in intracellular accumulation of K_{IR}2.1-EGFP indistinguishable from NH_4Cl and leupeptin induced accumulation (Jansen *et al.*, 2008), argues against this possibility. Moreover, pentamidine itself can act as a direct inhibitor of K_{IR}2.1, by a similar mode of molecular interaction with the channel as chloroquine (De Boer *et al.*, 2010b).

In transfected HEK293 cells, augmented functional K_{IR}2.1 expression has been demonstrated using inhibition of lysosomal degradation (Jansen *et al.*, 2008). In contrast, expression levels of the immature form of K_v11.1 are increased upon proteasome inhibition, with mature protein levels left unchanged (Gong *et al.*, 2005). Therefore, inhibition of proteasomal mediated

K_v11.1 degradation does not appear to be a feasible mode of action for rescue of normal I_{Kr} densities that rely on mature forms of K_v11.1. The recognition of channel specific correction of adverse drug effects as shown here, provides an additional opportunity in drug development to circumvent ion channel based cardiotoxicity. Thus far, prevention of adverse drug effects on ion channels has focused mainly on removing the chemical characteristics that induce the side effects, such as direct channel block. Trafficking interference as a side effect, on the other hand, receives much less attention. Therefore, compounds that specifically act to normalize ion channel expression levels could be effective in counteracting adverse drug effects. These actions might be incorporated into the compound itself, or alternatively, additional drugs could be administered as part of a multi-drug therapy. Here, we have used the antimalarial drug chloroquine to inhibit pentamidine-mediated downregulation of K_{IR}2.1 channels. Although this is an effective action of chloroquine, it cannot be prescribed for this purpose clinically, as it is also an effective I_{K1} channel inhibitor (Rodríguez-Menchaca *et al.*, 2008), as thus would augment the effect of pentamidine on I_{K1}.

Using the HEK293 ectopic expression system for ion channel research has proven very efficient (Thomas and Smart, 2005), but the system bears some limitations. As I_{K1} in cardiomyocytes results from multiple K_{IR}2.x isoforms, in our HEK293 system we investigated the effects of pentamidine on K_{IR}2.1 only. Another obvious limitation of HEK293 cells is the lack of ancillary subunit expression for most of the ion channels which is one factor that can result in temporal differences in ion channel protein synthesis, subcellular trafficking and degradation when comparing HEK293 with native cells. Another confounder is absence of intercalated discs and T-tubules in HEK293 cells, two characteristic features of cardiomyocytes to which many cardiac ion channels localize and anchor at high densities. Nevertheless, main findings in native cells can most often be reproduced in HEK293 cells, although kinetics and sensitivity might be different.

Conclusions

Cardiac ion channel proteins K_v11.1 and K_{IR}2.1 are both subject to pentamidine mediated downregulation, although the underlying cellular mechanisms differ. Additionally, partial rescue of K_{IR}2.1 ion channel expression levels, but not those of K_v11.1, can be achieved by inhibiting lysosomal degradation.

Acknowledgements

We would like to thank Dr. C.J. January (University of Wisconsin-Madison, USA) and Dr. A. IJzerman (LUMC, Netherlands) for HEK-hERG cells, Jet Beekman (UMCU, Netherlands) for providing canine cardiomyocytes, and Dr. T.A. Quinn (University of Oxford) for critically proofreading the manuscript. This work was supported by a grant from Top Institute Pharma, (D2-101), Leiden, The Netherlands (L.N.).

Chapter 6

Comparison of I_{Kr} blocking drugs Moxifloxacin and Dofetilide/E-4031 in 5 screening models of pro-arrhythmia reveals insufficient specificity of isolated cardiomyocytes.

Nalos L, Varkevisser R, Jonsson MKB, Houtman MJC, Beekman JDM, van der Nagel R, Thomsen MB, Duker G, Sartipy P, de Boer TP, Peschar M, Rook MB, van Veen TAB, van der Heyden MAG, Vos MA.

Br J Pharmacol. 2011 Jun 30. Manuscript accepted

Background and purpose: Drug discovery and development require testing of new chemical entities for possible adverse effects. For cardiac safety screening, improved assays are urgently needed and isolated adult cardiomyocytes (CM) and human embryonic stem cell-derived cardiomyocytes (hESC-CM) may open new opportunities to identify pro-arrhythmic compounds. In the present study, five assays were employed, in the same laboratory, to investigate their sensitivity and specificity for elucidating pro-arrhythmic properties of I_{Kr} blocking drugs using moxifloxacin (safe compound) and dofetilide or E-4031 (unsafe compounds).
Experimental approach: The assays included: 1. The anesthetized remodeled chronic complete AV-block (CAVB) dog, 2. The anesthetized methoxamine sensitized unremodeled rabbit, 3. Multi-cellular hESC-CM clusters, 4. Isolated CM obtained from the CAVB dog and 5. Isolated CM obtained from the normal rabbit. Arrhythmic outcome was defined as Torsade de Pointes (TdP) in the animal models, and early afterdepolarizations (EADs) in the cell models.
Key results: At clinically relevant concentrations (5-12 μM), moxifloxacin was free of pro-arrhythmic properties in all assays with the exception of the isolated CM, in which 10 μM induced EADs in 35% of the CAVB CM and in 23% of the rabbit CM. At supra-therapeutic concentrations (≥100 μM), moxifloxacin was pro-arrhythmic in the isolated rabbit CM (33%), in the hESC-CM clusters (18%), and in the methoxamine rabbit (17%). The unsafe agents, dofetilide and E-4031, induced EADs or TdP in all five assays (50-83%), and the induction correlated with a significant increase in beat-to-beat variability of repolarization.
Conclusion and implications: Isolated cardiomyocytes lack specificity to discriminate between TdP liability of the I_{Kr} blocking drugs moxifloxacin and dofetilide/E4031.

Introduction

Healthy cardiac tissue is rather resistant to proarrhythmic agents. Nevertheless, the clinical incidence of class III antiarrhythmic (dofetilide, sotalol) induced Torsade de Pointes arrhythmias (TdP) is 1-5% (Pedersen *et al.*, 2007; Sasse *et al.*, 1998), stressing the necessity of safety pharmacological testing of new pharmaceutical compounds. In animal models, and most ventricular multi-cellular preparations, blocking of a single repolarizing current (single hit) does not cause a proarrhythmic outcome. Only drugs or interventions

affecting multiple repolarizing currents (double hit) are proarrhythmic, and as a result, sensitization of the testing models is required (Vos, 2008; Biliczki *et al.*, 2002). This phenomenon is attributed to repolarization reserve (Roden, 1998a). Exceptions to the rule of sensitization that are known so far include human embryonic stem cell-derived cardiomyocyte (hESC-CM) clusters (He *et al.*, 2003; Jonsson *et al.*, 2010) and Purkinje fibers (Roden and Hoffman, 1985), in which an arrhythmic endpoint can be reached using only one hit. Both these models show phase 4 diastolic depolarization. However, in the course of this investigation, it has been reported that a single hit is sufficient for induction of a proarrhythmic outcome in isolated canine CM (Abi-Gerges *et al.*, 2010; Johnson *et al.*, 2010), which suggests that isolated cardiomyocytes may be considered a potentially attractive screening model.

The most common cause of drug-induced QT prolongation is inhibition of the rapid component of the delayed rectifier potassium current (I_{Kr}) (Sanguinetti and Tristani-Firouzi, 2006). Due to its I_{Kr} blocking activity, the widely prescribed antibiotic moxifloxacin is often used as a gold standard in safety pharmacology testing: the thorough QT study (Sarapa *et al.*, 2008; Matthys *et al.*, 2010). In humans/volunteers (phase I), the very stable biokinetics of moxifloxacin increase the QT interval by 7-12 ms reproducibly but without inducing any arrhythmias. The plasma concentration of moxifloxacin at a 400mg/day dose amounts to 3-6 μM (1.7-3.4 μg/ml) with a 40% protein binding (Stass *et al.*, 1998; Zeitlinger *et al.*, 2008). At this concentration, moxifloxacin has been considered to be safe (Faich *et al.*, 2004; Andriole *et al.*, 2005), although some recent reports have related clinical administration of moxifloxacin with induction of TdP (Sherazi *et al.*, 2008; Badshah *et al.*, 2009; Poluzzi *et al.*, 2010). It is important to stress that these tachyarrhythmias were often observed when moxifloxacin was combined with other long QT predisposing factors, such as the use of diuretics.

The blocking effect of moxifloxacin is well-studied in HEK-293 cells that express K_v11.1 (the α-subunit of human Ether-a-go-go-related gene channel - hERG), but this is not true for native I_{Kr} in cardiomyocytes which is the result of expression of the alpha and beta subunit (minK). The half maximal inhibitory concentration (IC_{50}) values derived from cell culture experiments vary considerably and range from 0.75 to 129 μM (Anderson *et al.*, 2001; Kang *et al.*, 2001; Alexandrou *et al.*, 2006). Using various animal models with an arrhythmogenic outcome, higher concentrations (30-100 μM) of moxifloxacin administration induced variable results (Vos, 2008). Part of this can be attributed to the different concentrations of moxifloxacin that were administered, however not all variability in the results can be explained in this way. Therefore, other aspects like the (animal) model of choice, the type of anesthesia, or the particular

test laboratory employed should be considered as well since these factors affect the response to moxifloxacin.

In an attempt to overcome these confounding variables, we employed five test assays in the present study, ranging from anesthetized chronic complete AV block (CAVB) dogs and the methoxamine sensitized rabbits as well-established models, to multi-cellular human embryonic stem cell-derived cardiomyocyte clusters (hESC-CM) and single CM, isolated from chronically remodeled dog hearts or normal, unremodeled, rabbit hearts, as new promising models. Based on the fact that two hits are necessary for induction of arrhythmias in models with stable resting membrane potential, the CAVB dog CMs were used as a model with decreased repolarization reserve due to electrical remodeling as a first hit. In all models, the endpoint has been an arrhythmogenic outcome, ranging from triggered ectopic beats and spontaneous TdP in the first two (Carlsson, 2008; Oros *et al.*, 2008), to induction of early afterdepolarizations (EADs) in the latter three models (Antoons *et al.*, 2010; Jonsson *et al.* 2010). Using this comprehensive set of model systems, moxifloxacin (safe compound) was compared dose-dependently to the unsafe compounds dofetilide or E-4031, which both are rather specific I_{Kr} blockers. In this way, the sensitivity (ability to detect an unsafe drug) and specificity (ability to identify a safe drug) for these drugs could be determined in our experimental models. In addition, the arrhythmogenic parameter beat-to-beat variability of repolarization (BVR), quantified as short-term variability of repolarization (STV), has been taken into consideration as a surrogate predictor for TdP risk (Thomsen *et al.*, 2004). Our results indicate that the isolated CM assays lack sufficient specificity to recognize moxifloxacin as a safe drug at therapeutic concentrations.

Methods

Animal care and handling was performed in accordance with the 'European Directive for the Protection of Vertebrate animals used for Experimental and Scientific Purpose, European Community Directive 86/609/CEE'. All experiments were approved by the Committee for Experiments on Animals of the Utrecht University, The Netherlands. Drug/molecular target nomenclature conforms to BJP's Guide to Receptors and Channels (Alexander *et al.*, 2009)

CAVB dog

AV block was induced in 5 dogs (Marshall, NY, USA) by radiofrequency ablation according to methods described previously (Schoenmakers *et al.*,

2003). Experiments were performed >4 weeks after ablation allowing cardiac remodeling to complete.

Complete anesthesia was induced by pentobarbital (25 mg/kg i.v.) and maintained by halothane (0.5% in O_2 and N_2O, 1:2). Besides ECG, monophasic action potentials (MAP) from the endocardium of the free walls of the left (LV) and right ventricle (RV) were recorded. Perioperative care, signal processing and data recording have been described in detail previously [4].

Experimental protocol

Moxifloxacin was tested twice, at 2 (low) and 8 mg/kg (intermediate dose) and administered intravenously as a bolus over 5 minutes. This results in moxifloxacin plasma levels of 10μM and 50μM respectively. Plasma samples for drug-concentration have been published previously using the same dogs, however with different anesthetics (Thomsen *et al.*, 2006).

ECG analysis

Mean RR and QT intervals from lead LL, a left lateral precordial lead placed in the 6th intercostal space near the sternum, were measured manually (ECGview, Maastricht University, The Netherlands). Durations of the MAP to 90% repolarization (MAPD) were determined semi-automatically (ECG-Auto, EMKA Technologies, France). QT intervals were corrected for heart rate (QTc) according to Van de Water's formula (Van de Water *et al.*, 1989). Measurements were performed during periods without extrasystolic activity as previously described [2]. BVR was quantified as STV using LV MAPD.

Methoxamine-sensitized rabbit

The methoxamine-sensitized rabbit model of TdP as described by Carlsson *et al.* (1990) was implemented with minor adjustments. A total of 16 female New Zealand White rabbits (2.7-4.0 kg) were used in this study. Anesthesia was induced with intramuscular ketamine (35 mg/kg) and xylazine (5 mg/kg), and maintained with inhaled isoflurane (1.5%) in O2-supplemented air (1:1). After induction of anesthesia, the analgesic rimadyl (50 mg i.v.) was administered. Subsequently, the animals were instrumented as follows. The thorax was shaved and defibrillation patches were placed on both sides and connected to an external defibrillator. The marginal ear vein and central ear artery were cannulated for infusion of drugs, measurement of arterial blood pressure and withdrawal of

arterial blood samples, respectively. Surface ECG (leads I-III, aVL, aVR, and aVF) was recorded and stored continuously with a 12 channel ECG amplifier and the custom made computer data acquisition system scapsys (custom made software, Maastricht University, The Netherlands, sampling frequency 500 Hz). To avoid large deviations in body temperature, a thermal mattress was used during all experiments.

Experimental protocol

After preparation and instrumentation, the animals were allowed to stabilize for 10 min. Baseline recordings were obtained during this entire period (Table 2). Subsequently, a continuous infusion of methoxamine (15 μg/kg/min, 2 ml/h) was started. Ten minutes later, either a low dose moxifloxacin (0.1 mg/kg/min, n=4) or a high dose moxifloxacin (3 mg/kg/min, n=6) was infused for a maximum of 30 min. Low dose infusion of moxifloxacin results in plasma concentrations of 7±3 μM at 15 min and 9±3 μM after 30 min. High dose infusion results in 95±17 μM after 15 min and 107±15 μM after 30 min (n=2). A separate group of 6 rabbits was treated with dofetilide (10 μg/kg/min) using the same protocol.

ECG analysis

ECG data were analyzed off-line using ECGview (custom made software, Maastricht University, The Netherlands). BVR was determined by semi-automatic measurement of 30 consecutive QT intervals (ECG-Auto, EMKA Technologies, France), whereas RR, PR, QRS duration and QT were measured manually at baseline, after 10 min methoxamine, and every 5 minutes during drug treatment. For each time point, the displayed intervals represent the average of 5 beats of sinoatrial origin from the lead that provided the clearest signal (mainly lead II or III). Heart-rate corrected QT values were calculated using the formula especially developed for this particular animal model (Carlsson *et al.*, 1993). At some predetermined time points, ECG intervals could not be obtained from all animals because of arrhythmias and frequent premature ventricular contractions (PVC). After the experiments, the animals were sacrificed.

Human Embryonic Stem Cell-derived Cardiomyocytes

Stem cell preparation

Generation of hESC-CM clusters was preformed as described previously (Synnergren *et al.*, 2008), using the hESC line SA002 (Cellartis AB, Göteborg). Spontaneously contracting clusters were identified by visual inspection and isolated from the cultures by mechanical dissection. All experiments were performed after 42-56 days of differentiation. Clusters were transferred to collagen coated cover slips and left to attach and recover at least 3 days prior to experiments. Culture medium consisted of DMEM supplemented with glutamax, 1% Pen/Strep, 1% NEAA, 0.1 mM β-mercapto-ethanol, and 20% heat-inactivated FBS. Only clusters with a beating rate low enough to allow electrical pacing at 1 Hz and with the ventricular action potential duration at 90% repolarization (APD90) > 300 ms were used (Jonsson *et al.*, 2010).

Action potential recordings and solutions

Measurements of field-stimulated APs were performed using a HEKA EPC-10 Double Plus amplifier (HEKA, Lambrecht/Pfalz, Germany) controlled by PatchMaster 2.20. APs were evoked by biphasic field stimulation (frequency 1 Hz, pulse length 2 ms) using two platinum electrodes and a Grass S88 stimulator (Grass technologies, West Warwick, USA).

AP recordings were performed using sharp microelectrodes filled with 3 M KCl (pipette resistance 60-80 MΩ) in a Tyrode buffer consisting of (in mmol/l) NaCl 130, KCl 4, $NaHCO_3$ 18, $MgCl_2$ 1.2, $CaCl_2$ 1.8, HEPES 10, glucose 10, pH7.4/NaOH. The bath was continuously perfused and kept at 37±0.5 ºC using a TC2BIP controller (Cell Microcontrols, Norfolk, VA, USA).

Isolated dog and rabbit cardiomyocytes

Isolation of CAVB dog cardiomyocytes

Dog CMs were enzymatically isolated from the hearts of 12 CAVB dogs. Hearts were quickly excised and washed with cold Ca^{2+} free standard buffer solution (in mmol/l: NaCl 130, KCl 5.4, KH_2PO_4 1.2, $MgSO_4$ 1.2, HEPES 6, Glucose 20, pH 7.2/NaOH). The left circumflex coronary artery was cannulated and perfused by gravity at a pressure of 80 mm H_2O with solutions warmed up to 37°C in the following order: 1) Ca^{2+} free standard buffer solution for 10 minutes,

2) Enzymatic solution (in 400 ml of standard buffer solution: Collagenase A (Roche) 420 mg, Protease (Sigma-Aldrich) 32 mg, 2.5% Trypsin 400 µl) for 25-35 minutes, 3) 0.2 mmol/l Ca^{2+} standard buffer solution (Ca^{2+} free standard buffer solution with 0.2 mmol/l $CaCl_2$) for 10 minutes. Finally, midmyocardial tissue of left ventricular free wall was minced and the cell suspension was filtered. Isolated CMs were stored at room temperature in 0.2 mmol/l Ca^{2+} standard buffer solution and used the same day.

Isolation of rabbit cardiomyocytes

Rabbit CMs were enzymatically isolated from 10 New Zealand White Rabbits. Hearts were quickly excised and washed with cold Rabbit Ca^{2+} free solution (in mmol/l: HEPES 16.8, NaCl 146, $KHCO_3$ 3.3, $NaHCO_3$ 0.988, KH_2PO_4 1.4, $MgCl_2$ 1.9, Glucose 11 and $CaCl_2$ 9.75 µmol/l). The ascending aorta was cannulated with a glass cannula and the heart was retrogradely perfused by gravity at a pressure of 90 mm H_2O with solutions warmed up to 37°C in the following order: 1) Rabbit Standard buffer solution (in mmol/l: NaCl 128.5, KCl 4.7, $CaCl_2$ 1.45, $MgCl_2$ 0.6, $NaHCO_3$ 27, NaH_2PO_4 0.4, Glucose 11) for 15 minutes, 2) Rabbit Ca^{2+} free solution for 20 minutes, 3) Rabbit Enzymatic solution (in mg/150 ml of Ca^{2+} free solution: Creatine hydrate (Sigma-Aldrich) 320, Collagenase P (Roche) 9, Collagenase B (Roche) 22, Hyaluronidase (Sigma-Aldrich) 25, Trypsine inhibitor (Roche) 15) for 30 minutes at a pressure of 60 mmH_2O. Thereafter, the left ventricle was opened, the endocardial layer removed, and midmyocardial cells of the free wall were harvested. Isolated midmyocardial cells were shaken (2Hz) in rabbit enzymatic solution at 37°C for 17 minutes. The solution was replaced by rabbit enzymatic solution with 1% bovine serum albumin and shaken (4Hz) for an additional 10 minutes. Finally the cell suspension was filtered and washed 2 times with washing solution (Rabbit Ca^{2+} free solution with 1% bovine serum albumin added). Isolated CMs were stored at room temperature in Rabbit Ca^{2+} free solution with addition of 0.35 mmol/l $CaCl_2$ and 1% bovine serum albumin and were used the same day.

Action potential recording

The initial criteria for selecting cells for AP recordings were that they were rod-shaped, silent, and did not show any spontaneous activity. Besides that, the myocytes should show clear and regular striation, a clean membrane, and sharp edges. APs were measured with an AxoPatch 200B amplifier controlled by pClamp 9 software (Molecular Devices, Sunnyvale, CA, USA) in the whole-cell current clamp mode. Patch pipettes were pulled with a Sutter

P-2000 puller (Sutter Instrument, Novato, CA, USA) and had resistances of 2-3 MΩ. Modified Tyrode solution with the following composition (in mmol/l) was used: NaCl 137, KCl 5.4, $CaCl_2$ 1.8, $MgCl_2$ 0.5, HEPES 11.8, Glucose 10, pH 7.4/NaOH. Pipette solution contained (in mmol/l): NaCl 10, KCl 130, HEPES 10, $MgCl_2$ 0.5, MgATP 5, pH 7.2/KOH. Cells were stimulated with 2 ms current injections at a cycle length of 2000 ms. AP duration was measured at 90% repolarization (APD90). All recordings were performed at 37±0.5 ºC in a temperature controlled perfusion chamber (Cell Microcontrols, Norfolk, VA, USA). Recordings were made for at least 10 minutes after infusion of the drug was started. EADs generally occurred within 4 minutes after infusion started, and in that case recordings were stopped earlier.

Drugs

Dofetilide was initially dissolved in DMSO (4.4 mg/ml) for *in vitro* experiments and in 0.1 ml 0.1 mM HCl for *in vivo* experiments respectively. Subsequently, it was diluted in Tyrode's buffer or in 0.9% saline respectively to the required concentration.

E-4031 (Sigma-Aldrich) was dissolved in H_20 and kept as 10 mM stock solution (frozen at -20°C) which was diluted in Tyrode's solution prior to each experiment.

Moxifloxacin-HCl (Avelox) was dissolved and diluted to the desired concentration in Tyrode's solution and used for cellular and hESC-CM cluster experiments. For *in vivo* experiments, moxifloxacin was dissolved and diluted in 0.5% lactic acid. Moxifloxacin was applied as a low, intermediate or high dose.

Methoxamine-HCl (Sigma-Aldrich) was dissolved and diluted in saline and used for *in vivo* rabbit experiments.

Calculations and statistical analysis

All values are presented as mean±SD. One or 2-way repeated measures ANOVA followed by a Tukey or Bonferroni Post Hoc test when appropriate or Student's t-test were used for statistical evaluation, and $P<0.05$ was considered statistically significant. Correlations were evaluated using Pearson product moment correlation.

BVR was assessed using STV (based on 30 consecutive beats) which was calculated using the formula $STV=\Sigma \mid D_{n+1}-D_n \mid /[30\sqrt{2}]$ where D represents APD90 in *in vitro* models, MAPD in CAVB dogs, and QT in the methoxamine-

sensitized rabbit model respectively, and describes the mean orthogonal distance to the line-of-identity on a Poincaré plot, as described previously (Thomsen *et al.*, 2004).

The cells were considered inducible (positive arrhythmogenic outcome) when at least three EADs were observed. In dogs and rabbits, 3 TdP episodes was set as a minimum for animals to be considered as TdP inducible. TdP was defined as a polymorphic ventricular tachyarrhythmia with at least 5 consecutive undulating QRS complexes with a typical twisting around the isoelectric line of the ECG. A run of 3 or more consecutive PVC was classified as a short run of ventricular tachycardia (VT).

Results

	baseline #1	moxi-low	baseline #2	moxi-intermediate
RR (ms)	1264±245	1360±315	1330±305	1575±400[a]
QT (ms)	415±85	435±85	430±90	530±110[a]
QTc (ms)	390±65	405±60	400±65	480±75[a]
LV MAPD (ms)	345±55	375±90	345±70	440±115[a]
RV MAPD (ms)	300±60	325±70[a]	315±65[a]	365±85[a]
ΔMAPD (ms)	45±10	50±20	25±25	75±35[b]
STV (ms)	2.3±1.2	2.5±2.6	1.9±0.5	3.2±1.3

Table 1. CAVB dog electrophysiological parameters (mean±SD, n=5). [a] $p<0.01$ vs. baseline #1, baseline #2, and low dose of moxifloxacin, [b] $p<0.05$ vs. baseline #2

The anaesthetized CAVB dog

At the lower dosage, moxifloxacin (2 mg/kg) did not significantly change any of the electrophysiological parameters measured, except RV MAPD (QTc was unchanged; 390±65 vs. 405±60, see Table 1 for other parameters). After 30 minutes of 2 mg/kg moxifloxacin (baseline #2), most of the repolarization characterizing values were still similar as original (baseline #1) values. The intermediate dosage of moxifloxacin (8 mg/kg) increased all ECG parameters significantly (QTc 400±65 to 480±75, $p<0.01$, Table 1), with the exception of STV which did not change (1.9±0.5 to 3.2±1.3 ms). No TdP (0/5) could be induced by either dose of moxifloxacin.

Using different types of anesthesia we have previously shown that dofetilide caused TdP in 76% of CAVB dogs using pentobarbital (Oros *et al.*, 2008) and 100% using thiopental as anesthetic (Thomsen *et al.*, 2006). The latter dogs are the same animals as used for the moxifloxacin experiments in

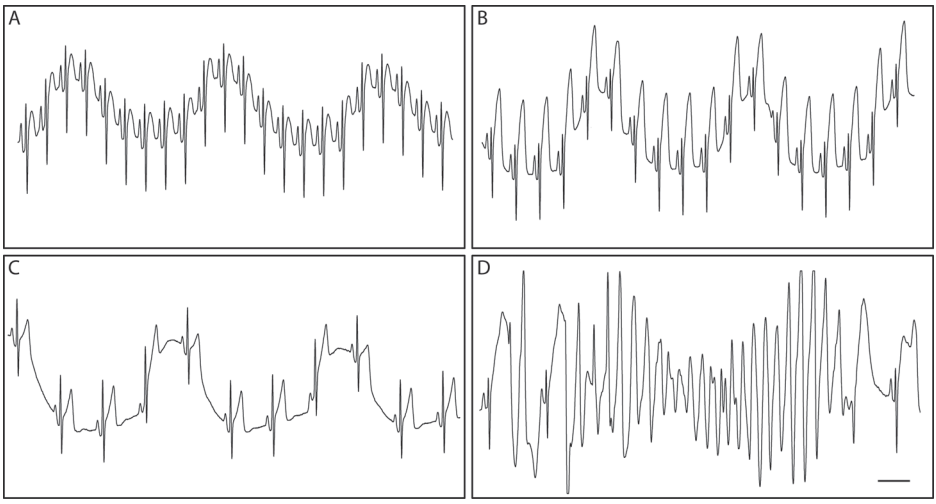

Figure 1. ECG recordings from the *in vivo* rabbit model. (A, C) rabbit treated with low dose moxifloxacin, A = baseline, C = 30 min moxifloxacin. (B,D) rabbit treated with high dose moxifloxacin showing TdP arrhythmia, B = baseline, D = 10 min moxifloxacin. Horizontal bar represents 0.5 seconds.

the present study, however pentobarbital was used as anesthetics. Dofetilide induced TdP was associated with a significant increase in QTc and STV.

The methoxamine-sensitized anesthetized rabbit

None of the animals experienced arrhythmias or PVCs during baseline. During infusion with methoxamine, mean blood pressure increased (62±11.2 to 93±22.7 mmHg) and the RR interval was prolonged (319±29 to 456±105

	base-line	**methox-amine**	**ML-1**	**ML-2**	**MH-1**	**MH-2**	**Dof**
RR (ms)	319±29	456±105[b]	513±127[b]	566±178[b]	534±100[b]	516±103[b]	632±156[ab]
PQ (ms)	78±12	81±12	88±9	90±8	94±20	100±21	93±21
QRS (ms)	50±4	51±5	53±3	52±3	56±6	63±13[ab]	75±18[ab]
QTc (ms)	170±12	160±13	165±9	181±6	223±37[ab]	291±73[abc]	244±36[abc]
STV (ms)	0.8±0.3	0.8±0.4	0.9±0.1	0.8±0.2	1.2±0.4	1.5±0.4	5.6±4.5[ab]

Table 2. Rabbit electrophysiological parameters (mean±SD). [a] $p<0.05$ vs methoxamine, [b] $p<0.05$ vs baseline, [c] $p<0.05$ vs ML-2. ML-1= low dose moxifloxacin at 5 min, ML-2= low dose moxifloxacin at 30 min, MH-1= high dose moxifloxacin at 5 min, MH-2= high dose moxifloxacin at 30 min, Dof= dofetilide at 5 min.

ms; n=16) (Table 2). Other ECG parameters remained unchanged and no arrhythmias or PVCs were observed. Subsequent infusion of moxifloxacin at a low (therapeutic, ML) or high (MH) concentration for 30 minutes caused significant QTc prolongation only in the high dose group (from 170±12 to ML 181±6, n=4 vs. MH 291±73 ms, n=6, $p<0.05$). STV did not increase significantly in any of the groups (from 0.8±0.3 to ML 0.8±0.2, n=4 vs. MH 1.5±0.4 ms, n=5). Moxifloxacin did not induce TdP at the low dosage (0/4), whereas at the high dose TdP was seen in 1 out of 6 rabbits (17%, Figure 1). This inducible animal experienced a total of 5 TdP episodes and 5 short runs of VT, which was

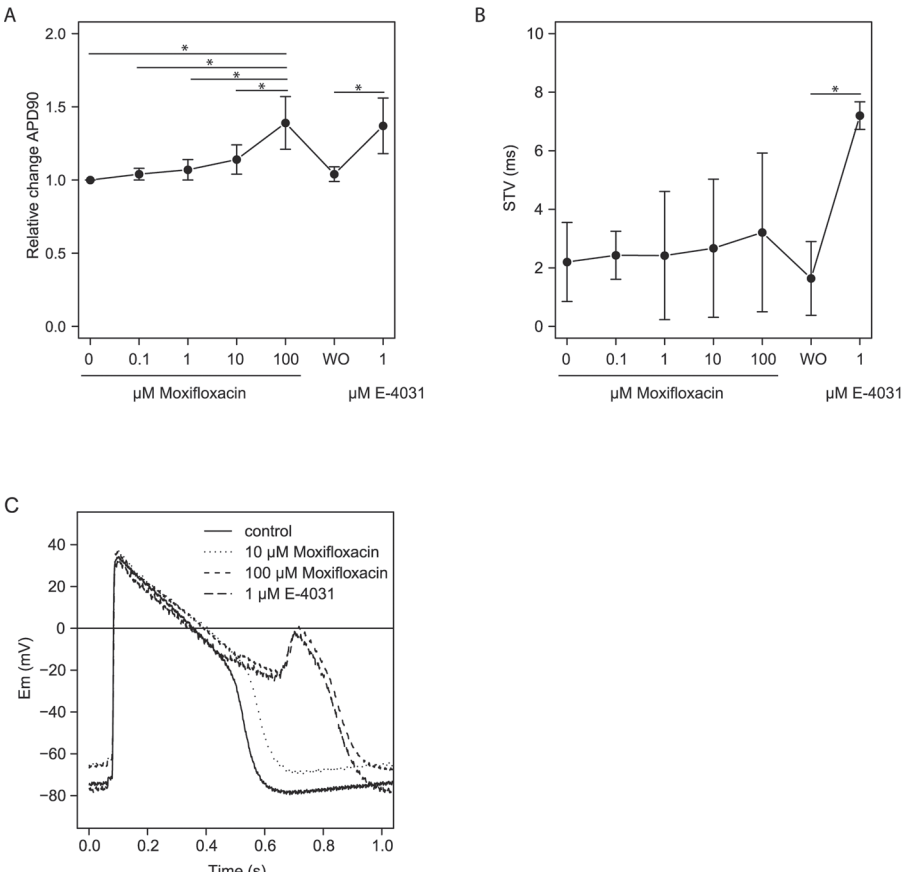

Figure 2. APD90, BVR and example of action potentials in hESC-CM. Alterations in APD90 (A) and BVR (B) after treatment with different concentrations of moxifloxacin (0.1, 1, 10 and 100 μM), or E-4031 (1 μM). (C) Example of action potential and induced EAD after treatment with either a low or a high concentration of moxifloxacin, or with E-4031.

associated with an STV increase to 25.7 ms just before the first TdP episode. In one other animal PVCs were observed at the high dose of moxifloxacin. All arrhythmias ceased within 20 minutes after the infusion of moxifloxacin was stopped.

At five minutes, dofetilide treatment caused prolongation of the RR, and QTc (244±36 ms; n=6), while STV was increased significantly to 5.6±4.5 ms (Table 2). In 5 out of 6 animals (83%) TdP was inducible. At the same time point, only the high dose of moxifloxacin significantly prolonged QTc, but not STV (Table 2, MH-1).

The multi-cellular hESC-CM clusters

In hESC-CM clusters, control APD90 was 381±47 ms (n=11) and STV 2.2±1.4 (n=10). 10 μM moxifloxacin (low concentration, within the therapeutic range) induced a small but not significant increase in APD90 (435±71 ms, n=11) and also STV was unchanged (2.7±2.4, n=9, Figure 2A and B). 100 μM moxifloxacin (high concentration) increased APD90 to 531±93 ms (n=11, $p<0.01$), comparable to the increase observed using 1 μM E-4031 (531±84 ms, n=8, $p<0.01$). The low concentration of moxifloxacin did not cause EADs, but an incidence of 18% (2/11) was seen with 100 μM (Figure 2C). In the same clusters, 1 μM E-4031 induced EADs in 50% (4/8). STV immediately prior to the first EAD was 5.2±4.3 (n=2, too low for statistical analysis) in the 100 μM moxifloxacin group and 9.4±3.7 (n=4, $p<0.05$ compared to control) for the E-4031 group.

The isolated remodeled canine ventricular myocyte

At 10 μM, moxifloxacin prolonged APD90 (324±57 to 402±120 ms, $p<0.01$), increased STV (15.7±7 to 34.5±24.5 ms, $p<0.01$), and induced EADs in 7/20 (35%) cells. An example is shown in Figure 3A. Dofetilide (1 μM) prolonged APD90 (384±111 to 490±134, $p<0.01$), increased STV (13.5±10.4 to 39.8±31.7 ms, $p<0.01$), and caused an EAD incidence of 15/25 (60%).

Analysis of the differences between inducible (n=7) and non-inducible (n=13) cells after 10 μM moxifloxacin revealed that baseline APD90 values were higher in inducible cells (365±62 vs. 302±43 ms, $p<0.05$), but STV (19.9±9.5 vs. 13.4±4 ms) was similar. In both groups, APD90 (492±142, $p<0.05$ vs. 354±74 ms, $p<0.01$) and STV (57±27.7 vs. 22.5±10.6 ms, $p<0.01$) were significantly prolonged following moxifloxacin infusion, but increases in APD90 and STV were significantly larger in the inducible cells (127 vs. 52 ms and 37 vs. 9 ms

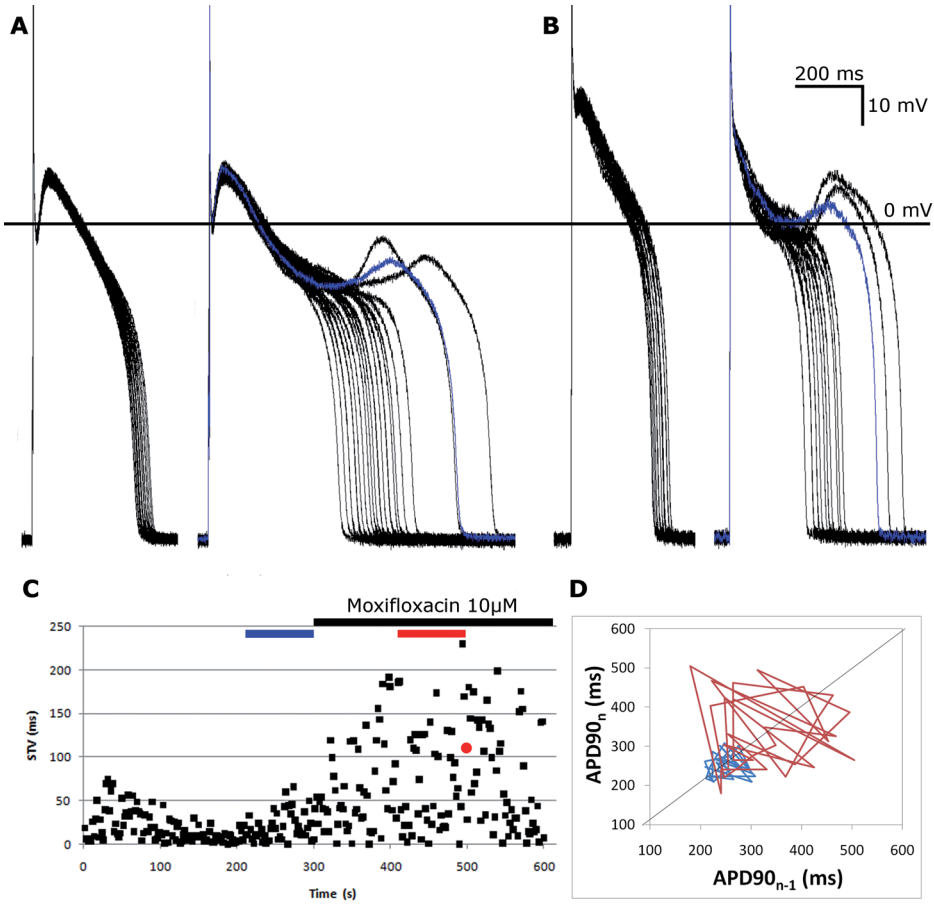

Figure 3. APD90, BVR and example of action potentials in hESC-CM. Alterations in APD90 (A) and BVR (B) after treatment with different concentrations of moxifloxacin (0.1, 1, 10 and 100 µM), or E-4031 (1 µM). (C) Example of action potential and induced EAD after treatment with either a low or a high concentration of moxifloxacin, or with E-4031.

respectively). Similarly, dofetilide (1µM) also increased APD90 and STV more in inducible cells (534±144 vs. 378±130 and 56.5±30.6 vs. 14.5±12.7, $p<0.01$; n=15) compared to non-inducible (423±98.7 vs. 394±79.9 and 14.8±8.2 vs. 12±5.7; $p>0.05$, n=10).

The isolated unremodeled rabbit ventricular myocyte

Moxifloxacin (10 µM) significantly increased APD90 (255±66 to 289±71 ms, $p<0.05$), STV (12±6.1 to 24±20.5 ms, $p<0.05$) and induced EADs in 3/13

cells (23%, Figure 3B). Example of the corresponding time-dependent behavior of APD90 and STV from a single rabbit CM is depicted in Figure 3C. In six cells that were resistant to EADs at 10 μM, infusion of 100 μM moxifloxacin resulted in a further increase in APD90 (482±163 ms, $p<0.05$), in STV (44.4±27.2 ms, $p<0.05$), and induced EADs in 2/6 cells.

Administration of 1 μM dofetilide significantly increased APD90 (277±45.8 to 528±241 ms, $p<0.01$), STV (15.4±3.5 to 66±38.7 ms, $p<0.01$) and EADs were observed in 5/8 cells (63%).

Overview of data

Arrhythmia incidence (TdP/EAD)	**Moxifloxacin**		**Dofetilide/E-4031**
	Low dose	**High dose**	
CAVB dog	0%[a]	76%[h]/100%[i]	
Methoxamine rabbit	0%[b]	17%[d]	83%[f]
hESC-CM clusters	0%[c]	18%[e]	50%[g]
Isolated rabbit CM	23%[c]	33%[e]	63%[g]
Isolated CAVB CM	35%[c]		60%[g]

Table 3. Arrhythmia inducibility by Moxifloxacin and Dofetilide/E-4031 in all models. [a] 2 mg/kg (10μM), [b] 0.1 mg/kg/min (9±3μM), [c] 10μM, [d] 3 mg/kg/min (107±15μM), [e] 100μM, [f] 10 μg/kg/min, [g] 1μM; [h] Oros *et al.*, 2008, [i] Thomsen *et al.*, 2006.

In Table 3, arrhythmogenic outcome for the different assays is summarized. It is clear that the isolated CM system provides acceptable sensitivity but lacks sufficient specificity to discriminate between the non- (moxifloxacin) and pro-arrhythmic (dofetilide) test drugs. The sensitivity (i.e., the ability to detect an unsafe drug – e.g. Dofetilide/E4031) is highest in animal models and lowest in hESC-CMs: 83% in methoxamine-sensitized rabbits, 76% in CAVB dogs, 63% in isolated rabbit CMs, 60% in isolated CAVB CMs, and 50% in hESC-CMs. The specificity (i.e., the ability to correctly detect a safe drug – i.e. low dose Moxifloxacin) is 100% in both *in vivo* models and the hESC-CM clusters, 77% in isolated rabbit CMs and 65% in isolated CAVB CMs.

Importantly, STV can be regarded as a parameter for detecting the pro-arrhythmic potential of the test drugs used since an increase in STV preceeds a subsequent arrhythmic outcome in all tested models.

Discussion

In the present work, we have demonstrated that all multi-cellular models tested were able to identify moxifloxacin as a safe compound despite the fact that this drug is an I_{Kr} blocker and prolongs the QT-interval. On the other hand, remodeled as well as unremodeled isolated cardiac ventricular myocytes lack sufficient specificity. The behavior of the arrhythmogenic marker STV was in line with the expectations and only a significant increase in STV corresponded to the occurrence of EADs or TdP.

Cardiac safety assessment

The current strategy of evaluating the cardiac toxicity of new drug candidates, as for instance applied by FDA, is based on the thorough QT/QTC study in healthy volunteers (ICH Guideline E14, 2005). If the QTc prolongation is less than 5 ms, the drug is considered to be safe, if it is more than 20 ms, the drug is labeled as unsafe. When the QTc prolongation is between 5 and 20 ms, additional verification of cardiac safety is required (ICH Guideline S7B, 2005). At the same time, the pharmaceutical industry is trying to identify possible unsafe drugs in early stages of drug development. For this purpose, a hERG assay is often used, in which the hERG blocking potency of the drug candidate is tested. Although informative, caution has been addressed that there is no clear correlation between hERG block/QT prolongation and proarrhythmic potential of the drug (Gintant, 2011; Martin *et al.*, 2004). Thus, a new assay that is not exclusively dependent on hERG block or QT prolongation is needed, preferably in combination with a surrogate parameter of pro-arrhythmia, such as STV.

Pre-clinical model systems for cardiac safety assessment

With the exception of the isolated ventricular myocytes, the other three assays used in the present study responded as anticipated. In the hESC-CM clusters and the methoxamine-sensitized rabbit, the low concentration of moxifloxacin (10 μM) did not induce any pro-arrhythmic endpoint, whereas the high concentration (> 100 μM) induced EADs (2/11) or TdP (1/6) respectively. In the anesthetized CAVB dog, only low and intermediate dosages were tested, and neither 2 mg/kg nor 8 mg/kg moxifloxacin did induce TdP. The observations were different in the isolated ventricular CMs. Already at the low concentrations (10 μM), moxifloxacin was able to induce EADs in a significant number of unremodeled rabbit CMs (3/13) and even more frequently (7/20) in the remodeled CAVB CMs. This clearly indicates a lower specificity of isolated ventricular CMs.

a. Intact animals

A previous study showed that moxifloxacin is safe (no QTc prolongation) at 10 mg/kg in conscious telemetered dogs (Chen *et al.*, 2005). Our results support that observation in an even more sensitive model, the anesthetized CAVB dog. This is in line with a previous report in which a different anesthetic was applied (Thomsen *et al.*, 2006).

In the methoxamine-sensitized rabbits, dofetilide induced TdP with comparable incidence that has been reported by others (Carlsson *et al.*, 2009). Moxifloxacin at high dosages (> 100 μM) induced TdP only in 1 out of 6 of our animals. Other authors reported no TdP arrhythmias using a similar dose, although experimental differences may account for this discrepancy (different type of anesthesia, dose, open thorax (Chiba *et al.*, 2004); different anesthesia regimen, lower moxifloxacin infusion rate (Anderson *et al.*, 2001).

b. Multi-cellular hESC-CM

This is the first time that a negative control has been tested in multi-cellular hESC-CM clusters. We and others have shown previously a somewhat higher sensitivity of these cells to hERG block (Caspi *et al.*, 2009; He *et al.*, 2003; Jonsson *et al.*, 2010; Pekkanen-Mattila *et al.*, 2010; Peng 2010), with APD prolongation, increase BVR, and formation of EADs (inducibility 60-69%) than our current study (50% inducibility). Here, we address specificity by showing that a therapeutic level of moxifloxacin results in slight but not significant APD prolongation and no increase in BVR or induction of EADs. Results from this model fit well with what is seen in other multi-cellular preparations, such as the rabbit ventricular wedge preparation and canine Purkinje fibers (Chen *et al.*, 2005), and show that this assay merits further validation for future safety pharmacology screening.

c. Isolated CM assay.

The ability of a single hit of dofetilide, ATXII or HMR1556 to induce EADs in isolated canine unremodeled ventricular myocytes has been published recently (Abi-Gerges *et al.*, 2010; Johnson *et al.*, 2010). Baseline STV calculated in the isolated CM from this study (15.7±7 in cAVB dog cells and 12.1±6.1 in rabbit CM) are comparable to those reported by Abi-Gerges et al (ranging from 9±2 to 16±4) and Johnson et al (estimated 8-10 at 0.5 Hz). In remodeled CAVB LV CM, we achieved moderately increased sensitivity (60%) for dofetilide-

induced EAD compared to unremodeled canine LV CM (55% and 42% (Abi-Gerges *et al.*, 2010; Johnson *et al.*, 2010)) at the same pacing frequency. Here, we demonstrate that even in unremodeled rabbit CMs, a single hit is enough to induce arrhythmias, whereas a second hit is mandatory in animal models and most multi-cellular preparations like canine RV papillary muscle (Biliczki *et al.*, 2002).

Unfortunately, no results concerning a negative control, like moxifloxacin, were provided in previous papers using the isolated CM test assay. Based on experience with multi-cellular preparations we originally chose the remodeled (predisposed) cells from CAVB dogs. In the course of these experiments, the CAVB dog myocytes responded with EADs already at the low concentration of moxifloxacin. As a comparison, we also included unremodeled myocytes from rabbits and evaluated the initiation of EADs. However, there was no major difference in arrhythmogenic outcome between these two types of cells with respect to moxifloxacin-induced EADs. This may be explained by the cell isolation procedure, which could lead to decreased repolarization reserve to such extent, that it overrides the effect of electrical remodeling of the CAVB dog cells. This hypothesis is in line with the increased STV levels in the uncoupled cells compared to the animal model from which they are derived. Although the exact mechanism of increased beat-to-beat variability of repolarization in isolated cells is not known, there are convincing data showing that beat-to-beat variability in calcium cycling results in BVR of APD through calcium sensitive channels. In multi-cellular preparations this variability is most likely attenuated by surrounding cells through electrotonic interaction (Pastore and Rosenbaum, 2000).

Another possible explanation could be the fact that we stimulated both cell types at 0.5 Hz. As the natural heart rate is much higher in rabbits than in dogs, this could be a confounding factor. At lower rates, the APD is increasing, making the cells more susceptible to hERG block (Bányász *et al.*, 2009).

STV as an alternative arrhythmogenic marker

In patients and animal models, STV has been proposed as a better or complementary predictor of arrhythmias than QT prolongation per se (e.g. Thomsen *et al.*, 2004; Hinterseer *et al.*, 2008; Takahara *et al.*, 2008; Carlsson *et al.*, 2009). In all assays tested in this study, STV was increased before the occurrence of TdP or EADs. In multi-cellular assays, STV increase was present only in inducible subjects. In isolated ventricular myocytes, STV was also significantly increased in non-inducible cells treated with moxifloxacin, but not with dofetilide. There is no obvious explanation for this observation.

In our experiments, the underlying STV calculation differed in the various models (MAPD in CAVB dogs, QTc in rabbits, and APD in hESC-CM clusters and isolated myocytes). It has been shown that in the *in vivo* animal models, changes in STV are comparable independently of the parameter used for calculating STV (Thomsen *et al.*, 2007). Whether BVR in cells or clusters has a similar etiology remains unknown.

Another way of assessing the proarrhythmic potential of a drug is by using TRIaD (Hondeghem *et al.*, 2001). Using three or four different parameters, an overall proarrhythmic score is given to the drug. Using TRIaD, a previous report predicted moxifloxacin to be safe at therapeutic concentrations, but with a small safety margin (Lawrence *et al.*, 2006). Dofetilide was identified as pro-torsadogenic at 20 nM (therapeutic concentration) and up in the same study. These results are in line with our multicellular and *in vivo* models, and support the hypothesis that isolated cardiomyocytes lack specificity to recognize moxifloxacin as a safe drug in the clinic.

Study limitation

Sensitivity and specificity data of the five models is based on one positive and one negative control compound only.

In summary, this study showed that a clinically relevant concentration of moxifloxacin did not cause arrhythmias in the three of the five multicellular assays tested, but was pro-arrhythmic in the two assays using isolated CMs. In this case, using isolated cardiomyocytes during safety pharmacology would result in a Type I error by falsely rejecting a safe drug. It is concluded that the sensitive isolated CM assay, irrespective whether obtained from remodeled or normal hearts, lacks specificity to recognize moxifloxacin as a safe drug. Clusters of hESC-CM are an attractive alternative for *in vivo* models as they combine sufficient sensitivity with high specificity.

Acknowledgements

This work was supported by a grant from Top Institute Pharma, (D2-101), Leiden, The Netherlands (L.N.) and by ZonMW-NWO (grant nr. 114000102 TAB vV).

Conflict of interest: Peter Sartipy is employed by Cellartis AB.

Chapter 7

General discussion

This thesis is focused on some important hurdles in cardiac safety assessment related to Torsade des Pointes (TdP) arrhythmia, which hampers development of new drugs. Within the larger framework in which this research was performed, we looked at these issues concerning development of new chemical entities (NCE) from three different angles (Fig. 1). From each expertise alone, development of NCE can be facilitated. However, in concert the three distinct fields facilitate each other. We have analyzed the issues from an electrophysiological perspective and demonstrate that state-of-the-art electrophysiology is very complementary to medicinal chemistry and in silico modeling and can place findings from these two fields into a physiological perspective.

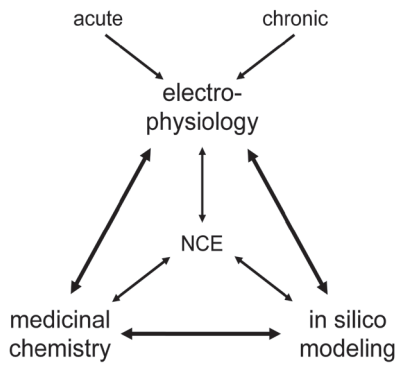

Figure 1. Concept of NCE development applied in this thesis

It is estimated, that about 75-86% of NCE is showing hERG inhibitory activity (Hoffmann and Warner 2006). Because of this, development of many promising NCE is presumably terminated because of their hERG channel inhibition potency. There are two possibilities how to circumvent this unwanted situation. First is to reduce hERG channel affinity of known NCE. Other possibility is to change the current approach in cardiac safety assessment in two ways. Cardiac safety assessment is based on the notion, that hERG block and/or significant QTc prolongation is associated with high risk of TdP arrhythmia. However, the correlation between hERG block, QTc prolongation and TdP arrhythmia is not always convincing (Gintant 2011). Thus, we suggest to make cardiac safety screening more specific to be able to identify safe drugs despite I_{Kr} block and action potential duration (APD) prolongation. It is also necessary to make cardiac safety assessment more sensitive in order to identify potentially unsafe drugs influencing other currents including channel protein trafficking.

Drug-channel interactions: Structure – Activity Relationship

Better understanding of the relation between the structure of a drug and its blocking activity can help in identification of chemical substructures in drugs that are responsible for hERG channel binding and block (a hERG blocker fingerprint). Replacement of these with inert substructures could allow the development of new drugs with low or no hERG blocking activity. A similar

approach applied to $K_{IR}2.x$ channel may be worthwhile in developing of a new specific I_{K1} blocker, which is needed for evaluation of the role of I_{K1} in cardiac arrhythmias including long QT syndrome. In chapters 2 and 4 we have combined different approaches to determine Structure – Activity Relationship (SAR) of the drug-channel interaction, including radioligand binding assay, patch clamp and in silico modeling. We have tested different analogues of known hERG (dofetilide) and $K_{IR}2.1$ (pentamidine) blockers.

In chapter 2, we have synthesized and tested 40 analogues of dofetilide and established SAR for their interaction with hERG. All analogues were evaluated in a radioligand binding assay. These experiments show two binding sites for dofetilide and some analogues, low and high affinity site. One selected analogue (#35), showing significantly higher affinity for low and similar affinity for high affinity site compared to dofetilide, was tested in patch clamp experiments to determine the relative contribution of these two binding sites to the hERG blocking effect in HEK293 cells expressing hERG channels. We have used a standard stimulation protocol to measure the peak of the hERG tail current and to determine the IC_{50} of block of both compounds (fig. 2A and B; chapter 2). The IC_{50} of both compounds was very close to K_i values for the high affinity site determined as by radioligand binding assay. For I_{Kr} block therefore only the high affinity binding site is physiologically relevant, because the K_i for the low affinity site is in the range where the current *in vivo* will be blocked completely. It is also obvious that binding to the low affinity site does not influence the drug binding to high affinity site as we have measured in patch clamp experiments slightly lower IC_{50} for dofetilide compared to compound 35.

Another interesting feature became apparent when we analyzed not only block of the tail current but also the block of the current elicited by depolarization. Dofetilide binds to the channel only when the cell is depolarized and the hERG channel is open or inactivated (Weerapura *et al.*, 2002). In steady state conditions the binding of dofetilide to the hERG channel is saturated and we did not see a large onset of the block during the depolarizing step (50% at the beginning, 54% at the end for 10 nM dofetilide). However, when we compared this to compound 35 (10 nM) we observed that at the beginning of the depolarization pulse only 15% of the channels were blocked whereas at the end of the depolarization step the block was 58% (fig. 2B). In our protocol the interval between two test pulses was 12 seconds and the cell was held at -80 mV during this period. At this membrane potential the hERG channel is closed (de-activated) and dofetilide as well as compound 35 cannot bind to the channel. It is likely that at this membrane potential both compounds are released from the channel binding site, but in the time frame used, it was not sufficient to release dofetilide in significant amount. On the other hand, compound 35 seems

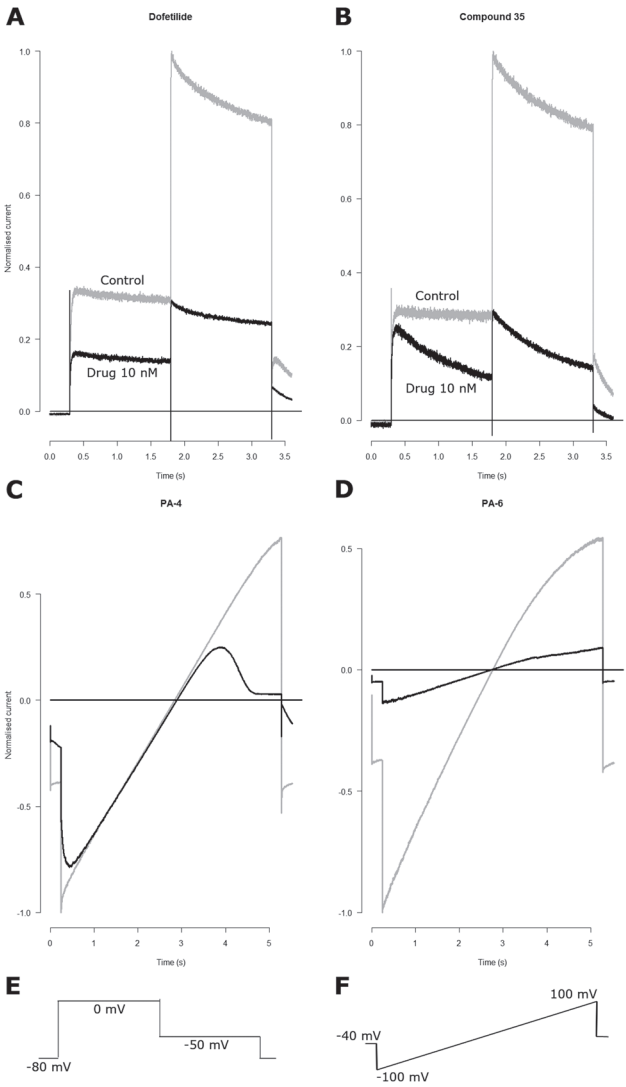

Figure 2. Time and voltage dependence of the hERG and $K_{IR}2.1$ block. During depolarization step dofetilide block is stable in time (panel A), whereas compound 35 block is increasing in time (panel B). During hyperpolarization PA-4 is released from the channel and channel is not blocked by PA-4 at negative membrane potentials, but the block occurs as the holding potential becomes more positive (panel C). The block with PA-6 is voltage insensitive (panel D). Holding protocols for hERG (E) and $K_{IR}2.1$ (F) measurements. Control measurements are colored gray, drug application is in black color.

to release relatively fast and following depolarization allows the drug to rapidly bind to the channel again. From this point of view dofetilide behaves as a stable blocking agent, whereas the blocking effect of compound 35 is dependent on duration of the test pulse (hERG channel open/inactivated) and the interval between subsequent test pulses (hERG channel closed/de-activated). When we try to translate this to the normal heart action, the effect of compound 35 will be dependent on the heart rate as well as on the duration of the action potential. It is also clear that at the beginning of the action potential the drug will not block the I_{Kr} with the same potency as at the end of the plateau phase. What consequences this finding has for the clinical use needs further investigation.

We have found voltage and time dependent block also during testing of the I_{K1} block by pentamidine analogues (chapter 4). When we compare the block of $K_{IR}2.1$ channel by PA-6 and PA-4, we can see that PA-6 blocks inward and outward component of I_{K1} to the same amount (fig. 2D). At the beginning of the testing pulse, when the test potential is negative (peak -100 mV with K+ reversal potential 0 mV), PA-4 is released from the binding site quite quickly, so when the testing pulse reaches -80 mV there is almost no block. As the test potential becomes positive, the drug again binds to the $K_{IR}2.1$ channel providing a block (fig. 2C). PA-4 is copying the behavior of the polyamines providing inward rectification to the $K_{IR}2.1$ channel. In contrast, PA-6 binds to the channel stably and it is not released by hyperpolarization. *In vivo* this might be relevant. We expect that PA-6 will block I_{K1} continuously and independently on the cardiac cycle because its effect is not voltage dependent. PA-4 will probably block I_{K1} preferably during the action potential, whereas resting membrane potential will be not influenced so strong. Thus PA-6 will be a useful tool to investigate roles of I_{K1} in cardiac arrhythmias. Conversely, PA-4 would be a better candidate in treating for example atrial fibrillation, because it will prolong action potential duration with no or restricted effect on resting membrane potential, keeping the heart excitability within safe margins.

These two examples show that including only IC_{50} values in cardiac safety assessment, might lead to the loss of information important for understanding of the behavior of the drug *in vivo*. Thus, testing protocols that will better reflect *in vivo* situation, like for example action potential clamp protocols would be a way to go.

Repolarization is not only mediated by I_{Kr}

It has been shown, that the correlation between hERG block and torsadogenicity of the drug is not very strong (Gintant 2011). hERG blockers with additional effects on other currents, like for example verapamil (I_{CaL}) or

ranolazine (late I_{NaL}) are in fact antiarrhythmic (Oros *et al.*, 2010; Antoons *et al.*, 2010). In chapter 3 we have demonstrated that drugs without significant acute hERG block still can have proarrhythmic properties because of a direct effect on other repolarizing current and an effect on channel protein trafficking during chronic treatment. This combined effect is associated with TdP incidence in patients (Kroll and Gettes 2002).

An increasing number of drugs are recognized as I_{K1} blocker, blocking the pore region or PIP_2-K_{IR}.2.1 interaction (for a review see van der Heyden and Sánchez-Chapula 2011). Moreover, enhancing I_{NaL} or blocking I_{Ks} was shown to potentiate the proarrhythmic effect of hERG channel block (Shimizu and Antzelevitch, 1997; Sun *et al.*, 2001; So *et al.*, 2006). In general, these drugs cannot induce TdP themselves, but in combination with another predisposition might be proarrhythmic.

It is also important to mention, that the heart is not a rigid system. Adrenergic stimulation accelerates gating of the I_{Ks} to compensate for the effect of sympathetic stimulation on I_{CaL} (Jost *et al.*, 2005). In this situation the importance of I_{Ks} in repolarization is increased and eventual block of this current might lead to TdP arrhythmia. Another example could be hypoxia of the heart that leads to opening of the I_{KATP} channels (Knopp *et al.*, 1999). This current is not contributing to the repolarization in normal situation. During hypoxia it becomes relevant and its block might significantly prolong the APD. Several chronic cardiac diseases are accompanied by electrical remodeling (reviewed in Wang and Hill 2010). Also in this situation the contribution of different repolarizing currents is changed compared to healthy heart. All these alterations might change sensitivity of the heart to different cardiac channel blockers and I_{Kr} does not necessarily have to remain the major repolarizing current.

In this perspective it is important to identify all currents that can be involved in TdP arrhythmia and to describe their relative contribution to repolarization, which is not fully known as yet. Based on these data, it is then necessary to develop an easy and high throughput drug screening assay that will comprise all major players.

Effect of drugs on channel trafficking and cardiac safety assessment

Trafficking of the ion channel proteins is not very well studied and thus poorly understood. However, drugs interfering with ion channel trafficking could be proarrhythmic (Van der Heyden *et al.*, 2008). This potential side effect of the drugs is not tested during drug development and such test is also not

required by the regulatory authorities. In chapters 3 and 5 we have shown that TdP arrhythmia linked to pentamidine treatment correlates with a combination of trafficking disruption of $K_{IR}2.1$ and hERG channels and direct blocking effect of pentamidine on the I_{K1}. Many drugs that disrupt protein trafficking are also directly inhibiting the membrane current (hERG: amoxapine, Obers *et al.*, 2010; fluconazole, Han *et al.*, 2010; desipramine, Staudacher *et al.*, 2011; $K_{IR}2.1$ + hERG: celastrol, Sun *et al.*, 2006; pentamidine, chapters 3 and 5 of this thesis). Conversely, other blockers are increasing protein levels. For example, expression of mutated hERG channel, which is deficient due to a mutation, is rescued by incubation of the cells with a potent hERG blocker E-4031 (Delisle *et al.*, 2003; Anderson *et al.*, 2006). Also our experiments with PA-6 in chapter 4 show increase in $K_{IR}2.1$ protein expression after 24 and 48 hour treatment. If this is just a coincidence or if the direct block (i.e. channel interaction) is necessary for the effect on protein trafficking is unclear.

In chapter 5 we have shown, that a single drug can disrupt trafficking of two structurally different channel proteins in different ways. Pentamidine prevents maturation of the hERG protein yielding less functional channels at the plasma membrane. The mechanism of trafficking disruption of $K_{IR}2.1$ remains unclear. Although ectopic expression systems, such as HEK293 cells, are informative in unraveling basic mechanisms, effort to study ion channel trafficking in cardiomyocytes should be increased, to fully appreciate all side effects on functional ion channel expression and to develop testing assays for detection of this type of adverse drug effect.

Models for testing torsadogenic potential of the drugs

In chapter 6 we compared five different testing models of TdP arrhythmia to assess their ability to distinguish between the unsafe drug dofetilide and the safe drug moxifloxacin. The main purpose of this study was to verify applicability of existing and new promising testing assays that are proposed to replace the current insufficient system. We have used two established animal models and compared them with *in vitro* assays. The animal models together with cell clusters of human embryonic stem cell derived cardiomyocytes (hESC-CM) were able to correctly recognize proarrhythmic properties of dofetilide and safety of moxifloxacin, whereas isolated adult cardiomyocytes (CM) were not. Recently, several drugs have been tested on isolated CMs (Abi-Gerges *et al.*, 2010; Johnson *et al.*, 2010) and CMs seemed to be sensitive enough to detect proarrhythmic drugs. In these studies selective I_{Kr} and I_{Ks} blockers and late sodium current enhancers showed arrhythmogenic outcome as expected. The multichannel blocker terfenadine showed a dose dependent behavior.

At low dosages its I_{Kr} blocking effect was prominent and isolated CMs were showing arrhythmogenic outcome. However, with increasing dose I_{CaL} block occurred and the proarrhythmic outcome disappeared. These findings suggest that isolated CMs are suitable to detect potentially dangerous drugs and drugs with multichannel action, but they will also give false positive results for safe drugs similar to moxifloxacin.

hESC-CM seem to be a promising model that can be used for cardiac safety assessment (Jonsson *et al.*, 2010). This model is able to distinguish between safe and unsafe I_{Kr} blockers (chapter 6). The main problem of hESC-CM is lack of I_{K1} current (Jonsson *et al.*, 2011). Potentially proarrhythmic I_{K1} blockers could not be detected in this assay. Moreover, the relatively low resting membrane potential, compared to adult CMs, is keeping sodium channels in the inactivated state and so they do not contribute much to the action potential. Therefore, safe multichannel blockers combining the effects on I_{Kr} and I_{NaL}, like for example ranolazine, will probably be detected by this assay as arrhythmogenic, although they are antiarrhythmic in reality. The less negative resting membrane potential also changes the behavior of I_{Kr}. It is slowing deactivation of the channel and also increasing the probability of the channel to open. Many I_{Kr} blockers bind to the open or inactivated state only, thus the output of this assay regarding I_{Kr} block needs to be interpreted with caution, because the blocking effect might be overestimated compared to the effect *in vivo*.

In chapters 4 and 6 we have tested short term variability (STV) of repolarization as a predicting marker for identifying drugs with proarrhythmic properties. STV was reasonably predicting the arrhythmogenic outcome in all models we have tested. We can propose STV of repolarization as a useful marker for cardiac safety assessment applicable in different models.

Conclusions and perspectives

In this thesis, I have commented on some weak points of the current drug cardiac safety assessment. Existing assays 1. rely too much on hERG channel block and QT prolongation. 2. measure hERG block at conditions not reflecting the *in vivo* situation and 3. determine acute drug effects only. Based on our findings what would be the perfect assay? First of all, such assay should include all major currents involved in repolarization of the human cardiac action potential, at best taking into account the relative contribution of each current. Secondly, this assay should also mimic the *in vivo* behavior of the channels during the action potential, preferably at different rates. And thirdly, it should also allow testing acute as well as chronic effects of the drugs on cardiac repolarization. It is unlikely, that we will be able to find an ideal and universal tool for testing the

torsadogenic potential of new compounds. Nevertheless combining advantages of new testing assays and improvement of the existing assays will definitely bring more new useful drugs and less unwarranted withdrawals of the drugs from the market.

If we want to find a high throughput assay, that even more is not very expensive, we have to focus on cell systems. A first option is to improve the current approach based on hERG assay and include also similar assays testing other currents shaping the phases 1-3 of the action potential (I_{Ks}, I_{K1}, I_{NaL}, I_{CaL} and others). Comparing the blocking profile of tested NCE with the profiles of drugs with known torsadogenicity could better predict the real arrhythmogenic potential of NCE than just the hERG assay. The stimulation protocol in these assays should mimic the normal cardiac action potential as much as possible to ensure that measured IC_{50} will be not over or underestimated.

Isolated cardiomyocytes are way too sensitive for direct use in cardiac safety assessment. One of the explanations for this could be higher baseline variability of APD in isolated cells (Pastore and Rosenbaum, 2000). The electrical coupling (coupling clamp) of two or more adult myocytes could be a way to stabilize the membrane potential and make isolated CMs less susceptible to arrhythmogenic hits and thus more specific (Zaniboni *et al.*, 2000).

hESC-CM are a very promising possibility, especially because the model is of human origin. The main disadvantage of this assay is lack of the I_{K1}. In the near future, increased understanding of the differentiation process may help us to produce more matured CMs with I_{K1} densities that will be similar to the adult human CMs.

Chapter 8

References

Abbott GW, Sesti F, Splawski I, Buck ME, Lehmann MH, Timothy KW, Keating MT, Goldstein SA (1999). MiRP1 forms IKr potassium channels with HERG and is associated with cardiac arrhythmia. Cell 97: 175-187.

Abi-Gerges N, Valentin JP, Pollard CE (2010). Dog left ventricular midmyocardial myocytes for assessment of drug-induced delayed repolarization: short-term variability and proarrhythmic potential. Br J Pharmacol 159: 77-92.

Ahmad K, Dorian P (2007). Drug-induced QT prolongation and proarrhythmia: an inevitable link? Europace 9: 16-22.

Aiba T, Shimizu W, Inagaki M, Noda T, Miyoshi S, Ding WG, Zankov DP, Toyoda F, Matsuura H, Horie M, Sunagawa K (2005). Cellular and ionic mechanism for drug-induced long QT syndrome and effectiveness of verapamil. J Am Coll Cardiol 45: 300-307.

Alexander SP, Mathie A, Peters JA. (2009). Guide to Receptors and Channels (GRAC), 4th edition (2009). Br J Pharmacol 158: S1-S254.

Alexander SPH, Mathie A, Peters JA (2008). Guide to receptors and channels (GRAC), 3rd edition (2008 revision). Br J Pharmacol 153: S1-S209.

Alexandrou AJ, Duncan RS, Sullivan A, Hancox JC, Leishman DJ, Witchel HJ, Leaney JL (2006). Mechanism of hERG K+ channel blockade by the fluoroquinolone antibiotic moxifloxacin. Br J Pharmacol 147: 905-916.

Anderson CL, Delisle BP, Anson BD, Kilby JA, Will ML, Tester DJ, Gong Q, Zhou Z, Ackerman MJ, January CT (2006). Most LQT2 mutations reduce Kv11.1 (hERG) current by a class 2 (trafficking-deficient) mechanism. Circulation 113: 365-373.

Anderson ME, Mazur A, Yang T, Roden DM (2001). Potassium current antagonist properties and proarrhythmic consequences of quinolone antibiotics. J Pharmacol Exp Ther 296: 806-810.

Andriole VT, Haverstock DC, Choudhri SH (2005). Retrospective analysis of the safety profile of oral moxifloxacin in elderly patients enrolled in clinical trials. Drug Saf 28: 443-452.

Antoons G, Oros A, Beekman JD, Engelen MA, Houtman MJ, Belardinelli L, Stengl M, Vos MA (2010). Late Na(+) current inhibition by ranolazine reduces torsades de pointes in the chronic atrioventricular block dog model. J Am Coll Cardiol 55: 801-809.

Antoons G, Oros A, Bito V, Sipido KR, Vos MA (2007). Cellular basis for triggered ventricular arrhythmias that occur in the setting of compensated hypertrophy and heart failure: considerations for diagnosis and treatment. J Electrocardiol 40: S8-14.

Antzelevitch C (2007). Ionic, molecular, and cellular bases of QT-interval prolongation and torsade de pointes. Europace 9: 4-15.

Anumonwo JMB, Lopatin AN (2010). Cardiac strong inward rectifier potassium channels. J Mol Cell Cardiol 48: 45-54.

Aronov AM (2006). Common pharmacophores for uncharged human ether-a-go-go-related gene (hERG) blockers. J Med Chem 49: 6917-6921.

Badshah A, Janjua M, Younas F, Halabi AR, Cotant JF (2009). Moxifloxacin-induced QT prolongation and torsades: an uncommon effect of a common drug. Am J Med Sci 338: 164-166.

Bakunova SM, Bakunov SA, Patrick DA, Suresh Kumar EVK, Ohemeng KW, Bridges AS, Wenzler T, Barszcz T, Kilgore Jones S, Werbovetz KA, Brun R, Tidwell RN (2009). Structure-activity study of pentamidine analogues as antiprotozoal agents. J Med Chem 52: 2016-2035.

Balijepalli S, Anderson CL, Lin EC, January CT (2010). Rescue of mutated cardiac ion channels in inherited arrhythmia syndromes. J Cardiovasc Pharmacol 56: 113-122.

Bányász T, Horváth B, Virág L, Bárándi L, Szentandrássy N, Harmati G, Magyar J, Marangoni S, Zaza A, Varró A, Nánási PP (2009). Reverse rate dependency is an intrinsic property of canine cardiac preparations. Cardiovasc Res 84: 237-244.

Bibler MR, Chou TC, Toltzis RJ, Wade PA (1988). Recurrent ventricular tachycardia due to Pentamidine-induced cardiotoxicity. Chest 94: 1303-1306.

Biliczki P, Virág L, Iost N, Papp JG, Varró A (2002). Interaction of different potassium channels in cardiac repolarization in dog ventricular preparations: role of repolarization reserve. Br J Pharmacol 137: 361-368.

Bilodeau MT, Balitza AE, Koester TJ, Manley PJ, Rodman LD, Buser-Doepner C, Coll KE, Fernandes C, Gibbs JB, Heimbrook DC, Huckle WR, Kohl N, Lynch JJ, Mao X, McFall RC, McLoughlin D, Miller-Stein CM, Rickert KW, Sepp-Lorenzino L, Shipman JM, Subramanian R, Thomas KA, Wong BK, Yu S, Hartman GD (2004). Potent N-(1,3-thiazol-2-yl)pyridin-2-amine vascular endothelial growth factor receptor tyrosine kinase inhibitors with excellent pharmacokinetics and low affinity for the hERG ion channel. J Med Chem 47: 6363-6372.

Bray PG, Barrett MP, Ward SA, De Koning HP (2003). Pentamidine uptake and resistance in pathogenic protozoa: past, present and future. Trends Parasitol 19: 232-239.

Brown AM (2004). Drugs, hERG and sudden death. Cell Calcium 35: 543-547.

Burashnikov A, Antzelevitch C (2002). Prominent I(Ks) in epicardium and endocardium contributes to development of transmural dispersion of repolarization but protects against development of early afterdepolarizations. J Cardiovasc Electrophysiol 13: 172-177.

Carlsson L (2008). The anaesthetised methoxamine-sensitised rabbit model of torsades de pointes. Pharmacol Ther 119: 160-167.

Carlsson L, Abrahamsson C, Andersson B, Duker G, Schiller-Linhardt G (1993). Proarrhythmic effects of the class III agent almokalant: importance of infusion rate, QT dispersion, and early afterdepolarisations. Cardiovasc Res 27: 2186-2193.

Carlsson L, Almgren O, Duker G (1990). QTU-prolongation and torsades de pointes

induced by putative class III antiarrhythmic agents in the rabbit: etiology and interventions. J Cardiovasc Pharmacol 16: 276-285.

Carlsson L, Andersson B, Linhardt G, Löfberg L (2009). Assessment of the ion channel-blocking profile of the novel combined ion channel blocker AZD1305 and its proarrhythmic potential versus dofetilide in the methoxamine-sensitized rabbit in vivo. J Cardiovasc Pharmacol 54: 82-89.

Caspi O, Itzhaki I, Kehat I, Gepstein A, Arbel G, Huber I, Satin J, Gepstein L (2009). In Vitro Electrophysiological Drug Testing using Human Embryonic Stem Cell Derived Cardiomyocytes. Stem Cells Dev 18: 161-172.

Cavalli A, Poluzzi E, De Ponti F, Recanatini M (2002). Toward a pharmacophore for drugs inducing the long QT syndrome: insights from a CoMFA study of HERG K(+) channel blockers. J Med Chem 45: 3844-3853.

Cens T, Rousset M, Leyris JP, Fesquet P, Charnet P (2006). Voltage- and calcium-dependent inactivation in high voltage-gated Ca(2+) channels. Prog Biophys Mol Biol 90: 104-117.

Cianchetta G, Li Y, Kang J, Rampe D, Fravolini A, Cruciani G, Vaz RJ (2005). Predictive models for hERG potassium channel blockers. Bioorg Med Chem Lett 15: 3637-3642.

Cordes JS, Sun Z, Lloyd DB, Bradley JA, Opsahl AC, Tengowski MW, Chen X, Zhou J (2005). Pentamidine reduces hERG expression to prolong the QT interval. Br J Pharmacol 145: 15-23.

Croft SL, Sundar S, Fairlamb AH (2006). Drug resistance in Leishmaniasis. Clin Microbiol Rev 19: 111-126.

Cross PE, Arrowsmith JE, Thomas GN, Gwilt M, Burges RA, Higgins AJ (1990). Selective class III antiarrhythmic agents. 1 Bis(arylalkyl)amines. J Med Chem 33: 1151-1155.

De Boer TP, Houtman MJC, Compier M, Van der Heyden MAG (2010a). The mammalian KIR2.x inward rectifier ion channel family: expression pattern and pathophysiology. Acta. Physiol. (Oxf) 199: 243-255.

De Boer TP, Nalos L, Stary A, Kok B, Houtman MJC, Antoons G, Van Veen TAB, Beekman HDM, De Groot BL, Opthof T, Rook MB, Vos MA, Van der Heyden MAG (2010b). The antiprotozoal drug pentamidine blocks KIR2.x-mediated inward rectifier current by entering the cytoplasmic pore region of the channel. Br J Pharmacol 159: 1532-1541.

De Boer TP, Van der Heyden MAG, Rook MB, Wilders R, Broekstra R, Kok B, Vos MA, De Bakker JMT, Van Veen TA (2006a). Pro-arrhythmogenic potential of immature cardiomyocytes is triggered by low coupling and cluster size. Cardiovasc Res 71: 704-714.

De Boer TP, Van Veen TA, Houtman MJ, Jansen JA, Van Amersfoorth SC, Doevendans PA, Vos MA, Van der Heyden MAG (2006b). Inhibition of cardiomyocyte automaticity

by electrotonic application of inward rectifier current from KIR2.1 expressing cells. Med Biol Eng Comput 44: 537-542.

Delisle BP, Anderson CL, Balijepalli RC, Anson BD, Kamp TJ, January CT (2003). Thapsigargin selectively rescues the trafficking defective LQT2 channels G601S and F805C. J Biol Chem 278: 35749-35754.

Dhamoon AS, Jalife J (2005). The inward rectifier current (IK1) controls cardiac excitability and is involved in arrhythmogenesis. Heart Rhythm 2: 316-324.

Diaz GJ, Daniell K, Leitza ST, Martin RL, Su Z, McDermott JS, Cox BF, Gintant GA (2004). The [3H]dofetilide binding assay is a predictive screening tool for hERG blockade and proarrhythmia: Comparison of intact cell and membrane preparations and effects of altering [K+]o. J Pharmacol Toxicol Methods 50: 187-199.

Dinges J, Albert DH, Arnold LD, Ashworth KL, Akritopoulou-Zanze I, Bousquet PF, Bouska JJ, Cunha GA, Davidsen SK, Diaz GJ, Djuric SW, Gasiecki AF, Gintant GA, Gracias VJ, Harris CM, Houseman KA, Hutchins CW, Johnson EF, Li H, Marcotte PA, Martin RL, Michaelides MR, Nyein M, Sowin TJ, Su Z, Tapang PH, Xia Z, Zhang HQ (2007). 1,4-Dihydroindeno[1,2-c]pyrazoles with acetylenic side chains as novel and potent multitargeted receptor tyrosine kinase inhibitors with low affinity for the hERG ion channel. J Med Chem 50: 2011-2029.

Dobrev D, Wettwer E, Kortner A, Knaut M, Schüler S, Ravens U (2002). Human inward rectifier potassium channels in chronic and postoperative atrial fibrillation. Cardiovasc Res 54: 397-404.

Donnelly H, Bernard EM, Rothkotter H, Gold JWM, Armstrong D (1988). Distribution of pentamidine in patients with AIDS. J Infect Dis 157: 985-989.

Dujardin JC, Campino L, Canavate C, Dedet JP, Gradoni L, Soteriadou K, Mazeris A, Ozbel Y, Boelaert M (2008). Spread of vector-borne diseases and neglect of Leishmaniasis, Europe. Emerg Infect Dis 14: 1013-1018.

Eckardt L, Breithardt G, Haverkamp W (2002). Electrophysiologic characterization of the antipsychotic drug sertindole in a rabbit heart model of torsade de pointes: low torsadogenic potential despite QT prolongation. J Pharmacol Exp Ther 300: 64-71.

Ehrlich JR (2008). Inward rectifier potassium currents as a target for atrial fibrillation therapy. J Cardiovasc Pharmacol 52: 129-135.

Eisenhauer MD, Eliasson AH, Taylor AJ, Coyne Jr, PE, Wortham DC (1994). Incidence of cardiac arrhythmias during intravenous pentamidine therapy in HIV-infected patients. Chest 105: 389-394.

Ekins S, Balakin KV, Savchuk N, Ivanenkov Y (2006). Insights for human ether-a-go-go-related gene potassium channel inhibition using recursive partitioning and Kohonen and Sammon mapping techniques. J Med Chem 49: 5059-5071.

El Harchi A, McPate MJ, Zhang YH, Zhang H, Hancox JC (2009). Action potential clamp and chloroquine sensitivity of mutant KIR2.1 channels responsible for variant 3

short QT syndrome. J Mol Cell Cardiol 47: 743-747.

Faich GA, Morganroth J, Whitehouse AB, Brar JS, Arcuri P, Kowalsky SF, Haverstock DC, Celesk RA, Church DA (2004). Clinical experience with moxifloxacin in patients with respiratory tract infections. Ann Pharmacother 38: 749-754.

Farid R, Day T, Friesner RA, Pearlstein RA (2006). New insights about HERG blockade obtained from protein modeling, potential energy mapping, and docking studies. Bioorg Med Chem 14: 3160-3173.

Ficker E, Taglialatela M, Wible BA, Henley CM, Brown AM (1994). Spermine and spermidine as gating molecules for inward rectifier K+ channels. Science 266: 1068-1072.

Fraley ME, Arrington KL, Buser CA, Ciecko PA, Coll KE, Fernandes C, Hartman GD, Hoffman WF, Lynch JJ, McFall RC, Rickert K, Singh R, Smith S, Thomas KA, Wong BK (2004). Optimization of the indolyl quinolinone class of KDR (VEGFR-2) kinase inhibitors: effects of 5-amido- and 5-sulphonamido-indolyl groups on pharmacokinetics and hERG binding. Bioorg Med Chem Lett 14: 351-355.

Friesen RW, Ducharme Y, Ball RG, Blouin M, Boulet L, Côté B, Frenette R, Girard M, Guay D, Huang Z, Jones TR, Laliberté F, Lynch JJ, Mancini J, Martins E, Masson P, Muise E, Pon DJ, Siegl PK, Styhler A, Tsou NN, Turner MJ, Young RN, Girard Y (2003). Optimization of a tertiary alcohol series of phosphodiesterase-4 (PDE4) inhibitors: structure-activity relationship related to PDE4 inhibition and human ether-a-go-go related gene potassium channel binding affinity. J Med Chem 46: 2413-2426.

Fujiwara Y, Kubo Y (2006). Functional roles of charged amino acid residues on the wall of the cytoplasmic pore of KIR2.1. J Gen Physiol 127: 401-419.

Gaborit N, Steenman M, Lamirault G, Le Meur N, Le Bouter S, Lande G, Léger J, Charpentier F, Christ T, Dobrev D, Escande D, Nattel S, Demolombe S (2005). Human atrial ion channel and transporter subunit gene-expression remodeling associated with valvular heart disease and atrial fibrillation. Circulation 112: 471-481.

Gintant G (2011). An evaluation of hERG current assay performance: Translating preclinical safety studies to clinical QT prolongation. Pharmacol Ther 129: 109-119.

Girgis I, Gualberti J, Langan L, Malek S, Mustaciuolo V, Costantino T, McGinn TG (1997). A prospective study of the effect of I.V. pentamidine therapy on ventricular arrhythmias and QTc prolongation in HIV-infected patients. Chest 112: 646-653.

Girmatsion Z, Biliczki P, Bonauer A, Wimmer-Greinecker G, Scherer M, Moritz A, Bukowska A, Goette A, Nattel S, Hohnloser SH, Ehrlich JR (2009). Changes in microRNA-1 expression and IK1 up-regulation in human atrial fibrillation. Heart Rhythm 6: 1802-1809.

Goa KL, Campoli-Richards DM (1987). Pentamidine isethionate: a review of its antiprotozoal activity, pharmacokinetic properties and therapeutic use in Pneumocystis carinii pneumonia. Drugs 33: 242-258.

Gong Q, Keeney DR, Molinari M, Zhou Z (2005). Degradation of trafficking-defective long QT syndrome type II mutant channels by the ubiquitin-proteasome pathway. J Biol Chem 280: 19419-19425.

Gonzalez A, Sager PT, Akil B, Rahimtoola SH, Bhandari AK (1991). Pentamidine-induced torsade de pointes. Am Heart J 122: 1489-1492.

Guo J, Massaeli H, Li W, Xu J, Luo T, Shaw J, Kirshenbaum LA, Zhang S (2007). Identification of IKr and its trafficking disruption induced by probucol in cultured neonatal rat cardiomyocytes. J Pharmacol Exp Ther 321: 911-920.

Han S, Zhang Y, Chen Q, Duan Y, Zheng T, Hu X, Zhang Z, Zhang L (2011). Fluconazole inhibits hERG K(+) channel by direct block and disruption of protein trafficking. Eur J Pharmacol 650: 138-144.

He J, Kargacin ME, Kargacin GJ, Ward CA (2003). Tamoxifen inhibits Na+ and K+ currents in rat ventricular myocytes. Am J Physiol Heart Circ Physiol 285: H661-668.

He JQ, Ma Y, Lee Y, Thomson JA, Kamp TJ (2003). Human embryonic stem cells develop into multiple types of cardiac myocytes: action potential characterization. Circ Res 93: 32-39.

Heginbotham L, Lu Z, Abramson T, MacKinnon R (1994). Mutations in the K+ channel signature sequence. Biophys J 66: 1061-1067.

Hinterseer M, Thomsen MB, Beckmann BM, Pfeufer A, Schimpf R, Wichmann HE, Steinbeck G, Vos MA, Kaab S (2008). Beat-to-beat variability of QT intervals is increased in patients with drug-induced long-QT syndrome: a case control pilot study. Eur Heart J 29: 185-190.

Hirano Y, Hiraoka M (1988). Barium-induced automatic activity in isolated ventricular myocytes from guinea-pig hearts. J Physiol 395: 455-472.

Hoffmann P, Warner B (2006). Are hERG channel inhibition and QT interval prolongation all there is in drug-induced torsadogenesis? A review of emerging trends. J Pharmacol Toxicol Methods 53: 87-105.

Hondeghem LM (2008). QT and TdP. QT: an unreliable predictor of proarrhythmia. Acta Cardiol 63: 1-7.

Hondeghem LM, Carlsson L, Duker G (2001). Instability and Triangulation of the Action Potential Predict Serious Proarrhythmia, but Action Potential Duration Prolongation Is Antiarrhythmic. Circulation 103: 2004-2013.

Hugnot JP, Pedeutour F, Le Calvez C, Grosgeorge J, Passage E, Fontes M, Lazdunski M (1997). The human inward rectifying K+ channel Kir 2.2 (KCNJ12) gene: gene structure, assignment to chromosome 17p11.1, and identification of a simple tandem repeat polymorphism. Genomics 39: 113-116.

Champeroux P, Viaud K, El Amrani AI, Fowler JS, Martel E, Le Guennec JY, Richard S (2005). Prediction of the risk of Torsade de Pointes using the model of isolated canine Purkinje fibres. Br J Pharmacol 144: 376-385.

Chapman H, Ramström C, Korhonen L, Laine M, Wann KT, Lindholm D, Pasternack M, Törnquist K (2005). Downregulation of the HERG (KCNH2) K(+) channel by ceramide: evidence for ubiquitin-mediated lysosomal degradation. J Cell Sci 118: 5325-5334.

Chen X, Cass JD, Bradley JA, Dahm CM, Sun Z, Kadyszewski E, Engwall MJ, Zhou J (2005). QT prolongation and proarrhythmia by moxifloxacin: concordance of preclinical models in relation to clinical outcome. Br J Pharmacol 146: 792-799.

Chézalviel-Guilbert F, Davy JM, Poirier JM, Weissenburger J (1995). Mexiletine antagonizes effects of sotalol on QT interval duration and its proarrhythmic effects in a canine model of torsade de pointes. J Am Coll Cardiol 26: 787-792.

Chiba K, Sugiyama A, Hagiwara T, Takahashi S, Takasuna K, Hashimoto K (2004). In vivo experimental approach for the risk assessment of fluoroquinolone antibacterial agents-induced long QT syndrome. Eur J Pharmacol 486: 189-200.

Chiba K, Sugiyama A, Satoh Y, Shiina H, Hashimoto K (2000). Proarrhythmic effects of fluoroquinolone antibacterial agents: in vivo effects as physiologic substrate for torsades. Toxicol Appl Pharmacol 169: 8-16.

Chiu PJ, Marcoe KF, Bounds SE, Lin CH, Feng JJ, Lin A, Cheng FC, Crumb WJ, Mitchell R (2004). Validation of a [3H]astemizole binding assay in HEK293 cells expressing HERG K+ channels. J Pharmacol Sci 95: 311-319.

Choe H, Nah KH, Lee SN, Lee HS, Lee HS, Jo SH, Leem CH, Jang YJ (2006). A novel hypothesis for the binding mode of HERG channel blockers. Biochem Biophys Res Commun 344: 72-78.

Ibarra J, Morley GE, Delmar M (1991). Dynamics of the inward rectifier K+ current during the action potential of guinea pig ventricular myocytes. Biophys J 60: 1534-1539.

ICH Harmonized Tripartite Guideline E14 (2005). The Clinical Evaluation of QT/QTc Interval Prolongation and Proarrhythmic Potential for Non-antiarrhythmic Drugs. Available at: http://www.ich.org/fileadmin/Public_Web_Site/ICH_Products/Guidelines/Efficacy/E14/Q_As/E14_Q__As_Final_Concept_Paper_March_15_2010x.pdf

ICH Harmonized Tripartite Guideline S7B (2005). The Non-Clinical Evaluation of the Potential for Delayed Ventricular Repolarization (QT Interval Prolongation) by Human Pharmaceuticals Available at: http://www.ich.org/fileadmin/Public_Web_Site/ICH_Products/Guidelines/Safety/S7B/Step4/S7B_Guideline.pdf

Imoto Y, Ehara T, Matsuura H (1987). Voltage- and time-dependent block of iK1 underlying Ba2+-induced ventricular automaticity. Am J Physiol 252: H325-333.

Irwin JJ, Shoichet BK (2005). ZINC--a free database of commercially available compounds for virtual screening. J Chem Inf Model 45: 177-182.

Ishihara K, Ehara T (2004). Two modes of polyamine block regulating the cardiac inward rectifier K+ current IK1 as revealed by a study of the KIR2.1 channel expressed

in a human cell line. J Physiol 556: 61-78.

Ishihara K, Yan DH (2007). Low-affinity spermine block mediating outward currents through KIR2.1 and KIR2.2 inward rectifier potassium channels. J Physiol 583: 891-908.

Iyengar RR, Lynch JK, Mulhern MM, Judd AS, Freeman JC, Gao J, Souers AJ, Zhao G, Wodka D, Doug Falls H, Brodjian S, Dayton BD, Reilly RM, Swanson S, Su Z, Martin RL, Leitza ST, Houseman KA, Diaz G, Collins CA, Sham HL, Kym PR (2007). An evaluation of 3,4-methylenedioxy phenyl replacements in the aminopiperidine chromone class of MCHr1 antagonists. Bioorg Med Chem Lett 17: 874-878.

Jamieson C, Moir EM, Rankovic Z, Wishart G (2006). Medicinal chemistry of hERG optimizations: Highlights and hang-ups. J Med Chem 49: 5029-5046.

Jansen JA, De Boer TP, Wolswinkel R, Van Veen TA, Vos MA, Van Rijen HV, Van der Heyden MAG (2008). Lysosome mediated KIR2.1 breakdown directly influences inward rectifier current density. Biochem Biophys Res Commun 367: 687-692.

Johnson DM, Heijman J, Pollard CE, Valentin JP, Crijns HJ, Abi-Gerges N, Volders PG (2010). I(Ks) restricts excessive beat-to-beat variability of repolarization during beta-adrenergic receptor stimulation. J Mol Cell Cardiol 48: 122-130.

Johnson CH, VanTassell VJ (1991). Acute barium poisoning with respiratory failure and rhabdomyolysis. Ann Emerg Med 20: 1138-1142.

Jonsson MK, de Boer TP, Duker G, Sartipy P, Vos MA, van Veen TAB (2011). Human embryonic stem cell-derived cardiomyocytes as a new model for screening of pro-arrhythmia: predictive value beyond hERG block. Heart Rhythm 8: S184.

Jonsson MK, Duker G, Tropp C, Andersson B, Sartipy P, Vos MA, van Veen TA (2010). Quantified Proarrhythmic Potential of Selected Human Embryonic Stem Cell-derived Cardiomyocytes. Stem Cell Res 4: 189-200.

Joshi A, Dimino T, Vohra Y, Cui C, Yan GX (2004). Preclinical strategies to assess QT liability and torsadogenic potential of new drugs: the role of experimental models. J Electrocardiol 37: 7-14.

Jost N, Virág L, Bitay M, Takács J, Lengyel C, Biliczki P, Nagy Z, Bogáts G, Lathrop DA, Papp JG, Varró A (2005). Restricting excessive cardiac action potential and QT prolongation: a vital role for IKs in human ventricular muscle. Circulation 112: 1392-1399.

Judd AS, Souers AJ, Wodka D, Zhao G, Mulhern MM, Iyengar RR, Gao J, Lynch JK, Freeman JC, Falls HD, Brodjian S, Dayton BD, Reilly RM, Gintant G, Limberis JT, Mikhail A, Leitza ST, Houseman KA, Diaz G, Bush EN, Shapiro R, Knourek-Segel V, Hernandez LE, Marsh KC, Sham HL, Collins CA, Kym PR (2007). Identification of diamino chromone-2-carboxamides as MCHr1 antagonists with minimal hERG channel activity. Bioorg Med Chem Lett 17: 2365-2371.

Kang J, Wang L, Chen XL, Triggle DJ, Rampe D (2001). Interactions of a series of

fluoroquinolone antibacterial drugs with the human cardiac K+ channel HERG. Mol Pharmacol 59: 122-126.

Kannankeril PJ, Roden DM (2007). Drug-induced long QT and torsade de pointes: recent advances. Curr Opin Cardiol 22: 39-43.

Kawai M, Nakamura H, Sakurada I, Shimokawa H, Tanaka H, Matsumizu M, Ando K, Hattori K, Ohta A, Nukui S, Omura A, Kawamura M (2007). Discovery of novel and orally active NR2B-selective N-methyl-D-aspartate (NMDA) antagonists, pyridinol derivatives with reduced HERG binding affinity. Bioorg Med Chem Lett 17: 5533-5536.

Knopp A, Thierfelder S, Koopmann R, Biskup C, Böhle T, Benndorf K (1999). Anoxia generates rapid and massive opening of KATP channels in ventricular cardiac myocytes. Cardiovasc Res 41: 629-640.

Kramer C, Beck B, Kriegl JM, Clark T (2008). A composite model for HERG blockade. ChemMedChem 3: 254-265.

Kroll CR, Gettes LS (2002). T wave alternans and Torsades de Pointes after the use of intravenous pentamidine. J Cardiovasc Electrophysiol 13: 936-938.

Kubo Y, Murata Y (2001). Control of rectification and permeation by two distinct sites after the second transmembrane region in Kir2.1 K+ channel. J Physiol 531: 645-660.

Kuryshev YA, Ficker E, Wang L, Hawryluk P, Dennis AT, Wible BA, Brown AM, Kang J, Chen XL, Sawamura K, Reynolds W, Rampe D (2005). Pentamidine-induced long QT syndrome and block of hERG trafficking. J Pharmacol Exp Ther 312: 316-323.

Lai A Fat EJSK, Vrede MA, Soetosenojo RM, Lai A Fat RFM (2002). Pentamidine, the drug of choice for the treatment of cutaneous leishmaniasis in Surinam. Int J Dermatol 41: 796-800.

Lawrence CL, Bridgland-Taylor MH, Pollard CE, Hammond TG, Valentin JP (2006). A Rabbit Langendorff Heart Proarrhythmia Model: Predictive Value for Clinical Identification of Torsades de Pointes. Br J Pharmacol 149: 845-860.

Lengyel C, Dézsi L, Biliczki P, Horváth C, Virág L, Iost N, Németh M, Tálosi L, Papp JG, Varró A (2004). Effect of a neuroprotective drug, eliprodil on cardiac repolarisation: importance of the decreased repolarisation reserve in the development of proarrhythmic risk. Br J Pharmacol 143: 152-158.

Lengyel C, Varró A, Tábori K, Papp JG, Baczkó I (2007). Combined pharmacological block of I(Kr) and I(Ks) increases short-term QT interval variability and provokes torsades de pointes. Br J Pharmacol 151: 941-951.

Lidman C, Bronner U, Gustafsson LL, Rombo L (1994). Plasma pentamidine concentrations vary between individuals with Pneumocystis carinii pneumonia and the drug is actively secreted by the kidney. J Antimicrob Chemother 33: 803-810.

Liew R, Stagg MA, MacLeod KT, Collins P (2004). Raloxifene acutely suppresses ventricular myocyte contractility through inhibition of the L-type calcium current. Br J Pharmacol 142: 89-96.

Liu H, Ji M, Luo X, Shen J, Huang X, Hua W, Jiang H, Chen K (2002). New p-methylsulfonamido phenylethylamine analogues as class III antiarrhythmic agents: design, synthesis, biological assay, and 3D-QSAR analysis. J Med Chem 45: 2953-2969.

Liu H, Jin MW, Xiang JZ, Huang Y, Sun HY, Chiu SW, Lau CP, Li GR (2007). Raloxifene inhibits transient outward and ultra-rapid delayed rectifier potassium currents in human atrial myocytes. Eur J Pharmacol 563: 61-68.

Liu XK, Katchman A, Ebert SN, Woosley RL (1998). The antiestrogen tamoxifen blocks the delayed rectifier potassium current, IKr, in rabbit ventricular myocytes. J Pharmacol Exp Ther 287: 877-883.

Lopatin AN, Makhina EN, Nichols CG (1994). Potassium channel block by cytoplasmic polyamines as the mechanism of intrinsic rectification. Nature 372: 366-369.

Lopatin AN, Nichols CG (2001). Inward rectifiers in the heart: an update on I(K1). J Mol Cell Cardiol 33: 625-638.

Lu Z (2004). Mechanism of rectification in inward-rectifier K+ channels. Annu Rev Physiol 66: 103–129.

Makhina EN, Kelly AJ, Lopatin AN, Mercer RW, Nichols CG (1994). Cloning and expression of a novel human brain inward rectifier potassium channel. J Biol Chem 269: 20468-20474.

Martin R, McDermott J, Salmen H, Palmatier J, Cox B, Gintant GA (2004). The Utility of hERG and Repolarization Assays in Evaluating Delayed Cardiac Repolarization: Influence of Multi-Channel Block. J Cardiovasc Pharmacol 43: 369-379.

Matasi JJ, Caldwell JP, Zhang H, Fawzi A, Higgins GA, Cohen-Williams ME, Varty GB, Tulshian DB (2005). 2-(2-Furanyl)-7-phenyl[1,2,4]triazolo[1,5-c]pyrimidin-5-amine analogs as adenosine A2A antagonists: the successful reduction of hERG activity. Part 2. Bioorg Med Chem Lett 15: 3675-3678.

Matsuda H, Saigusa A, Irisawa H (1987). Ohmic conductance through the inwardly rectifying K channel and blocking by internal Mg2+. Nature 325: 156-159.

Matthys G, Park JW, McGuire S, Wire MB, Zhang J, Bowen C, Williams D, Jenkins JM, Peng B (2010). Eltrombopag does not affect cardiac repolarization: results from a definitive QTc study in healthy subjects. Br J Clin Pharmacol 70: 24-33.

McCauley JA, Theberge CR, Romano JJ, Billings SB, Anderson KD, Claremon DA, Freidinger RM, Bednar RA, Mosser SD, Gaul SL, Connolly TM, Condra CL, Xia M, Cunningham ME, Bednar B, Stump GL, Lynch JJ, Macaulay A, Wafford KA, Koblan KS, Liverton NJ (2004). NR2B-selective N-methyl-D-aspartate antagonists: synthesis and evaluation of 5-substituted benzimidazoles. J Med Chem 47: 2089-2096.

Meyers KM, Méndez-Andino JL, Colson AO, Warshakoon NC, Wos JA, Mitchell MC, Hodge KM, Howard JM, Ackley DC, Holbert JK, Mittelstadt SW, Dowty ME, Obringer CM, Reizes O, Hu XE (2007). Aminomethyl tetrahydronaphthalene ketopiperazine MCH-R1 antagonists--Increasing selectivity over hERG. Bioorg Med Chem Lett 17:

819-822.

Miake J, Marbán E, Nuss HB (2002). Biological pacemaker created by gene transfer. Nature 419: 132-133.

Ming X, Ju W, Wu H, Tidwell RR, Hall JE, Thakker DR (2009). Transport of dicationic drugs pentamidine and furamidine by human organic cation transporters. Drug Metab Dispos 37: 424-430.

Mitchell P, Dodek P, Lawson L, Kiess M, Russell J (1989). Torsades de pointes during intravenous pentamidine isethionate therapy. Can Med Assoc J 140: 173-174.

Mitcheson JS, Chen J, Lin M, Culberson C, Sanguinetti MC (2000). A structural basis for drug-induced long QT syndrome. Proc Natl Acad Sci U S A 97: 12329-12333.

Mukaiyama H, Nishimura T, Kobayashi S, Komatsu Y, Kikuchi S, Ozawa T, Kamada N, Ohnota H (2008). Novel pyrazolo[1,5-a]pyrimidines as c-Src kinase inhibitors that reduce IKr channel blockade. Bioorg Med Chem 16: 909-921.

Murphy CA, Dargie HJ (2007). Drug-induced cardiovascular disorders. Drug Saf 30: 783-804.

Nagase S, Fukushima Kusano K, Yoshida M, Ohe T (2007). Electrophysiologic characteristics of an Andersen syndrome patient with KCNJ2 mutation. Heart Rhythm 4: 512-515.

Nalos L, De Boer TP, Houtman MJC, Rook MB, Vos MA, Van der Heyden MAG (2011a). Inhibition of lysosomal degradation rescues pentamidine-mediated decreases of KIR2.1 ion channel expression but not that of Kv11.1. Eur J Pharmacol 652: 96-103.

Nalos L, Varkevisser R, Jonsson M, Houtman M, Beekman J, van der Nagel R, Thomsen M, Duker G, Sartipy P, de Boer T, Peschar M, Rook M, van Veen T, van der Heyden M, Vos M (2011b). Comparison of I(Kr) blocking drugs Moxifloxacin and Dofetilide/E-4031 in 5 screening models of pro-arrhythmia reveals insufficient specificity of isolated cardiomyocytes. Br J Pharmacol manuscript accepted.

Noujaim SF, Stuckey JA, Ponce-Balbuena D, Ferrer-Villada T, López-Izquierdo A, Pandit S, Calvo CJ, Grzeda KR, Berenfeld O, Chapula JA, Jalife J (2010). Specific residues of the cytoplasmic domains of cardiac inward rectifier potassium channels are effective antifibrillatory targets. FASEB J 24: 4302-4312.

Obers S, Staudacher I, Ficker E, Dennis A, Koschny R, Erdal H, Bloehs R, Kisselbach J, Karle CA, Schweizer PA, Katus HA, Thomas D (2010). Multiple mechanisms of hERG liability: K+ current inhibition, disruption of protein trafficking, and apoptosis induced by amoxapine. Naunyn Schmiedebergs Arch Pharmacol 381: 385-400.

OMIM® - Online Mendelian Inheritance in Man® http://www.ncbi.nlm.nih.gov/omim

Oros A, Beekman JD, Vos MA (2008). The canine model with chronic, complete atrio-ventricular block. Pharmacol Ther 119: 168-178.

Oros A, Houtman MJ, Neco P, Gomez AM, Rajamani S, Oosterhoff P, Attevelt NJ,

Beekman JD, van der Heyden MA, Ver Donck L, Belardinelli L, Richard S, Antoons G, Vos MA; CONTICA investigators (2010). Robust anti-arrhythmic efficacy of verapamil and flunarizine against dofetilide-induced TdP arrhythmias is based upon a shared and a different mode of action. Br J Pharmacol 161: 162-175.

Owens Jr., R.C., 2004. QT prolongation with antimicrobial agents: understanding the significance. Drugs 64, 1091-1124.

Paine MF, Wang MZ, Generaux CN, Boykin DW, Wilson WD, De Koning HP, Olson CA, Pohlig G, Burri C, Brun R, Murilla GA, Thuita JK, Barrett MP, Tidwell RR (2010). Diamidines for human African trypanosomiasis. Curr Opin Investig Drugs 11: 876-883.

Pastore JM, Rosenbaum DS (2000). Role of structural barriers in the mechanism of alternans-induced reentry. Circ Res 87: 1157-1163.

Pathak CK, Dhawan D, Lindner DJ, Borden EC, Farver C, Yi T (2002). Pentamidine is an inhibitor of PRL phosphatases with anticancer activity. Mol Cancer Ther 1: 1255-1264.

Pearlstein R, Vaz R, Rampe D (2003a). Understanding the structure-activity relationship of the human ether-a-go-go-related gene cardiac K+ channel. A model for bad behavior. J Med Chem 46: 2017-2022.

Pearlstein RA, Vaz RJ, Kang J, Chen XL, Preobrazhenskaya M, Shchekotikhin AE, Korolev AM, Lysenkova LN, Miroshnikova OV, Hendrix J, Rampe D (2003b). Characterization of HERG potassium channel inhibition using CoMSiA 3D QSAR and homology modeling approaches. Bioorg Med Chem Lett 13: 1829-1835.

Pedersen HS, Elming H, Seibaek M, Burchardt H, Brendorp B, Torp-Pedersen C, Køber L; DIAMOND Study Group (2007). Risk factors and predictors of Torsade de pointes ventricular tachycardia in patients with left ventricular systolic dysfunction receiving Dofetilide. Am J Cardiol 100: 876-880.

Pegan S, Arrabit C, Zhou W, Kwiatkowski W, Collins A, Slesinger PA, Choe S (2005). Cytoplasmic domain structures of KIR2.1 and KIR3.1 show sites for modulating gating and rectification. Nat Neurosci 8: 279-287.

Pekkanen-Mattila M, Chapman H, Kerkelä E, Suuronen R, Skottman H, Koivisto AP, Aalto-Setälä K (2010). Human embryonic stem cell-derived cardiomyocytes: demonstration of a portion of cardiac cells with fairly mature electrical phenotype. Exp Biol Med 235: 522-530.

Peng S, Lacerda AE, Kirsch GE, Brown AM, Bruening-Wright A (2010). The action potential and comparative pharmacology of stem cell-derived human cardiomyocytes. J Pharmacol Toxicol Methods 61: 277-286.

Petrecca K, Atanasiu R, Akhavan A, Shrier A (1999). N-linked glycosylation sites determine HERG channel surface membrane expression. J Physiol 515: 41-48.

Plaster NM, Tawil R, Tristani-Firouzi M, Canún S, Bendahhou S, Tsunoda A, Donaldson MR, Iannaccone ST, Brunt E, Barohn R, Clark J, Deymeer F, George AL Jr, Fish FA,

Hahn A, Nitu A, Ozdemir C, Serdaroglu P, Subramony SH, Wolfe G, Fu YH, Ptácek LJ (2001). Mutations in KIR2.1 cause the developmental and episodic electrical phenotypes of Andersen's syndrome. Cell 105: 511-519.

Poluzzi E, Raschi E, Motola D, Moretti U, De Ponti F (2010). Antimicrobials and the risk of Torsade de Pointes. The contribution from data mining of the US FDA adverse event reporting system. Drug Saf 33: 303-314.

Ponce-Balbuena D, López-Izquierdo A, Ferrer T, Rodríguez-Menchaca AA, Aréchiga-Figueroa IA, Sánchez-Chapula JA (2009). Tamoxifen inhibits KIR2.x family of inward rectifier channels by interfering with PIP2-channel interactions. J Pharmacol Exp Ther 331: 563-573.

Price DA, Armour D, de Groot M, Leishman D, Napier C, Perros M, Stammen BL, Wood A (2006). Overcoming HERG affinity in the discovery of the CCR5 antagonist maraviroc. Bioorg Med Chem Lett 16: 4633-4637.

Quadrel MA, Atkin SH, Jaker MA (1992). Delayed cardiotoxicity during treatment with intravenous pentamidine: two case reports and a review of the literature. Am Heart J 123: 1377-1379.

Rajamani S, Eckhardt LL, Valdivia CR, Klemens CA, Gillman BM, Anderson CL, Holzem KM, Delisle BP, Anson BD, Makielski JC, January CT (2006). Drug-induced long QT syndrome: hERG K+ channel block and disruption of protein trafficking by fluoxetine and norfluoxetine. Br J Pharmacol 149: 481-489.

Ramakers C, Ruijter JM, Lekanne Deprez RH, Moorman AFM (2003). Assumption-free analysis of quantitative real-time polymerase chain reaction (PCR) data. Neurosci Lett 339: 62-66.

Ravens U, Cerbai E (2008). Role of potassium currents in cardiac arrhythmias. Europace 10: 1133-1137.

Recanatini M, Cavalli A, Masetti M (2008). Modeling HERG and its interactions with drugs: recent advances in light of current potassium channel simulations. ChemMedChem 3: 523-535.

Recanatini M, Poluzzi E, Masetti M, Cavalli A, De Ponti F (2005). QT prolongation through hERG K(+) channel blockade: current knowledge and strategies for the early prediction during drug development. Med Res Rev 25: 133-166.

Redell JB, Tempel BL (1998). Multiple promoter elements interact to control the transcription of the potassium channel gene, KCNJ2. J Biol Chem 273: 22807-22818.

Redfern WS, Carlsson L, Davis AS, Lynch WG, MacKenzie I, Palethorpe S, Siegl PK, Strang I, Sullivan AT, Wallis R, Camm AJ, Hammond TG (2003). Relationships between preclinical cardiac electrophysiology, clinical QT interval prolongation and torsade de pointes for a broad range of drugs: evidence for a provisional safety margin in drug development. Cardiovasc Res 58: 32-45.

Roden DM (1998a). Mechanisms and management of proarrhythmia. Am J Cardiol 82:

491-571.

Roden DM (1998b). Taking the “idio” out of “idiosyncratic”: predicting Torsades des Pointes. Pacing Clin Electrophysiol 21: 1029-1034.

Roden DM (2004). Drug-induced prolongation of the QT interval. N Engl J Med 350: 1013-1022.

Roden DM (2008). Cellular basis of drug-induced torsades de pointes. Br J Pharmacol 154: 1502-1507.

Roden DM, Hoffman BF (1985). Action potential prolongation and induction of abnormal automaticity by low quinidine concentrations in canine Purkinje Fibers. Circ Res 56: 857-867.

Roden DM, Lazzara R, Rosen M, Schwartz PJ, Towbin J, Vincent GM (1996). Multiple mechanisms in the long-QT syndrome. Current knowledge, gaps, and future directions. The SADS Foundation Task Force on LQTS. Circulation 94: 1996-2012.

Rodríguez-Menchaca AA, Navarro-Polanco RA, Ferrer-Villada T, Rupp J, Sachse FB, Tristani-Firouzi M, Sánchez-Chapula JA (2008). The molecular basis of chloroquine block of the inward rectifier KIR2.1 channel. Proc Natl Acad Sci USA 105: 1364-1368.

Roza O, Berman LB (1971). The pathophysiology of barium: hypokalemic and cardiovascular effects. J Pharmacol Exp Ther 177: 433-439.

Saint DA, Chung SH (1999). Variability of channel subconductance states of the cardiac sodium channel induced by protease. Receptors Channels 6: 283-294.

Sands M, Kron MA, Brown RB (1985). Pentamidine: a review. Rev Infect Dis 7: 625-633.

Sanguinetti MC, Jurkiewicz NK (1990). Two components of cardiac delayed rectifier K+ current. Differential sensitivity to block by class III antiarrhythmic agents. J Gen Physiol 96: 195-215.

Sanguinetti MC, Tristani-Firouzi M (2006). hERG potassium channels and cardiac arrhythmia. Nature 440: 463-469.

Sarapa N, Nickens DJ, Raber SR, Reynolds RR, Amantea MA (2008). Ritonavir 100 mg does not cause QTc prolongation in healthy subjects: a possible role as CYP3A inhibitor in thorough QTc studies. Clin Pharmacol Ther 83: 153-159.

Sasse M, Paul T, Bergmann P, Kallfelz HC (1998). Sotalol associated torsades de pointes tachycardia in a 15-month-old child: successful therapy with magnesium aspartate. Pacing Clin Electrophysiol 21: 1164-1166.

Shamovsky I, Connolly S, David L, Ivanova S, Nordén B, Springthorpe B, Urbahns K (2008). Overcoming undesirable HERG potency of chemokine receptor antagonists using baseline lipophilicity relationships. J Med Chem 51: 1162-1178.

Sherazi S, DiSalle M, Daubert JP, Shah AH (2008). Moxifloxacin induced Torsade de Pointes. Cardiol J 15: 71-73.

Shimizu W, Antzelevitch C (1997). Sodium channel block with mexiletine is effective in reducing dispersion of repolarization and preventing torsade des pointes in LQT2 and LQT3 models of the long-QT syndrome. Circulation 96: 2038-2047.

Schoenmakers M, Ramakers C, van Opstal JM, Leunissen JD, Londono C, Vos MA (2003). Asynchronous development of electrical remodeling and cardiac hypertrophy in the complete AV block dog. Cardiovasc Res 59: 351-359.

Schroeder BC, Waldegger S, Fehr S, Bleich M, Warth R, Greger R, Jentsch TJ (2000). A constitutively open potassium channel formed by KCNQ1 and KCNE3. Nature 403: 196-199.

Schwalbe RA, Rudin A, Xia SL, Wingo CS (2002). Site-directed glycosylation tagging of functional Kir2.1 reveals that the putative pore-forming segment is extracellular. J Biol Chem 277: 24382-24389.

Singleton DH, Boyd H, Steidl-Nichols JV, Deacon M, Groot MJ, Price D, Nettleton DO, Wallace NK, Troutman MD, Williams C, Boyd JG (2007). Fluorescently labeled analogues of dofetilide as high-affinity fluorescence polarization ligands for the human ether-a-go-go-related gene (hERG) channel. J Med Chem 50: 2931-2941.

Sisko JT, Tucker TJ, Bilodeau MT, Buser CA, Ciecko PA, Coll KE, Fernandes C, Gibbs JB, Koester TJ, Kohl N, Lynch JJ, Mao X, McLoughlin D, Miller-Stein CM, Rodman LD, Rickert KW, Sepp-Lorenzino L, Shipman JM, Thomas KA, Wong BK, Hartman GD (2006). Potent 2-[(pyrimidin-4-yl)amine}-1,3-thiazole-5-carbonitrile-based inhibitors of VEGFR-2 (KDR) kinase. Bioorg Med Chem Lett 16: 1146-1150.

Slee DH, Moorjani M, Zhang X, Lin E, Lanier MC, Chen Y, Rueter JK, Lechner SM, Markison S, Malany S, Joswig T, Santos M, Gross RS, Williams JP, Castro-Palomino JC, Crespo MI, Prat M, Gual S, Díaz JL, Jalali K, Sai Y, Zuo Z, Yang C, Wen J, O'Brien Z, Petroski R, Saunders J (2008). 2-Amino-N-pyrimidin-4-ylacetamides as A2A receptor antagonists: 2. Reduction of hERG activity, observed species selectivity, and structure-activity relationships. J Med Chem 51: 1730-1739.

Snyders DJ, Chaudhary A (1996). High affinity open channel block by dofetilide of HERG expressed in a human cell line. Mol Pharmacol 49: 949-955.

So PP, Hu XD, Backx PH, Puglisi JL, Dorian P (2006). Blockade of IKs by HMR 1556 increases the reverse rate-dependence of refractoriness prolongation by dofetilide in isolated rabbit ventricles. Br J Pharmacol 148: 255-263.

Soltysinska E, Olesen SP, Christ T, Wettwer E, Varró A, Grunnet M, Jespersen T (2009). Transmural expression of ion channels and transporters in human nondiseased and end-stage failing hearts. Pflugers Arch 459: 11-23.

Spector PS, Curran ME, Zou A, Keating MT, Sanguinetti MC (1996). Fast inactivation causes rectification of the IKr channel. J Gen Physiol 107: 611-619.

Stanfield PR, Davies NW, Shelton PA, Sutcliffe MJ, Khan IA, Brammar WJ, Conley EC (1994). A single aspartate residue is involved in both intrinsic gating and blockage by Mg2+ of the inward rectifier, IRK1. J Physiol 478: 1-6.

Stansfeld PJ, Gedeck P, Gosling M, Cox B, Mitcheson JS, Sutcliffe MJ (2007). Drug block of the hERG potassium channel: insight from modeling. Proteins 68: 568-580.

Stass H, Dalhoff A, Kubitza D, Schühly U (1998). Pharmacokinetics, safety, and tolerability of ascending single doses of moxifloxacin, a new 8-methoxy quinolone, administered to healthy subjects. Antimicrob Agents Chemother 42: 2060-2065.

Staudacher I, Wang L, Wan X, Obers S, Wenzel W, Tristram F, Koschny R, Staudacher K, Kisselbach J, Koelsch P, Schweizer PA, Katus HA, Ficker E, Thomas D (2011). hERG K+ channel-associated cardiac effects of the antidepressant drug desipramine. Naunyn Schmiedebergs Arch Pharmacol 383: 119-139.

Su J, McKittrick BA, Tang H, Burnett DA, Clader JW, Greenlee WJ, Hawes BE, O'Neill K, Spar B, Weig B, Kowalski T, Sorota S, Li C, Liu T (2007). SAR study of bicyclo[4.1.0]heptanes as melanin-concentrating hormone receptor R1 antagonists: taming hERG. Bioorg Med Chem 15: 5369-5385.

Sun H, Liu X, Xiong Q, Shikano S, Li M (2006). Chronic inhibition of cardiac Kir2.1 and HERG potassium channels by celastrol with dual effects on both ion conductivity and protein trafficking. J Biol Chem 281: 5877-5884.

Sun T, Zhang Y (2008). Pentamidine binds to tRNA through non-specific hydrophobic interactions and inhibits aminoacylation and translation. Nucl Acids Res 36: 1654-1664.

Sun ZQ, Thomas GP, Antzelevitch C (2001). Chromanol 293B inhibits slowly activating delayed rectifier and transient outward currents in canine left ventricular myocytes. J Cardiovasc Electrophysiol 12: 472-478.

Synnergren J, Akesson K, Dahlenborg K, Vidarsson H, Améen C, Steel D, Lindahl A, Olsson B, Sartipy P (2008). Molecular signature of cardiomyocyte clusters derived from human embryonic stem cells. Stem Cells 26: 1831-1840.

Taglialatela M, Ficker E, Wible BA, Brown AM (1995). C-terminus determinants for Mg2+ and polyamine block of the inward rectifier K+ channel IRK1. EMBO J 14: 5532-5541.

Tai K, Stansfeld J, Sansom MSP (2009). Ion-blocking sites of the KIR2.1 channel revealed by multiscale modeling. Biochemistry 48: 8758-8763.

Takahara A, Nakamura Y, Sugiyama A (2008). Beat-to-beat variability of repolarization differentiates the extent of torsadogenic potential of multi ion channel-blockers bepridil and amiodarone. Eur J Pharmacol 596: 127-131.

Thai KM, Ecker GF (2008). A binary QSAR model for classification of hERG potassium channel blockers. Bioorg Med Chem 16: 4107-4119.

Thomas P, Smart TG (2005). HEK293 cell line: a vehicle for the expression of recombinant proteins. J Pharmacol Toxicol Methods 51: 187-200.

Thomsen MB, Beekman JD, Attevelt NJ, Takahara A, Sugiyama A, Chiba K, Vos MA (2006). No proarrhythmic activity of the antibiotics moxifloxacin and azythromycin in anesthetized dogs with chronic AV-block. Br J Pharmacol 149: 1039-1048.

Thomsen MB, Oros A, Schoenmakers M, van Opstal JM, Maas JN, Beekman JD, Vos MA (2007). Proarrhythmic electrical remodelling is associated with increased beat-to-beat variability of repolarisation. Cardiovasc Res 73: 521-530.

Thomsen MB, Verduyn SC, Stengl M, Beekman JD, de Pater G, van Opstal J, Volders PG, Vos MA (2004). Increased short-term variability of repolarization predicts d-sotalol-induced torsades de pointes in dogs. Circulation 110: 2453-2459.

Tong Y, Brandt GS, Li M, Shapovalov G, Slimko E, Karschin A, Dougherty DA, Lester HA (2001). Tyrosine decaging leads to substantial membrane trafficking during modulation of an inward rectifier potassium channel. J Gen Physiol 117: 103-118.

Topliss JG (1972). Utilization of operational schemes for analog synthesis in drug design. J Med Chem 15: 1006-1011.

Tristani-Firouzi M, Jensen JL, Donaldson MR, Sansone V, Meola G, Hahn A, Bendahhou S, Kwiecinski H, Fidzianska A, Plaster N, Fu YH, Ptácek LJ, Tawil R (2002). Functional and clinical characterization of KCNJ2 mutations associated with LQT7 (Andersen syndrome). J Clin Invest 110: 381-388.

Valentin JP, Hammond T (2008). Safety and secondary pharmacology: successes, threats, challenges and opportunities. J Pharmacol Toxicol Methods 58: 77-87.

Valentin JP, Hoffmann P, De Clerck F, Hammond TG, Hondeghem L (2004). Review of the predictive value of the Langendorff heart model (Screenit system) in assessing the proarrhythmic potential of drugs. J Pharmacol Toxicol Methods 49: 171-181.

Valenzuela F, Vassalle M (1991). Role of membrane potential in Ba2+ induced automaticity in guinea pig cardiac myocytes. Cardiovasc Res 25: 421-430.

Van de Water A, Verheyen J, Xhonneux R, Reneman RS (1989). An improved method to correct the QT interval of the electrocardiogram for changes in heart rate. J Pharmacol Methods 22: 207-217.

van der Heyden MA, Sánchez-Chapula JA (2011). Toward specific cardiac I(K1) modulators for in vivo application: Old drugs point the way. Heart Rhythm 8: 1076-1080.

van der Heyden MA, Smits ME, Vos MA (2008). Drugs and trafficking of ion channels: a new pro-arrhythmic threat on the horizon? Br J Pharmacol 153: 406-409.

Van Opstal JM, Leunissen JD, Wellens HJ, Vos MA (2001). Azimilide and dofetilide produce similar electrophysiological and proarrhythmic effects in a canine model of Torsade de Pointes arrhythmias. Eur J Pharmacol 412: 67–76.

Vandenberg CA (1987). Inward rectification of a potassium channel in cardiac ventricular cells depends on internal magnesium ions. Proc Natl Acad Sci U S A 84: 2560-2564.

Volders PG, Sipido KR, Carmeliet E, Spätjens RL, Wellens HJ, Vos MA (1999). Repolarizing K+ currents ITO1 and IKs are larger in right than left canine ventricular midmyocardium. Circulation 99: 206-210.

Volders PG, Stengl M, van Opstal JM, Gerlach U, Spätjens RL, Beekman JD, Sipido KR, Vos MA (2003). Probing the contribution of IKs to canine ventricular repolarization: key role for beta-adrenergic receptor stimulation. Circulation 107: 2753-2760.

Vos MA (2008). Literature based evaluation of four hard end-points models for assessing drug induced Torsades de Pointes liability. Br J Pharmacol 154: 1523-1527.

Vos MA, van Opstal JM, Leunissen JD, Verduyn SC (2001). Electrophysiologic parameters and predisposing factors in the generation of drug-induced Torsade de Pointes arrhythmias. Pharmacol Ther 92: 109-122.

Vos MA, Verduyn SC, Gorgels AP, Lipcsei GC, Wellens HJ (1995). Reproducible induction of early afterdepolarizations and torsade de pointes arrhythmias by d-sotalol and pacing in dogs with chronic atrioventricular block. Circulation 91: 864-872.

Waalkes TP, Denham BA, DeVita VT (1970). Pentamidine: clinical pharmacologic correlations in man and mice. Clin Pharmacol 11: 505-512.

Waldman RH, Pearce DE, Martin RA (1973). Pentamidine isothionate levels in lungs, livers, and kidneys of rats after aerosol or intramuscular administration. Am Rev Respir Dis 108: 1004-1006.

Wang L, Wible BA, Wan X, Ficker E (2007). Cardiac glycosides as novel inhibitors of human ether-a-go-go-related gene channel trafficking. J Pharmacol Exp Ther 320: 525-534.

Wang Y, Hill JA (2010). Electrophysiological remodeling in heart failure. J Mol Cell Cardiol 48: 619-632.

Warf MB, Nakamori M, Matthys CM, Thornton CA, Berglund JA (2009). Pentamidine reverses the splicing defects associated with myotonic dystrophy. Proc Natl Acad Sci USA 106: 18551-18556.

Warmke JW, Ganetzky B (1994). A family of potassium channel genes related to eag in Drosophila and mammals. Proc Natl Acad Sci U S A 91: 3438-3442.

Weerapura M, Hébert TE, Nattel S (2002). Dofetilide block involves interactions with open and inactivated states of HERG channels. Pflugers Arch 443: 520-531.

Werbovetz K (2006). Diamidines as antitrypanosomal, antileishmanial and antimalarial agents. Curr Opin Investig Drugs 7: 147-157.

White NJ (2007). Cardiotoxicity of antimalarial drugs. Lancet Infect Dis 7: 549-558.

Wible BA, Taglialatela M, Ficker E, Brown AM (1994). Gating of inwardly rectifying K+ channels localized to a single negatively charged residue. Nature 371: 246-249.

Wilke RA, Lin DW, Roden DM, Watkins PB, Flockhart D, Zineh I, Giacomini KM, Krauss RM (2007). Identifying genetic risk factors for serious adverse drug reactions: current progress and challenges. Nat Rev Drug Discov 6: 904-916.

Wilson WD, Tanious FA, Mathis A, Tevis D, Hall JE, Boykin DW (2008). Antiparasitic compounds that target DNA. Biochimie 90, 999-1014.

Witchel HJ, Milnes JT, Mitcheson JS, Hancox JC (2002). Troubleshooting problems with in vitro screening of drugs for QT interval prolongation using HERG K+ channels expressed in mammalian cell lines and Xenopus oocytes. J Pharmacol Toxicol Methods 48: 65-80.

Xia M, Jin Q, Bendahhou S, He Y, Larroque MM, Chen Y, Zhou Q, Yang Y, Liu Y, Liu B, Zhu Q, Zhou Y, Lin J, Liang B, Li L, Dong X, Pan Z, Wang R, Wan H, Qiu W, Xu W, Eurlings P, Barhanin J, Chen Y (2005). A KIR2.1 gain-of-function mutation underlies familial atrial fibrillation. Biochem Biophys Res Commun. 332: 1012-1019.

Xiao J, Zhen XG, Yang J (2003). Localization of PIP2 activation gate in inward rectifier K+ channels. Nat Neurosci 6: 811-818.

Yang BF, Xu DH, Xu CQ, Li Z, Du ZM, Wang HZ, Dong DL (2004). Inactivation gating determines drug potency: a common mechanism for drug blockade of HERG channels. Acta Pharmacol Sin 25: 554-560.

Yang J, Jan YN, Jan LY (1995b). Control of rectification and permeation by residues in two distinct domains in an inward rectifier K+ channel. Neuron 14: 1047-1054.

Yang T, Kupershmidt S, Roden DM (1995a). Anti-minK antisense decreases the amplitude of the rapidly activating cardiac delayed rectifier K+ current. Circ Res 77: 1246-1253.

Yokoyama H, Nakamura Y, Iwasaki H, Hoshiai K, Mitsumori Y, Sugiyama A (2009). Effects of acute intravenous administration of pentamidine, a typical hERG-trafficking inhibitor, on the cardiac repolarization process of halothane-anesthetized dogs J Pharmacol Sci 110: 476-482.

Yoshizumi T, Takahashi H, Miyazoe H, Sugimoto Y, Tsujita T, Kato T, Ito H, Kawamoto H, Hirayama M, Ichikawa D, Azuma-Kanoh T, Ozaki S, Shibata Y, Tani T, Chiba M, Ishii Y, Okuda S, Tadano K, Fukuroda T, Okamoto O, Ohta H (2008). A novel class of cycloalkano[b]pyridines as potent and orally active opioid receptor-like 1 antagonists with minimal binding affinity to the hERG K+ channel. J Med Chem 51: 4021-4029.

Zaniboni M, Pollard AE, Yang L, Spitzer KW (2000). Beat-to-beat repolarization variability in ventricular myocytes and its suppression by electrical coupling. Am J Physiol Heart Circ Physiol 278: H677-687.

Zeegelaar JE, Steketee WH, Van Thiel PPAM, Wetsteyn JCFM, Kager FA, Faber WR (2005). Changing pattern of imported cutaneous leishmaniasis in the Netherlands. Clin Exp Dermatol 30: 1-5.

Zeitlinger M, Sauermann R, Fille M, Hausdorfer J, Leitner I, Müller M (2008). Plasma protein binding of fluoroquinolones affects antimicrobial activity. J Antimicrob Chemother 61: 561-567.

Zhang H, Garratt CJ, Zhu J, Holden AV (2005c). Role of up-regulation of IK1 in action potential shortening associated with atrial fibrillation in humans. Cardiovasc Res 66: 493-502.

Zhang HC, Derian CK, McComsey DF, White KB, Ye H, Hecker LR, Li J, Addo MF, Croll D, Eckardt AJ, Smith CE, Li Q, Cheung WM, Conway BR, Emanuel S, Demarest KT, Andrade-Gordon P, Damiano BP, Maryanoff BE (2005a). Novel indolylindazolylmaleimides as inhibitors of protein kinase C-beta: synthesis, biological activity, and cardiovascular safety. J Med Chem 48: 1725-1728.

Zhang L, Benson DW, Tristani-Firouzi M, Ptácek LJ, Tawil R, Schwartz PJ, George AL, Horie M, Andelfinger G, Snow GL, Fu YH, Ackerman MJ, Vincent GM (2005b). Electrocardiographic features in Andersen-Tawil syndrome patients with KCNJ2 mutation. Characteristic T-U-wave patterns predict the KCNJ2 genotype. Circulation 111: 2720-2726.

Zhang S (2006). Isolation and characterization of IKr in cardiac myocytes by Cs+ permeation. Am J Physiol Heart Circ Physiol 290: H1038-1049.

Zhang Y, Li Z, Pilch DS, Leibowitz MJ (2002). Pentamidine inhibits catalytic activity of group I intron Ca.LSU by altering RNA folding. Nucl Acids Res 30: 2961-2971.

Zhou Z, Gong Q, January CT (1999). Correction of defective protein trafficking of a mutant HERG potassium channel in human long QT syndrome. J Biol Chem 274: 31123-31126.

Zhou Z, Gong Q, Ye B, Fan Z, Makielski JC, Robertson GA, January CT (1998). Properties of HERG channels stably expressed in HEK 293 cells studied at physiological temperature. Biophys J 74: 230-241.

Zhu BY, Jia ZJ, Zhang P, Su T, Huang W, Goldman E, Tumas D, Kadambi V, Eddy P, Sinha U, Scarborough RM, Song Y (2006). Inhibitory effect of carboxylic acid group on hERG binding. Bioorg Med Chem Lett 16: 5507-5512.

Chapter 9

Summary/ Samenvatting

Excessive prolongation of cardiac repolarization, manifested as QT prolongation on ECG, is common unwanted side effect of many drugs and drug candidates. Prolongation of QT interval may lead to life threatening cardiac arrhythmia – Torsade de Point (TdP). Number of drugs was withdrawn from the market and development of many new drug candidates is terminated because of this side effect. Block of the hERG channel is believed to be the principal reason of QT prolongation and thus current safety testing assays are based on determining the hERG block potency of new drug candidates.

Here we demonstrate that focus on hERG block is counterproductive. Drugs affecting other repolarizing currents might be proarrhythmic as well. In the same time, potent hERG blocker with effect on depolarizing currents is not always proarrhythmic. We also show, that TdP can occur after chronic treatment due to effect on protein trafficking. This chronic effect is not tested in cardiac safety assessment at all.

We have designed and synthesized 40 analogues of potent hERG blocker dofetilide to analyze molecular substructures required for hERG block. This approach may help design new drugs with low affinity to hERG channel.

We identify pentamidine as a direct blocker of another important repolarizing current - I_{K1}. The role of this current in cardiac arrhythmias is poorly studied, mainly because of absence of a specific I_{K1} blocker. We have tested 7 pentamidine analogues to find a specific and effective I_{K1} blocker applicable in vivo.

Based on our findings, to improve current cardiac safety assessment, we employed five test assays and compare their sensitivity and specificity using hERG blockers with known proarrhythmic potential. We demonstrate that isolated cardiomyocytes lack sufficient specificity to correctly identify safe hERG blocker moxifloxacin. On the other hand, hESC-CM seems to be a promising alternative to current assays.

Een overmatige verlenging van cardiale repolarisatie, zich uitend als QT verlenging in het ECG, is een veel voorkomende, ongewenste, bijwerking van bestaande en potentieel nieuwe medicijnen. Deze QT verlenging kan soms tot levensbedreigende hartritmestoornissen leiden, de zogenoemde Torsade de Pointes aritmie.

Als gevolg van deze ernstige bijwerking is een aantal bestaande medicijnen van de markt gehaald en is de verdere ontwikkeling van veelbelovende experimentele medicijnen stopgezet. De onderliggende oorzaak is veelal blokkade van het hERG ionkanaal, en daarom maakt het onderkennen van deze blokkade een belangrijk deel uit van medicijn veiligheidsonderzoek.

Uit ons onderzoek blijkt dat deze focus op het hERG ionkanaal contraproductief is. Zo kan remming van andere ionkanalen op zichzelf ook pro-aritmisch zijn. Aan de andere kant, een medicijn dat meerdere ionkanalen tegelijkertijd remt, is niet per definitie pro-aritmisch, en kan zelfs volledig veilig zijn. We tonen ook aan dat Torsade de Pointes aritmiën het gevolg kunnen zijn van fouten in intracellulair transport van het ionkanaal-eiwit wat is veroorzaakt door een medicijn. Dit aspect is momenteel niet opgenomen in het standaard medicijn veiligheidsonderzoek.

We hebben veertig analogen van een sterke hERG ionkanaal remmer, dofetilide, ontworpen en geproduceerd. Hiermee hebben we op moleculair niveau inzicht verkregen in de structuren die het hERG ionkanaal zullen remmen, hetgeen een waardevolle bijdrage levert aan medicijn-ontwikkeling waarin hERG blokkade dient te worden vermeden.

We tonen hier ook aan dat het medicament pentamidine een directe remmer is van een ander belangrijk repolariserend ionkanaal, namelijk het zogenoemde I_{K1} kanaal. De rol van dit kanaal in hartritmestoornissen is nog onduidelijk wegens het ontbreken van een specifieke remmer. We hebben daarom een zevental pentamidine-analogen onderzocht om zodoende tot een specifieke en efficiënte I_{K1} remmer te komen die in proefdieronderzoek kan worden gebruikt.

Omdat medicijn veiligheidsonderzoek beter moet, hebben wij vijf verschillende testen met elkaar vergeleken op basis van hun specificiteit en gevoeligheid voor een onveilige en een veilige hERG remmer. We laten zien dat testen die zijn gebaseerd op geïsoleerde hartspiercellen onvoldoende specificiteit bezitten om veilige van onveilige medicijnen te kunnen onderscheiden. Dit in tegenstelling tot hartspiercellen die uit menselijke embryonale stamcellen worden gemaakt. We denken daarom dat menselijke stamcellen een veelbelovend alternatief kunnen zijn voor bestaande testsystemen.

Chapter 10

Acknowledgements

I am greatly indebted to all colleagues and co-workers who contributed to studies that form the backbone of this thesis. My thanks go especially to:

Marc, my principal supervisor, for teaching me a straightforward way of thinking and for his patients with all my shortcomings.

Marcel, my daily supervisor, for teaching me the daily scientific routine and for convincing me, that molecular biology is not an ugly nightmare.

Martin, my kind mentor and supervisor, for showing me the deepest secrets of the cellular electrophysiology.

Gudrun, my original supervisor, for guiding me through the first steps in patch-clamping.

My gratitude also goes to Maaike, Teun, Marien and Tonny for their collegiate help, friendship and knowledge.

I would like to express my sincere thanks to all other co-workers in the Department of Physiology, UMC Utrecht, for their efforts and helpful attitude during my stay there, particularly to Toon, Harold, Jacques, Tobias, Maria, Marti, Joost, Bart, Roel, Leonie, Vincent, John, Sanne, Malin, Maartje, Peter, Siddarth, Thom, Rosanne, Linda, Magda, Christian, Mohamed, Avram, Stephan, Mèra, Jet, Shirley, Tamara, Wendy and all others that formed an amazing atmosphere in which it was a privilege to work.

Zvláštní poděkování patří také mým kolegům a přátelům z Ústavu Fyziologie LF UK v Plzni a kamarádům, kteří mě podporovali a dodávali mi další sílu v boji s nástrahami bádání i sepisování.

Last but not least, I wish to acknowledge the advice and support of my parents as well as an exceptional patience, love and understanding of my wife. Finally this work is dedicated to our wonderful children.

Curriculum vitae

Lukáš Nalos was born on March 5th, 1976 in Ústí nad Labem, Czech Republic. He attended Gymnazium Jateční in Ústí nad Labem. After his graduation in 1994 he continued his study at the Charles University in Prague, Medical Faculty in Pilsen, Czech Republic, where he acquired his MD degree in 2000. Since 2000 he worked and did PhD traineeship at the Department of Physiology, Faculty of Medicine in Pilsen, Charles University in Prague. In 2007 he started his PhD training and performed the research presented in this thesis, in the laboratory of Medical Physiology, University Medical Center in Utrecht, under supervision of prof. Marc Vos, dr. Marcel van der Heyden and dr. Martin Rook.

Vydal vlastním nákladem
Lukáš Nalos, Slunečnicová 19, 32600 Plzeň
Plzeň 2011
Vydání 1.